Cytokinin-inducible *DIRIGENT13* involved in lignan synthesis and ROS accumulation promotes root growth and abiotic stress tolerance in *Arabidopsis*

Alesia Melnikava[1,2], François Perreau[3], Candelas Paniagua[1†], Sy-Chyi Cheng[4,5], Li-Min Huang[4,5], Elena Ubogoeva[6,7], Elena Zemlyanskaya[6,7], Yu-Liang Yang[4,5], Grégory Mouille[3], Dominique Arnaud[1,‡]* and Jan Hejatko[1,2]*

[1]CEITEC - Central European Institute of Technology, Masaryk University, Brno, Czech Republic

[2]National Centre for Biomolecular Research, Faculty of Science, Masaryk University, Brno, Czech Republic

[3]Université Paris-Saclay, INRAE, AgroParisTech, Institut Jean-Pierre Bourgin (IJPB), 78000, Versailles, France

[4]Agriculture Biotechnology Research Center, Academia Sinica, Taipei City, Taiwan

[5]Academia Sinica Biotechnology Center in Southern Taiwan, Tainan City, Taiwan

[6]Institute of Cytology and Genetics, Siberian Branch of Russian Academy of Sciences, Novosibirsk, Russia

[7]Novosibirsk State University, Novosibirsk, Russia

[†]Recent address: Institute for Mediterranean and Subtropical Horticulture "La Mayora", IHSM-UMA-CSIC, University of Málaga, Málaga, Spain

[‡]Recent address: Center of Plant Systems Biology and Biotechnology, 4000 Plovdiv, Bulgaria

***Correspondence:** D.A (dominiquearnaud.fr@gmail.com) and J.H. (lead corresponding author, jan.hejatko@ceitec.muni.cz); requests for materials should be addressed to J.H..

Running title: DIR13 promotes root growth and stress tolerance

Abstract

Dirigent (DIR) proteins mediate regio- and stereoselectivity of phenoxy radical coupling of monolignols for (neo)lignan or lignin synthesis. However, the role of DIR proteins and lignans in plant development and response to environmental stresses remains elusive. Here, we

provide a functional characterization of the cytokinin-responsive *DIRIGENT13* (*DIR13*) in *Arabidopsis thaliana*. DIR13 was localized to the root endodermis and at the margins of lateral root primordia and lateral roots. While not necessary for Casparian strip formation, DIR13 promoted both main and lateral root growth. Untargeted metabolomics and imaging mass spectrometry analyses unveiled the role of DIR13 in facilitating (neo)lignan synthesis in primary and lateral roots. Interestingly, DIR13 activated the production of putative oxomatairesinol and matairesinol-cysteine which are oxidative derivatives of the lignan matairesinol. Our data also identified DIR13 as an enhancer of salt and drought tolerance. Particularly, *DIR13* attenuated salt stress-mediated inhibition of germination and root growth. Moreover, DIR13 activated reactive oxygen species (ROS) accumulation both under control and salt stress conditions, and cytokinin further enhanced the salt-induced ROS production specifically in the *DIR13* overexpressing line. Our results uncover a role for DIR13-produced lignans in the priming of ROS accumulation, mediating both abiotic stress tolerance and the control of root architecture.

Keywords: dirigent, DIR13, lignan, ROS, cytokinins, stress response, salt, root architecture, Arabidopsis

Introduction

As sessile organisms, plants experience abiotic stress caused by multiple environmental factors, such as drought, salinity, and osmotic stress, which in turn induce alterations in plant physiological and biochemical processes, leading to compromised plant growth and developmental modifications (Zhao *et al.*, 2020). Salt stress represents a critical environmental challenge with profound implications for crop growth and productivity, thereby leading to significant economic repercussions in agriculture (Qadir *et al.*, 2014). Salt stress can detrimentally reduce photosynthesis, and impede seed germination and root growth (Zhao *et al.*, 2020; Zou, Zhang and Testerink, 2022; Balasubramaniam *et al.*, 2023).

Reactive oxygen species (ROS) play crucial roles in plant development and stress responses (Mittler, 2017; Mhamdi and Van Breusegem, 2018; Smirnoff and Arnaud, 2019). Various (a)biotic stresses induce an increase in ROS production in plants and hydrogen peroxide (H_2O_2) is particularly implicated in stress sensing, signaling, and adaptation (Miller *et al.*, 2010;

57 Smirnoff and Arnaud, 2019). However, excessive ROS generation under stresses leads to direct
58 oxidative damage of DNA, lipids and proteins (Smirnoff and Arnaud, 2019). Besides their role
59 in stress response, ROS also function as signaling molecules for optimal root growth and
60 development (Tsukagoshi, 2016; Eljebbawi *et al.*, 2020; Mase and Tsukagoshi, 2021). Basal
61 ROS level and localized production are essential for cell expansion, root hair growth, lateral
62 root development, cell polarity, and Casparian strip (CS) formation (Takeda *et al.*, 2008; Lee *et*
63 *al.*, 2013; Manzano *et al.*, 2014; Mangano *et al.*, 2017). Although ROS have the ability to
64 modulate root growth to some degree autonomously, they also engage in complex crosstalk
65 with other signaling molecules including hormones (Mase and Tsukagoshi, 2021). However,
66 despite its central importance, our knowledge of the mechanisms controlling localized ROS
67 production in plants is still in its infancy.

68 The phenolic compounds lignans and neolignans are found throughout the plant kingdom and
69 are thought to play roles in various physiological processes, including response to
70 environmental stresses [(Paniagua *et al.*, 2017) and references there in]. Lignan biosynthesis
71 starts with the dimerization/radical coupling of two coniferyl alcohol molecules from the
72 phenylpropanoid and monolignol pathways leading to (+/-)-pinoresinol formation (Davin *et*
73 *al.*, 1997; Suzuki and Umezawa, 2007). The term lignan refers to a class of phenolic secondary
74 metabolites linked by an 8-8´ bond, while alternative dimers from 8-O-4' and 8-5' coupling are
75 known as neolignans (Moss, 2000; Umezawa, 2003). Through a series of enzymatic reactions
76 involving pinoresinol/lariciresinol reductase (PLR) and secoisolariciresinol dehydrogenase,
77 pinoresinol can be converted *via* lariciresinol to secoisolariciresinol and matairesinol (Davin
78 and Lewis, 2003; Suzuki and Umezawa, 2007). A variety of lignans can be derived from
79 pinoresinol, lariciresinol, secoisolariciresinol, and matairesinol through aromatic substituent
80 modification, such as glycosylation, hydroxylation, methylation, and cysteine addition
81 (Umezawa, 2003; Niculaes *et al.*, 2014). A number of pharmacological studies, mostly in
82 mammal cells, showed that many (neo)lignans exhibit potent antioxidant properties (Zálešák,
83 Bon and Pospíšil, 2019) while others have prooxidant activities (Hwang *et al.*, 2012; Ko *et al.*,
84 2021). Surprisingly, their roles in ROS metabolism in plants are poorly documented. It was
85 suggested that the poplar phenylcoumaran benzylic ether reductase (PCBER) and related
86 enzymes, such as PLRs, reduce (neo)lignans *in planta* to form antioxidants for protection
87 against oxidative damage (Niculaes *et al.*, 2014).

88 The first dirigent (DIR) protein was found to be responsible for the regio- and stereo-selective
89 specificity of coniferyl alcohol dimerization during (+)-pinoresinol formation (Davin *et al.*,
90 1997; Gang *et al.*, 1999). DIRs do not possess oxidizing or any other enzymatic activity but rely
91 on laccases (LAC) or apoplastic peroxidases (PER) to generate phenoxy radicals, which are then
92 guided *via* oriented binding to DIR trimers towards regio- and enantioselective product
93 formation (Davin *et al.*, 1997; Halls *et al.*, 2004; Gasper *et al.*, 2016; Paniagua *et al.*, 2017). DIR
94 and DIR-like proteins have been identified in almost all vascular plants and were classified into
95 six subfamilies DIR-a to DIR-f (Ralph *et al.*, 2006; Ralph *et al.*, 2007). In Arabidopsis, the DIR
96 family consists of 25 members, but for most of them, their physiological functions remain
97 unknown. Within the DIR-a subfamily, DIR5 and DIR6 participate in (-)-pinoresinol biosynthesis
98 (Kim *et al.*, 2012), and DIR12/DP1 is specific to the outer seed coat and essential for neolignans
99 biosynthesis (Yonekura-Sakakibara *et al.*, 2021). ESB1/DIR10, crucial for CS positioning, and
100 DIR9, DIR16, DIR21, and DIR24 (DIR-e subfamily) were shown to be responsible for the
101 majority of lignin deposition during CS formation (Lee *et al.*, 2013; Gao *et al.*, 2023). DIR13
102 (At4G11190) is the closest paralog of DIR5, DIR6, DIR14, and DIR12 but lacks the conserved
103 residues necessary for (-)-pinoresinol formation and exhibits strong, although not exclusive,
104 expression in the root (Kim *et al.*, 2012). *DIR* genes are induced by biotic and abiotic stresses
105 (Paniagua *et al.*, 2017) and overexpression of some *DIRs* can lead to improved tolerance to
106 biotic and abiotic stresses (dos Santos *et al.*, 2022; Li *et al.*, 2022).

107 Cytokinins are plant growth regulators controlling many important developmental and growth
108 processes such as cell division and differentiation (Kieber and Schaller, 2018; Yang *et al.*, 2021;
109 Svolacchia and Sabatini, 2023). Cytokinins and the cytokinin signaling pathway are also
110 involved in regulating biotic and abiotic stress response (Cortleven *et al.*, 2019; Skalak *et al.*,
111 2021). Several studies have demonstrated that cytokinins can exert both beneficial and
112 detrimental effects on stress tolerance or resistance (Nishiyama *et al.*, 2011; Reguera *et al.*,
113 2013; Arnaud *et al.*, 2017). The transcription factors type-B ARABIDOPSIS RESPONSE
114 REGULATORs (ARRs) ARR1, ARR10, and ARR12 transcriptionally regulate a number of
115 cytokinin-responsive genes (Taniguchi *et al.*, 2007; Bhargava *et al.*, 2013; Zubo *et al.*, 2017; Xie
116 *et al.*, 2018), but the functional importance of the majority of type-B ARR targets remains to
117 be clarified.

118 In this paper, we describe the spatiotemporal specificity of *DIR13* expression and DIR13
119 protein localization in the root and demonstrate that *DIR13* is under control of cytokinins and
120 type-B ARRs. DIR13 activated the accumulation of several putative lignans and neolignans in
121 the roots and primed ROS accumulation leading to improved plant adaptation to salinity and
122 drought, and modifications of root architecture toward growth promotion. These
123 observations imply a link between DIR13-mediated lignan production, ROS signaling, and
124 regulation of plant development and stress acclimation.

125

126 **Results**

127 **The root-expressed *DIR13* is upregulated by cytokinins**

128 To determine precisely the localization of DIR13 in root cells, we generated Arabidopsis lines
129 expressing the *pDIR13:NLS-3xGFP* construct. In the early (3-day-old) seedling development,
130 we observed the activity of *DIR13* promoter predominantly in the root, covering the region
131 ranging approximately from the root-shoot junction up to the root transition zone
132 (Supplemental Figures 1A, B). Weak expression was detectable also in the shoot apical
133 meristem (Supplemental Figure 1C). In the older (7-day-old) seedlings, *DIR13* promoter was
134 active dominantly in the endodermis, but also in the epidermis, cortex, and pericycle of the
135 root transition zone (Figure 1A), as well as in cells surrounding the lateral root (LR) primordia
136 (Figure 1B).

137 *DIR13* expression was proposed to be controlled by cytokinins (Taniguchi *et al.*, 2007;
138 Bhargava *et al.*, 2013). Accordingly, we observed that exogenous cytokinin application, 6-
139 Benzylaminopurine (BAP) for 4 or 24 hours, significantly enhanced *DIR13* promoter activity in
140 the root apical meristem (RAM) where only a weak signal was detectable under control
141 conditions (Figures 1C, D). These observations were confirmed by RT-qPCR analyses showing
142 a prompt upregulation of *DIR13* transcripts in roots from 3 hours after cytokinin treatment
143 (Figure 1E). In the *DIR13* promoter, we found the presence of binding regions recognized by
144 the type-B response regulators *ARR1, ARR10* and *ARR12* involved in cytokinin signaling [(Xie
145 *et al.*, 2018); Supplemental Figure 1D]. In line with that, we observed a significant decrease in
146 *DIR13* expression in single *arr1-3, arr10-5* and *arr12-1* mutants compared to Col-0 WT
147 (Supplemental Figure 1E). Even a more pronounced decrease in *DIR13* transcript levels was

148 detectable in double *arr1,10, arr10,12* and *arr1,12* mutant backgrounds, both in the presence
149 or absence of exogenous cytokinin (Figure 1F). In summary, our findings provide evidence for
150 root-dominant expression of *DIR13* being under positive control of cytokinin signaling.

151

152 **DIR13 protein localizes to the root endodermis and periphery of developing lateral roots**

153 Using *pDIR13:DIR13-mCherry* Arabidopsis lines, we found DIR13 being localized to the
154 endodermis of the root differentiation zone at a domain resembling the Casparian strip (CS)
155 (Figure 2A–C). However, compared to CASP1-GFP and ESB1-mCherry (Supplemental Figure 2),
156 which are known to determine the CS positioning and regulate CS formation (Roppolo *et al.*,
157 2011; Hosmani *et al.*, 2013), DIR13 localization pattern was more diffuse and of weaker signal
158 intensity. That might be due to the weak binding of DIR13 to the cell wall and possible wash-
159 out during specimen preparation (see Materials and Methods). Following 24 h of BAP
160 treatment, the DIR13 signal was observed earlier (more distally) in the root differentiation
161 zone compared to control-treated samples (Figure 2D–E). Besides the endodermis of the main
162 root, a strong DIR13 signal was also recognizable at the periphery of developing lateral roots,
163 forming a ring-like distribution surrounding the lateral root primordia (LRP) and persisting
164 there up to the lateral root (LR) emergence (Figure 2F–I). Therefore, the DIR13 localization to
165 the root endodermis and peripheral cells of LRs suggests involvement of DIR13 in CS and/or
166 LR formation.

167

168 **DIR13 does not interfere with Casparian strip formation**

169 To explore the function of *DIR13* in root growth and development, we produced the *DIR13*
170 overexpressing (OE) lines *35S:DIR13* #6 and #8 with expression levels about 33 and 85 times
171 higher than WT respectively (Supplemental Figure 3A). Because only knock-down T-DNA
172 insertion mutants (*dir13-1*, *dir13-2*, and *dir13-3*) were available, we used CRISPR-Cas9 genome
173 editing to generate a knock-out *dir13-4* mutant producing truncated *DIR13* transcripts at
174 position 128 of the coding sequence (Supplemental Figure 3B-D). Importantly, the expression
175 level of the closest *DIR13* homologs *DIR6* and *DIR14,* as well as *DIR10 (ESB1),* was not affected
176 in *DIR13* OE and *dir13-4* mutant lines (Supplemental Figure 3 E), *DIR5* and *DIR12* being not
177 expressed in the root.

178 According to previous reports (Roppolo *et al.*, 2011; Hosmani *et al.*, 2013), the examination of
179 lignin autofluorescence indicated a complete loss of well-organized CS structure leading to a
180 patchy and disrupted morphology in mutants deficient in *ESB1* or *CASP1/3* (Supplemental
181 Figure 4). In contrast, no visible changes in the structure of CS were detectable in *DIR13*
182 deficient *dir13-4* or *DIR13* OE lines when compared to Col-0 WT (Supplemental Figure 4A–F).
183 We performed propidium iodide (PI) staining to assay any potential delay in the formation of
184 a CS-mediated apoplastic barrier (Supplemental Figure 4G–N). We confirmed previous
185 findings (Roppolo *et al.*, 2011; Hosmani *et al.*, 2013) demonstrating a delayed CS development
186 in *casp1-1;3-1* and *esb1-1* mutants with an extended penetrability of PI into the central
187 cylinder of about 15 endodermal cells in comparison to Col-0 WT (Supplemental Figure 4L–O).
188 In the *dir13-4* mutant and *DIR13* OE line, no significant delay in CS formation was observed
189 (Supplemental Figure 4G–K, O). Overall, our data suggest that in contrast to ESB1/DIR10,
190 DIR13 is not essential for CS formation and function.

191

192 **DIR13 controls root architecture**

193 In the developing lateral roots, DIR13-mCherry, CASP1-GFP and ESB1-mCherry exhibited
194 distinct localization patterns. While CASP1 was nearly absent in the LRP (Supplemental Figure
195 5A–C), ESB1 localization is restricted to the endodermal cells of newly formed LR, contrasting
196 with the localization of DIR13 to the peripheral cells surrounding the LRP and emerged LR
197 (Supplemental Figure 5D–K).

198 To determine whether DIR13 contributes to root growth and development, we examined root
199 phenotypes of 9-, 11- and 15-day-old *dir13-4* and *DIR13* OE seedlings. In *DIR13* OE lines, the
200 lateral root growth was enhanced as indicated by a higher number of emerged LRs, and an
201 increase in LR density and total LR length (Figure 3A, C–D). In addition, the LR density and total
202 LR length were decreased in the *dir13-4* mutant, although the reduced number of emerged
203 LRs remained not statistically significant when compared to Col-0 WT (Figure 3B, F–H). Besides
204 the positive effects on the LR growth, the overexpression of *DIR13* also increased the length
205 of primary roots and the RAM size (higher number of meristematic cells) compared to WT
206 (Supplemental Figures 5L-Q). However, no changes in primary root growth or RAM size were
207 detected for the *dir13-4* mutant. Altogether, our findings indicate that DIR13 controls root

208 architecture by promoting lateral root formation and growth. And when overexpressed, DIR13
209 has the potential to enhance the main root growth.

210

211 **DIR13 improves salt stress tolerance**

212 Considering the potential role of DIRIGENTs in plant response to environmental constraints
213 (Paniagua *et al.*, 2017; dos Santos *et al.*, 2022; Li *et al.*, 2022), we inspected the possible role
214 of DIR13 in the salt stress response. When placed on control media (0 mM NaCl), the
215 germination rate of the *DIR13* OE or *DIR13*-deficient lines was similar to Col-0 WT
216 (Supplemental Figure 6A, D). In the presence of 150 mM NaCl, the germination rates of *DIR13*
217 OE and *dir13-4* seeds were higher and lower, respectively, than in Col-0 WT (Figure 4A, B), and
218 at 50 and 100 mM NaCl, the *DIR13* OE lines also showed improved germination rate
219 (Supplemental Figure 6B–C, E–F).

220 The effects of salt stress on root growth were examined after transferring 5-day-old seedlings
221 to 150 mM NaCl-supplemented media. The *DIR13* OE lines were more resistant to NaCl-
222 induced inhibition of root growth with a significant increase in primary root elongation,
223 number of emerged LR, LR density, and LR length compared to Col-0 WT (Figure 4C–D;
224 Supplemental Figure 6G, I). Conversely, the *dir13-4* mutant was more sensitive than WT to salt
225 stress for all these root phenotypes (Figure 4E–F; Supplemental Figure 6H–J). Importantly, the
226 observed relative differences in the increased or decreased root growth between the *DIR13*
227 OE or *dir13-4* lines respectively, and Col-0 WT were more pronounced upon salt treatment
228 than in control condition (Figure 4C-F). Therefore, besides promoting root growth, DIR13 also
229 improves tolerance to salt stress.

230 We have also inspected the role of DIR13 in the response to progressive salt stress by watering
231 4-week-old plants grown on soil with increasing NaCl concentrations every week (see
232 Materials and Methods). In the absence of stress (water control), the growth and
233 development of Col-0 WT and *DIR13* OE were indistinguishable (Supplemental Figure 7A-B).
234 After 4 weeks of salt stress, a similar reduction in rosette area was observed for Col-0 WT and
235 *DIR13* OE lines (Supplemental Figure 7B). However, while Col-0 WT plants exhibited a striking
236 yellowish leaf phenotype and defects in the root growth, the *DIR13* OE plants remained green,
237 revealing higher dark-adapted quantum efficiency of photosystem II (*Fv/Fm*) and enhanced

238 root system when compared to WT controls, suggesting improved stress tolerance (Figure 4G–
239 I). Altogether, these findings suggest that *DIR13* promotes salt stress tolerance throughout
240 plant development from seed germination to adult plants.

241

242 **Plant drought tolerance is enhanced when *DIR13* is overexpressed**

243 To further investigate DIR13 function in plant response to abiotic stresses, we performed
244 drought stress experiments on 4-week-old Col-0 WT and *DIR13* OE plants exposed to 3 weeks
245 of water withholding. The plants were then rewatered for recovery. Compared to Col-0 WT,
246 *DIR13* OE plants exhibited higher tolerance to drought stress, as evidenced by a lower
247 percentage of wilted plants (Supplemental Figure 7C) and a greater survival rate after 5 days
248 of recovery (Supplemental Figure 7D, E). *DIR13* OE plants also showed larger shoot area during
249 the drought stress stage compared to Col-0 WT plants which was even more notable during
250 the recovery phase (Supplemental Figure 7F). Additionally, higher *Fv/Fm* was detected in
251 drought-stressed *DIR13* OE compared to Col-0 WT plants, indicating a better PSII efficiency
252 (Supplemental Figure 7G). Collectively, these data suggest that DIR13 positively regulates
253 acclimation to abiotic stresses and may play an important role in plant responses to
254 environmental challenges.

255

256 **DIR13 activates ROS accumulation in roots**

257 Salt stress triggers the accumulation of ROS which act as an important signaling messenger or
258 a toxic by-product of stress responses (Miller *et al.*, 2010). To further clarify the role of DIR13
259 in response to salt treatment (150 mM NaCl for 30 min), in the presence and absence of
260 cytokinin (BAP), we analyzed the level of intracellular ROS in the cortex and epidermis of the
261 root differentiation zone using the ROS fluorescent dye 2',7'-dichlorodihydrofluorescein-
262 diacetate (H_2DCFDA; Figure 5). Interestingly, in control conditions, the basal ROS level in roots
263 was significantly higher (1.3 times) in *DIR13* OE line and lower (0.67 times) in *dir13-4* mutant
264 than in Col-0 WT. Moreover, NaCl-triggered ROS accumulation was more pronounced in *DIR13*
265 OE and reduced in *dir13-4* compared to WT. Pretreatment with BAP did not change the ROS
266 levels in all the lines when compared to the control condition. However, when combined with
267 salt stress, BAP further enhanced the salt-induced ROS production only in the *DIR13* OE line

268 (Figure 5). In summary, DIR13 promotes ROS accumulation under normal and salt stress
269 conditions, and cytokinin enhances salt-mediated ROS production when *DIR13* is
270 overexpressed.

271 The production of apoplastic ROS was also tested by luminol assays in leaves and roots after
272 treatment with flg22, an epitope of the bacterial flagellin eliciting immune responses in plants
273 (Felix *et al.*, 1999). Albeit statistically not significant, flg22-triggered ROS burst was stronger in
274 the leaves and particularly the roots of *DIR13* OE line when compared to Col-0 WT
275 (Supplemental Figure 8A, B). In contrast, disease symptoms and bacteria content were similar
276 between Col-0 WT and *DIR13* OE line 3 days after spray-inoculation with the virulent bacteria
277 *Pseudomonas syringae* pv. tomato DC3000 (Supplemental Figure 8C, D). Based on these
278 observations, it seems that DIR13 plays a preferential role in the response to abiotic stress.
279 However, the positive role of DIR13 in pathogen-elicited ROS production cannot be excluded.

280

281 **DIR13 promotes the production of putative (neo)lignans promoting lateral root formation**

282 It was shown that DIR12, a close homolog of DIR13, is involved in neolignan biosynthesis
283 (Yonekura-Sakakibara *et al.*, 2021). To provide more insights into the possible role of DIR13 in
284 (neo)lignan production, two untargeted metabolome analyses of root extracts from 10-day-
285 old *DIR13* OE lines or *dir13-4* mutant were performed by HPLC-MS/MS together with Col-0 WT
286 as a control. For the experiment with *DIR13* OE lines, 1221 and 1382 compounds were
287 detected in ElectroSpray Ionization in positive (ESI+) and negative (ESI-) modes, respectively
288 (Supplemental Table 1). For the *dir13-4* mutant, 1214 and 872 compounds were identified in
289 ESI+ and ESI- modes (Supplemental Table 2). Pairwise comparisons with Col-0 WT identified
290 143 (ESI+) and 225 (ESI-) differentially accumulated metabolic features (DAMF) at $P \leq 0.05$ in
291 the *DIR13* OE lines, and 36 (ESI+) and 26 (ESI-) DAMF in the *dir13-4* mutant. Principal
292 component analysis and the heatmaps built using correlation distance and average linkage
293 illustrated the differences in metabolite accumulation within tested genotypes (Figure 6A;
294 Supplemental Figures 9A, B and 10A).

295 The majority of identified compounds had no annotation in homemade or public libraries.
296 Metabolites with ≥1.5- or ≤0.5-fold change in accumulation between *DIR13* OE or *dir13-4* and
297 Col-0 WT and with the highest significant differences at $P \leq 0.01$ were selected for annotations

298 (see Materials and Methods). Interestingly, for *DIR13* OE line in ESI+ mode, among 16
299 annotated compounds, 12 of them were putative lignans and neolignans, such as
300 matairesinol-cysteine (5a; compound # is shown in parenthesis in the further text, see also
301 Supplemental Figure 9C and Table 1), oxomatairesinol (6) and lariciresinol 4-O-glucoside (11),
302 two of them were annotated as flavonoids [2-arylbenzofuran (8) and kaempferol-hexoside-
303 rhamnoside (9)], and compound (7) corresponded to a fatty acid. Matairesinol (5b) was
304 considered as an in-source fragment of matairesinol-cysteine (5a) suggesting that matairesinol
305 is mainly oxidized by cysteine addition in Arabidopsis roots. Most of the putative (neo)lignans
306 [compounds (1) to (7) and (12) to (16)] were up-regulated in *DIR13* OE compared to Col-0 WT
307 except the monolignol glucoside syringin (10) and the lignan lariciresinol 4-O-glucoside (11)
308 that were down-regulated (Supplemental Figure 9C). For the *dir13-4* mutant, among nine
309 DAMF selected for identification in ESI+ mode, six compounds (1)-(6) were annotated as
310 putative lignans or neolignans and were also identified in *DIR13* OE (Supplemental Figure 10B
311 and Table 2). Compared to Col-0 WT, these six putative (neo)lignans were over-accumulated
312 in *DIR13* OE but down-regulated in *dir13-4* mutant (Figure 6B and Supplemental Figure 13).
313 The putative fatty acid compound (7) and flavonoid compounds (8) and (9), were also
314 commonly identified in both overexpressing and mutant lines, where compounds (7) and (8)
315 had an opposite abundance between *DIR13* OE and *dir13-4* and compound (9) was down-
316 regulated in both *DIR13* OE and *dir13-4* roots (Supplemental Figures 9C and 10B). Surprisingly,
317 in ESI- mode, putative (neo)lignans were not detected among 31 DAMF selected for
318 annotation in *DIR13* OE lines (Supplemental Table 1), while in *dir13-4* mutant, out of 16
319 metabolites selected for identification in ESI-, four corresponded to (neo)lignans
320 (Supplemental Table 2). In addition, no significant difference in the accumulation of
321 anthocyanins between Col-0 WT and *DIR13* OE lines was observed (Supplemental Figure 9D).

322 To test the possible role of lignans in the control of root architecture, Arabidopsis seedlings
323 were grown in the presence of matairesinol. Interestingly, we observed that when applied at
324 low concentrations (1 and 10 nM), matairesinol promoted both LR density and the main root
325 elongation (Supplemental Figure 12). This result suggests that matairesinol and possibly other
326 (neo)lignans upregulated by DIR13 may have the potential to promote root growth.

327 Collectively, our data suggest that DIR13 promotes (neo)lignans synthesis with consequences
328 on the accumulation of other phenolic compounds in Arabidopsis roots. Furthermore, the

329 DIR13-mediated upregulation of matairesinol and possibly other (neo)lignans seems to have
330 the potential to control root growth.

331

332 **DIR13-mediated accumulation of (neo)lignans in diverse root areas**

333 Imaging mass spectrometry (IMS) has been widely used to analyze the spatial abundance of
334 metabolites in plant tissues (Boughton *et al.*, 2016). We developed a new matrix-assisted laser
335 desorption/ionization (MALDI)-IMS method with a spatial resolution of 50 µm by using
336 carboxymethylcellulose (CMC) to stabilize 11-day-old Arabidopsis roots on the sample target
337 (see Materials and Methods). By employing this approach, we examined the spatial
338 distribution of (neo)lignans along the root in *DIR13* OE and *dir13-4* lines. For the imaging, we
339 selected six putative (neo)lignans in ESI+ mode that were both up-regulated in *DIR13* OE line
340 and down-regulated in *dir13-4* mutant [compounds (1) to (6) (Figure 6 B)] or only up-regulated
341 in *DIR13* OE line [compounds (12 to 16) (Supplemental Figure 9 C)]. Many ions identified as
342 putative (neo)lignans by LC-MS/MS have similar mass-to-charge (*m/z*) ratios that cannot be
343 distinguished by IMS with a mass range of ± 0.1 Da (Figure 6C and Supplemental Figure 11).
344 Nevertheless, in meristematic and mature areas of the main root and in the lateral roots
345 (Figure 6C), we were able to detect signals in positive-ion mode at *m/z* 355.1 related to lignans
346 (3) and (14), *m/z* 343.1 for putative lignans (4) and (13), and *m/z* 480.2 corresponding to
347 matairesinol-cysteine (5a). Compared to Col-0 WT, these putative lignans (at *m/z* 355.1, 343.1
348 and 480.2) were more abundant in *DIR13* OE line, preferentially in the mature portion of the
349 main root while in the *dir13-4* mutant, the signal of these ions was weaker in all root areas.

350 No apparent difference in the distribution of the ion at *m/z* 373.1 corresponding to putative
351 (neo)lignans (1), (2), (6) and syringin (10) was detected between Col-0 WT, *DIR13* OE line and
352 *dir13-4* mutant (Supplemental Figure 11), possibly because syringin was found to be down-
353 regulated in *DIR13* overexpressing lines by LC-MS/MS analysis (Supplemental Figure 9C). The
354 ions at *m/z* 359.1 and 583.2 probably related to putative matairesinol (5b) and the neolignan
355 (15) respectively, were only downregulated in the *dir13-4* mutant root compared to Col-0 WT
356 (Supplemental Figure 11). Even if ionization by $NH4^+$ is unlikely to occur during IMS, the signals
357 of putative lignan (12) at *m/z* 512.2 and neolignan (16) at *m/z* 556.2 from possible ionization
358 by $NH4^+$ or at *m/z* 494.1 (12) and 539.2 (16) from ionization by H^+ indicate that these ions

359 might also be up- and down-regulated in the roots of *DIR13* OE and *dir13-4* lines, respectively
360 (Supplemental Figure 11). Altogether, the IMS results support our LC-MS/MS metabolomic
361 data and strongly suggest that DIR13 promotes the accumulation of (neo)lignans in diverse
362 areas of Arabidopsis root.

363

364 **Discussion**

365 **Does DIR13-mediated lignan production control ROS formation?**

366 Our data from the MS-based metabolomic profiling and imaging approaches demonstrate that
367 DIR13 is involved in the (neo)lignan production that correlates with increased ROS production.
368 The positive impact of DIR13 on the ROS accumulation can be seen under control conditions,
369 but particularly in the salt stress-induced roots. Stress-induced apoplastic ROS production is
370 dominantly mediated via peroxidases (PERs) and NADPH oxidases (NOXs), the latter referred
371 to as respiratory burst oxidase homologs (RBOHs) in plants [(Suzuki *et al.*, 2011; Chapman *et*
372 *al.*, 2019; Smirnoff and Arnaud, 2019; Castro *et al.*, 2021) and references there in].

373 The ability of (neo)lignans to impact ROS homeostasis was demonstrated previously. On one
374 hand, lignans and neolignans, including DIR13-upregulated matairesinol, are known
375 antioxidants and ROS scavengers (Lee *et al.*, 2012; Zálešák *et al.*, 2019). On the other hand,
376 several lignans are able to upregulate ROS production. For instance, (+)-medioresinol
377 mediates its antifungal activities via inducing intracellular ROS accumulation in *Candida*
378 *albicans* (Hwang *et al.*, 2012). Gomisin L1, a lignan isolated from *Schisandra berries*, induces
379 apoptotic cell death by upregulating intracellular ROS production via activating NOX activity
380 (Ko *et al.*, 2021).

381 Another mechanism of DIR13-mediated ROS regulation can be associated with lignan
382 biosynthesis. Synthesis of (neo)lignans leads to the consumption of H_2O_2 or O_2 if the
383 monolignol substrates are oxidized by apoplastic peroxidases (PERs) or laccases (LAC),
384 respectively (Davin *et al.*, 1997). It was suggested that DIR12/DP1, a close homolog of DIR13,
385 works with LAC5 for neo(lignan) synthesis in seeds (Yonekura-Sakakibara *et al.*, 2021). If this
386 is the case also for DIR13, then oxygen will be consumed for oxidizing monolignols leaving
387 H_2O_2 (not used by PERs) accumulating in the apoplast. Moreover, PER enzymes have a dual
388 function depending on the biological context. PERs consume H_2O_2 through the peroxidase

389 cycle for cell wall cross-linking, lignan synthesis or lignification, or produce ROS through the
390 oxidative cycle upon stress perception (Bolwell *et al.*, 2002; Smirnoff and Arnaud, 2019). PERs
391 substrates are phenolic compounds and our metabolomic analysis indicates a decrease in
392 putative syringin, a glycosylated monolignol, in *DIR13* OE lines. It is therefore possible that
393 DIR13-mediated (neo)lignan accumulation induces changes in PER activity and subsequently
394 ROS accumulation. This scenario is further supported by the occurrence of an oxomatairesinol
395 and matairesinol-cysteine, putative oxidized forms of the lignan matairesinol, that we found
396 to be up- and down-regulated in *DIR13 OE* and *dir13-4* mutant respectively. Formation of
397 cysteine adducts of coniferyl alcohol by PER activity was observed *in vitro* in the presence of
398 H_2O_2 (Cong *et al.*, 2013) and cysteine dilignols accumulated in the poplar with attenuated ROS
399 scavenging capacity (Niculaes *et al.*, 2014). However, whether some of the DIR13-synthesized
400 lignans contribute to the regulation of the activity of ROS-producing enzymes, remains to be
401 identified.

402

403 **DIR13 is involved in the control of root growth**

404 ROS were demonstrated as potent regulators of root architecture, controlling both main root
405 growth and lateral root formation (Mase & Tsukagoshi, 2021). For the regulatory role of ROS,
406 its precise localization and chemical nature seems to play an important role. RBOHs catalyze
407 the reduction of oxygen to superoxide ($O_2^{\bullet--}$), which rapidly dismutates to H_2O_2. Besides their
408 role in lignan and lignin formation, a reaction consuming H_2O_2, PER can also produce ROS ($O_2^{\bullet-}$,
409 $OH^{\bullet}$ and H_2O_2) depending on the chemical environment (Smirnoff and Arnaud, 2019). In the
410 main root, a differential distribution of H_2O_2 and superoxide along the root axis was observed
411 (Dunand, Crèvecoeur and Penel, 2007). Superoxide may stimulate cell division in the RAM,
412 while H_2O_2 might promote cell differentiation (Tsukagoshi, Busch and Benfey, 2010). Several
413 PERs are implicated in the control of main root growth via regulating ROS distribution in the
414 RAM (Passardi *et al.*, 2006; Tsukagoshi, Busch and Benfey, 2010). The highly localized ROS
415 production is also necessary for the CS formation in the endodermis, where RBHOF with the
416 possible contribution of RBHOD were shown to be the main ROS-producing enzymes (Lee, *et*
417 *al.*, 2013; Fujita *et al.*, 2020).

418 ROS also regulates LR formation. A number of *PERs* were found to be expressed during LR
419 formation, and both H_2O_2 and superoxide accumulate in the LRP (Manzano *et al.*, 2014).
420 Notably, *per7* and *per57* mutants have a lower number of LRs and reduced main root length.
421 MYB DOMAIN PROTEIN 36 (MYB36)-regulated PRX9/64 might also be important for LR
422 emergence (Fernández-Marcos *et al.*, 2017). H_2O_2 was found to accumulate in the middle
423 lamellae of cortical and endodermal cells overlying newly formed LRPs and several RBOHs
424 were found to be expressed in the developing LRP, particularly at their edges (Orman-Ligeza
425 *et al.*, 2016). It was suggested the role of RBOHs in facilitating the LR emergence via ROS-
426 mediated cell wall remodeling in the overlying tissues (Orman-Ligeza *et al.*, 2016). However,
427 other studies indicate that RBOHD/F inhibit LR development (Ma *et al.*, 2012; Li *et al.*, 2015).
428 The *rbohD/F* mutant exhibits increased LR density that was correlated with an increase in PER
429 activity and superoxide accumulation in the mature root zone (Li *et al.*, 2015).

430 Our results showed that *DIR13*, expressed in the endodermis of the main root and at the
431 margin of LRs, is necessary for main root growth and LR emergence and growth. While we
432 cannot exclude a direct role of (neo)lignans in root growth independently of ROS, it is likely
433 that, DIR13-regulated ROS accumulation (due to its ROS scavenging and/or altered activity of
434 ROS-producing enzymes) regulates both main root and LR growth. The highly specific
435 localization of DIR13 supports this type of regulation. In the main root, DIR13 overlaps with
436 the CS domain in the endodermis and localizes to the outskirts of LRP, i.e., in the tissues where
437 the functional importance of ROS homeostasis in the control over the main root and LR
438 formation, respectively, was demonstrated. This is well in line with tight spatial control over
439 ROS production/homeostasis and its functional importance in plant development and stress
440 response (Castro *et al.*, 2021; Mase and Tsukagoshi, 2021). The absence of DIR13 does not
441 prevent the plant from forming CS or LRs. In the case of CS, this may be attributed to the
442 functional redundancy with other DIRs, as recently demonstrated for DIR9, DIR16, DIR21, and
443 DIR24, shown to be responsible for the majority of lignin formation in the CS (Gao *et al.*, 2023).
444 Nonetheless, rather than being directly involved in the cell wall lignification, DIR13-mediated
445 lignan production seems to provide an additional regulatory mechanism, fine-tuning the ROS-
446 regulated control over the root architecture, facilitating thus the plant's accommodation to
447 physiological and/or developmental status.

448

449 **DIR13-induced ROS production facilitates salt and drought adaptation**

450 Our results clearly show that DIR13 plays an important role in salt and drought stress tolerance
451 for different assays including seed germination, root growth and progressive stress to soil-
452 grown plants. This is in agreement with previous findings based on expression analyses,
453 suggesting the role of dirigent genes in various stress responses (Paniagua *et al.*, 2017; Luo *et*
454 *al.*, 2022). For instance, recent studies have shown that silencing of pepper *CaDIR7* weakened
455 plant defense and increased susceptibility to biotic and salt stresses (Khan *et al.*, 2018).
456 Another example is the overexpression of sugarcane *ScDIR* genes in *Nicotiana benthamiana*
457 leading to enhanced drought tolerance (Li *et al.*, 2022). However, the precise mechanism of
458 DIRs action in stress adaptation remains unknown.

459 Induced ROS production as a signaling molecule and activation of antioxidant machinery to
460 scavenge harmful ROS have an essential role in the response and adaptation to salt, one of
461 the most severe abiotic stresses in plants (Miller *et al.*, 2010; Kesawat *et al.*, 2023). We showed
462 that DIR13 activates a rapid (1 h) overaccumulation of ROS upon salt treatment. An initial
463 increase in apoplastic ROS mediated by NADPH oxidases or PERs is one of the mechanisms by
464 which plants respond to (a)biotic stress (Smirnoff and Arnaud, 2019). PERs participate in plant
465 resistance to pathogens but their precise role in response to abiotic stresses remains unclear.
466 Nevertheless, both RBOHD and RBOHF play a crucial role in salt stress tolerance (Jiang *et al.*,
467 2012; Ma *et al.*, 2012) and RBOHD/F-dependent ROS production is required for salt-induced
468 antioxidant defense and ROS-scavenging enzymatic activities in Arabidopsis (Ben Rejeb *et al.*,
469 2015). Besides being the key mechanism for the local stress response, ROS production also
470 mediates the systemic acquired acclimation, the response induced by abiotic stress and
471 activating resistance or acclimation pathways in tissues that were not yet subjected to the
472 stress [reviewed in (Castro *et al.*, 2021; Kesawat *et al.*, 2023; Mittler & Blumwald, 2015; Wang
473 *et al.*, 2024)].

474 The observation that *DIR13* overexpression improved plant tolerance to long-term salt
475 treatment suggests a better protection against oxidative damage. Considering our data
476 implying the positive role of DIR13 in the ROS production under both control and stress
477 conditions, we hypothesize that DIR13-mediated upregulation of ROS levels is a signal to
478 induce higher salt and drought tolerance, probably via an H_2O_2-priming mechanism (Hossain
479 *et al.*, 2015).

480

481 **Cytokinin-controlled DIR13 provides a possible link between hormonal- and ROS-mediated**
482 **regulations**

483 We showed that both basal expression of *DIR13* and its upregulation by exogenous cytokinins
484 are dependent on the presence of functional RRBs ARR1, ARR10 and ARR12 transcription
485 factors, activating cytokinin signaling (Sakai *et al.*, 2001; Argyros *et al.*, 2008). Like DIR13,
486 cytokinins were found to regulate root growth and stress adaptation. Cytokinins are potent
487 regulators of the root architecture with contrasting effects depending on root developmental
488 areas (Ramireddy, Chang and Schmülling, 2014; Yamoune *et al.*, 2021). On one hand,
489 cytokinins promote root growth by stimulating stem cell activity (Higuchi *et al.*, 2004;
490 Nishimura *et al.*, 2004; Köllmer *et al.*, 2014). On the other one, cytokinins restrict root growth
491 by inducing the differentiation of the dividing cells which results in a reduction of the RAM
492 size (Dello Ioio *et al.*, 2007, 2008; Street *et al.*, 2016; Di Mambro *et al.*, 2019). Cytokinins also
493 inhibit LR initiation and early development (Miyawaki *et al.*, 2006; Kuderová *et al.*, 2008;
494 Laplaze *et al.*, 2008; Chang, Ramireddy and Schmülling, 2013) but seem to promote LR
495 elongation at later stages (Rani Debi, Taketa and Ichii, 2005; Li *et al.*, 2006). The ROS-mediated
496 regulation of root growth was shown to be both auxin- and cytokinin-independent
497 (Tsukagoshi, Busch and Benfey, 2010). However, the cytokinin kinetin induces the
498 accumulation of two lignans (phyllanthin and hypophyllanthin) in *Phyllanthus amarus* shoot
499 cultures (Sparzak-Stefanowska and Krauze-Baranowska, 2022). Therefore, cytokinin-regulated
500 (neo)lignan production through DIR13 might connect the ROS- and hormonal-mediated
501 regulations of root architecture.

502 Cytokinin signaling generally inhibits numerous stress responses including salt and drought
503 stresses with some exceptions showing positive effects on plant tolerance to environmental
504 constraints (Cortleven *et al.*, 2019; Skalak *et al.*, 2021). One mechanism could be the cytokinin-
505 mediated ROS production (Novák *et al.*, 2013; Wang *et al.*, 2015; Arnaud *et al.*, 2017; Nongpiur
506 *et al.*, 2024). Cytokinin-induced ROS production through ARR2-mediated transcriptional
507 regulation of several apoplastic peroxidases (e.g. *PER33/34*) promotes Arabidopsis resistance
508 to *Pseudomonas syringae* bacteria (Arnaud *et al.*, 2017). Moreover, an increase in endogenous
509 cytokinin levels by induction of *ISOPENTENYL TRANSFERTASE* (*IPT*) expression in tobacco
510 (*Nicotiana tabacum*) induces ROS accumulation in leaves (Novák *et al.*, 2013). The

511 overexpression of Arabidopsis *IPT8* leads to higher ROS production only under salt stress
512 condition (Wang *et al.*, 2015). This was correlated with transcriptional upregulation of *RBOH*
513 genes and downregulation of genes for ROS scavenging enzymes including *PERs*. Altogether,
514 this suggests that changes in the cytokinin homeostasis may sensitize or prime the plant to
515 the salt stressor, leading to higher ROS production (Hossain *et al.*, 2015; Cortleven *et al.*, 2019).
516 A similar mechanism, possibly including synergistic effects of DIR13-mediated lignan
517 production and exogenously applied cytokinin can explain the cytokinin-upregulated ROS
518 production specifically in the *DIR13* OE lines. Nonetheless, the detailed molecular mechanisms
519 underlying the cytokinin-dependent lignan-mediated regulation of ROS production and its
520 developmental importance remain to be identified.

521

522 **Model for the DIR13-regulated ROS production and root growth control**

523 Our findings demonstrate the novel role of the DIR13 protein in the regulation of ROS
524 accumulation, root architecture and stress adaptation. We propose that in response to
525 different developmental and/or environmental signals, *DIR13* is activated, at least in part via
526 the cytokinin signaling pathway, inducing (neo)lignan production in roots. This leads to ROS
527 accumulation, helping the plant to fine-tune the root architecture under stress conditions
528 which are nearly permanently present in nature (Figure 7). Noteworthy, DIR13-mediated root
529 growth and the potential benefits of (neo)lignans for plant stress tolerance as well as human
530 health (Adlercreutz, 2007) make DIR13 and possibly other DIRs an attractive breeding target.

531

532 **Materials and Methods**

533 **Plant material and growth conditions**

534 The mutant and reporter lines used in this study are in *Arabidopsis thaliana* Col-0 background.
535 *dir13-1* (N838075), *dir13-2* (N808825 in Col-3 background), *dir13-3* (N565236) were obtained
536 from the Nottingham Arabidopsis Stock Centre and T-DNA insertions were confirmed by PCR
537 genotyping with primers listed in Supplemental Table 3. T-DNA insertion sites for the *dir13*
538 mutants were determined by sequencing. The type-B ARR mutants *arr1-3* (N6971), *arr2-5*
539 (N425801), *arr10-5* (N39989), *arr11-3* (N506544), *arr12-1* (N6978), *arr1-3 arr10-5* (N39990),

540 *arr1-3 arr12-1* (N6981), and *arr10-5 arr12-1* (N39991) were previously described (Mason *et*
541 *al.*, 2005; Argyros *et al.*, 2008; Hill *et al.*, 2013). *CASP1-GFP* and *ESB1-mCherry* lines used for
542 Casparian strip visualization were generated and described by Roppolo *et al.* (2011) and
543 Hosmani *et al.* (2013) respectively. Mutants *casp1-1;3-1* and *esb1-1* were previously described
544 by Baxter *et al.* (2009) and Roppolo *et al*. (2011).

545 Surface sterilized seeds were sown on half-strength Murashige–Skoog (1/2 MS) medium
546 (Duchefa) MES-KOH pH 5.7 (Duchefa), and 1 % (w/v) plant agar (Duchefa)and stratified for 2
547 days at 4°C in the dark. Seedlings were grown under long-day conditions (16 hours light at
548 21°C/8 hours dark at 19°C) with the light intensity at 130 µmol m^{-2} s^{-1}.

549 For cytokinin treatment followed by either confocal microscopy or gene expression analysis,
550 6 or 11-day-old seedlings were transferred in 2 ml of liquid 1/2 MS media (pH 5.7) and
551 incubated for 2 h in the growth chamber for recovery. Then, 6-Benzylaminopurine (BAP,
552 Duchefa) at a final concentration of 5 µM or 0.1 % DMSO as a control were added and
553 seedlings were further incubated in the growth chamber for 1 to 24 hours.

554 For drought and salt stress experiments on adult plants, stratified seeds were cultivated on
555 soil in a growth chamber under short-day conditions (10 hours light at 22 °C / 14 hours dark
556 at 19 °C) with a relative humidity of 40 - 60 % and the light intensity at 130 µmol m^{-2} s^{-1}.

557

558 **Cloning and generation of transgenic plants**

559 To generate *DIR13* promoter fusion line with GFP (*pDIR13:NLS-3xGFP*) and *DIR13*
560 overexpression lines (*35S:DIR13)*, we applied Ligase Independent Cloning (LIC) according to
561 (de Rybel *et al.*, 2011). To produce the *pDIR13:NLS-3xGFP* reporter construct, 3.1 Kb of *DIR13*
562 promoter was PCR-amplified using Phusion DNA Polymerase (Thermo Fisher Scientific) from
563 Col-0 gDNA. The amplified fragment, including LIC adapter sites, was introduced into the
564 pPLV04 LIC-based vector containing 3 repeats of Green Fluorescent Protein (3xGFP) fused to
565 the nuclear localization signal (NLS). For the generation of *35S:DIR13* overexpression lines, the
566 full-length coding sequence (CDS) of *DIR13* was PCR-amplified from Col-0 gDNA, including LIC
567 adapter sites and the fragment was inserted into pPLV26 LIC-based vector with the 35S
568 promoter from cauliflower mosaic virus. The primers with appropriate adapter sites used for
569 the cloning are listed in Supplemental Table 3. To generate the translational fusion of DIR13

570 with mCherry (*pDIR13:DIR13-mCherry*), the region ~3.1 Kb upstream of ATG along with the
571 CDS of *DIR13* prior to the stop codon, was PCR-amplified using Herculase II Fusion DNA
572 polymerase (Agilent Technologies) and primers containing PacI and SnaBI restriction sites
573 (Supplemental Table 3). The PCR products were digested and cloned into the intermediate
574 vector pZEO-mCherryT35S (Samalova *et al.*, 2023), and then sub-cloned through the
575 GATEWAY^{TM} LR reaction in the pFAST-G01 destination vector (Shimada, Shimada and Hara-
576 Nishimura, 2010). The fidelity of the constructs was confirmed by sequencing. Arabidopsis Col-
577 0 plants were transformed using the GV3101 strain of Agrobacterium tumefaciens according
578 to the floral dip protocol (Clough and Bent, 1998). Transgenic lines were isolated on 1/2 MS
579 media supplemented with appropriate antibiotics. Transgenic lines were screened for 3:1
580 segregation of the resistance marker and raised to homozygous T3 lines. 3, 3 and 5
581 independent lines were selected for further experiments for *pDIR13:NLS-3xGFP, 35S:DIR13*
582 and *pDIR13:DIR13-mCherry,* respectively.
583 For the generation of the *dir13-4* knock-out mutant line, we applied CRISPR/Cas9 genome
584 editing technology. The cloning was performed by the ProTech Facility/CRISPR lab at Vienna
585 Biocenter Core Facilities GmbH (Richter *et al.*, 2018). The vector was created using a Golden
586 Gate-based cloning system to simultaneously target two locations with two single-guide RNAs
587 (sgRNAs) in the *DIR13* gene and delete the coding sequence at position 128 from the start
588 codon along with the 3'-UTR, leading to a null mutation of *DIR13* (Supplemental Table 3;
589 Supplemental Figure 3). The final vector was transformed into *A. tumefaciens* GV3101 cells
590 containing the pGreen helper plasmid pSOUP (Hellens *et al.*, 2000). Agrobacterium-mediated
591 transformation of Arabidopsis was performed as described above. T1 transgenic plants were
592 selected with YFP fluorescent seed coat marker and grown in soil. The deletion event was
593 confirmed by PCR amplification of the target sites and sequencing using primers specified in
594 Supplemental Table 3. Potential heterozygous plants were propagated to T2 generation. T2
595 seeds lacking YFP fluorescence were grown in soil and screened by PCR to confirm the absence
596 of Cas9 nuclease gene and the deletion of *DIR13* gene. 10 lines of T3 plants were screened to
597 ensure homozygosity for the *dir13* mutation and 2 selected for further experiments. *DIR13*
598 expression was checked by semi-quantitative PCR and RT-qPCR (Supplemental Table 3).

599

600 **Gene expression analysis**

601 Total RNA was extracted from 11-day-old roots using Trizol reagent (Invitrogen). Genomic
602 DNA (gDNA) contamination was removed by DNase I digestion (DNA-free; Thermo Fisher
603 Scientific) according to the manufacturer's protocol. First-strand cDNA was synthesized from
604 1 µg of total RNA using RevertAid First Strand cDNA Synthesis Kit and oligo $(dT)_{18}$ primers
605 (Thermo Fisher Scientific) and diluted 2 times prior to use. Real-time PCR was performed on
606 the cDNAs using FastStart SYBR Green Master (Roche) with primers listed in Supplemental
607 Table 3. Real-time quantification was made using the Rotor-Gene Q 72-slots system and
608 analyzed with the Rotor-Gene Q Series Software (QIAGEN). The cycling conditions were as
609 follows: an initiation denaturation step at 95 °C for 5 minutes, then 45 cycles of 30 seconds at
610 95 °C, 30 seconds at 60 °C, and 60 seconds at 72 °C. The amplified samples were normalized
611 against the reference genes *Elongation factor 1α* (*EF-1α* At5G60390) and *Ubiquitin 1* (*UBQ1*
612 At3G52590). For semi-quantitative PCR, the first-strand cDNA was diluted 10-fold and used as
613 a template for PCR amplification (using Dream-Taq DNA polymerase (ThermoFisher), 10mM
614 dNTPs and *EF-1α/DIR13* primers). The primers are specified in Supplemental Table 3.

615

616 **Confocal laser scanning microscopy and image analysis**

617 To visualize the cell wall, propidium iodide (PI, Sigma) staining was done as described
618 previously (Alassimone, Naseer and Geldner, 2010). Alternatively, seedlings cleared overnight
619 in ClearSee solution were then stained in 0.1 % Calcofluor White (Sigma) according to (Ursache
620 *et al.*, 2018). For more details see Suppl. Materials and Methods. A Zeiss LSM 880 laser-
621 scanning microscope with a 25X objective (LD LCI Plan-Apochromat, 0.8 Imm Korr DIC M27)
622 was used to observe the fluorescence from GFP, mCherry, PI and Calcofluor White staining
623 with the pinhole set to 1 airy unit. The excitation and emission wavelengths were set as
624 follows: GFP, 488 and 490–550 nm; propidium iodide (PI), 561 and 595–700 nm. mCherry
625 fluorescence was detected at a wavelength range 580-650 nm with 561-nm laser excitation.
626 Calcofluor White staining was excited at 405-nm laser and detected at 425–475 nm to visualize
627 the cell wall. Images were processed with ZEN2 (blue edition) and/or using Image J 1.53m.
628 GFP fluorescence quantification of the *pDIR13:NLS-3xGFP* line was done using IMARIS 9.2

629 software (Bitplane, http://www.bitplane.com/imaris/imaris). The GFP and mCherry signal was
630 confirmed in at least three independent lines.

631

632 **ROS localization and quantification in the root cells**

633 To visualize the accumulation of intracellular ROS in the root differentiation zone, 2′,7′-
634 dichlorofluorescein diacetate (H_2DCFDA, Sigma) was used, following the protocol described by
635 Achard *et al.* (2008) with some modifications. 6- to 7-day-old seedlings were transferred to
636 1/2 MS liquid media and placed back for 2 hours in the growth chamber for recovery. For
637 cytokinin treatment, the seedlings were pre-treated with 5 µM BAP or 0.1 % DMSO (control)
638 in liquid 1/2 MS media for 2 hours. The liquid media was then gently removed from the wells
639 and replaced with a solution of 50 µM H_2DCFDA (dissolved in liquid 1/2 MS media) and 150
640 mM NaCl or water as a control. The samples were incubated in the dark at 4 °C for 30 minutes.
641 Seedlings were then washed with a solution containing 10 mM MES, 0.1 mM KCl, and 0.1 mM
642 $CaCl_2$ (pH 6.0) and incubated in liquid 1/2 MS media at room temperature for 30 minutes
643 before microscopy. H_2DCFDA fluorescence was observed with a Zeiss LSM 880 laser-scanning
644 microscope after excitation at 488 nm and emission was detected at 500–550 nm with the
645 pinhole set to 1 airy unit. Quantification of H_2DCFDA fluorescence of the same regions of
646 interest for each sample was performed using Image J 1.53m and results are shown in arbitrary
647 units.

648

649 **Seed germination assay under salt stress treatment**

650 Surface-sterilized seeds of *DIR13* overexpression and knock-out mutant lines with their
651 respective wild-type controls from matched seed lots were sown on 1/2 MS agar plates
652 supplemented with different concentrations of NaCl (0, 50, 100, or 150 mM) (Lachner). After
653 stratification, the seed germination was monitored every 24 hours for 7 days and scored as
654 the percentage of seeds with an obvious protrusion of the radicle through the seed coat.

655

656 **Root phenotyping**

657 To analyze root architecture, Arabidopsis seedlings were grown vertically on MS/2 plates
658 (under normal or salt-stressed conditions) and scanned after 9, 11 and 15 days of growth using
659 a desktop scanner (Epson Perfection V700). Measurements of primary root length (in cm),
660 average number of emerged lateral roots, lateral root density (in mm^{-1}), and total lateral root
661 length per seedling (in cm) were performed using ImageJ 1.53m. Primary root length was
662 determined by measuring from the root tip to the base of the hypocotyl. The number of
663 emerged lateral roots per seedling was determined by counting the visible lateral roots that
664 penetrated the root epidermis. Lateral root density in the root branching zone was settled as
665 the number of emerged lateral roots divided by the length of the primary root from the shoot
666 base to the most rootward emerged LR. And, the total lateral root length was established by
667 summing the length of all emerged lateral roots per seedling.

668

669 **Root growth assay under NaCl treatment *in vitro***

670 5-day-old plants vertically grown on agar plates were transferred to fresh plates
671 supplemented with 0 and 150 mM NaCl. At the time of transfer, the position of the root cap
672 was marked for each root. After 7 days, the length of the primary root was measured from the
673 marked area to assess the primary root elongation under salt stress. For the measurements,
674 the plates were scanned using a desktop scanner (Epson Perfection V700), and primary root
675 growth, LR length, number, and density were quantified with Image J 1.53m software as
676 described above.

677

678 **Salt stress assays**

679 To evaluate the response of plants to progressive salt stress, 4-week-old plants initially grown
680 on soil under normal conditions were exposed to an additional 4-week treatment with
681 increasing concentrations of NaCl (100, 150, 200, and 300 mM) each week or water as control.
682 The watering regime was adjusted to incorporate the NaCl solutions. Representative pictures
683 were taken at the onset of salt stress symptoms (e.g. yellowing of the leaves). To assess the
684 efficiency of Photosystem II maximum quantum yield (QY) under salt stress, chlorophyll
685 fluorescence measurements were taken on the 23d day of salt stress using the automatic

686 phenotyping platform (PlantScreen™ SC Root System, Photon System Instrument (PSI).
687 Maximum quantum yield (*Fv/Fm*) representing the maximal photochemical efficiency.

688

689 **Extraction of phenolic compounds from root tissue**

690 Phenolic compounds were extracted from 10-day-old Arabidopsis roots using a modified
691 protocol from (Routaboul *et al.*, 2006). The samples were collected and ground in liquid
692 nitrogen using the Qiagen Tissue Lyser for 2 minutes at 18 Hz with metal beads. To extract the
693 phenolic compounds, the samples were homogenized in 1 mL cold acetonitrile/water (75:25,
694 v/v) by vortexing for 1 minute and then sonicated on ice for 20 minutes. An internal standard,
695 1 µg of apigenin (Sigma), was added to the samples. After centrifugation at 16000 *g*, for 10
696 minutes at 4 °C, the pellet was further extracted with 1 ml acetonitrile/ water (75:25; v/v)
697 overnight at 4 °C. The two extracts were pooled together, centrifuged again and the
698 supernatants were used for HPLC-MS/MS analysis.

699

700 **HPLC–MS/MS analysis of phenolic compounds and data processing**

701 The samples containing the phenolic compounds were dried down in a SpeedVac vacuum
702 concentrator (o/n) and resuspended in 200 µl of ULC/MS grade water (Biosolve). Untargeted
703 metabolomic data were acquired using a UHPLC system (Ultimate 3000 Thermo) coupled to a
704 quadrupole time of flight mass spectrometer (Q-Tof Impact II Bruker Daltonics, Bremen,
705 Germany).
706 A Nucleoshell RP 18 plus reversed-phase column (2 x 100 mm, 2.7 µm; Macherey-Nagel) was
707 used for chromatographic separation with mobile phases (A) 0.1 % formic acid in H_2O; and (B)
708 0.1 % formic acid in acetonitrile. The flow rate was 400 µL min^{-1}. Data-dependent acquisition
709 methods were used for mass spectrometer data in positive and negative ESI modes using the
710 following parameters: capillary voltage, 4.5 kV; nebulizer gas flow, 2.1 bar; dry gas flow, 6 L
711 min^{-1} ; drying gas in the heated electrospray source temperature, 140 °C. Samples were
712 analyzed at 8 Hz with a mass range of 100–1500 *m/z*. Stepping acquisition parameters were
713 created to improve the fragmentation profile with a collision RF from 200 to 700 Vpp, a
714 transfer time from 20 to 70 µsec, and collision energy from 20 to 40 eV. Each cycle included a
715 MS full scan and 5 MS/MS Collision Induced Dissociation on the 5 main ions of the previous

716 MS spectrum. HPLC–MS/MS data processing was performed as described in Boutet *et al.*
717 (2022).
718

719 **Metabolite annotation of untargeted metabolomic data**

720 Metabolite annotation was performed as described previously by (Boutet *et al.*, 2022). For
721 differentially accumulated metabolites that had no or unclear annotation, we used SIRIUS 4.0
722 software (https://bio. informatik.uni-jena.de/software/sirius/) which proposes molecular
723 structures using LC–MS/MS data (Djoumbou Feunang *et al.*, 2016; Dührkop *et al.*, 2021). Not
724 annotated differentially accumulated metabolites that belong to molecular network clusters
725 containing annotated metabolites were assigned to the same chemical family and their
726 MS/MS spectra were tentatively annotated manually. Raw data were normalized with the
727 internal standard (Apigenin) and the weight of the material used for the extraction.
728 Metaboanalyst (https://www.metaboanalyst.ca/) and R software (R Core Team,
729 https://www.R-project.org) were used for statistical analysis.
730

731 **Principal component analysis and heatmaps**

732 Principal component analysis (PCA) and heatmaps were created by using ClustVis software
733 (columns were centered, unit variance scaling was applied to columns,
734 (https://biit.cs.ut.ee/clustvis/) (Metsalu and Vilo, 2015) based on the correlation distance and
735 average linkage illustrating the difference between genotypes in the accumulation of
736 significantly different abundant compounds.

737

738 **Imaging mass spectrometry analysis**

739 To stabilize the roots on the stainless steel sample target, 100 µl carboxymethylcellulose
740 (CMC, Sigma) 2 % (w/v) solution dissolved in water was spread and let dry evenly on a pre-
741 heated target at 40 °C using a razor blade. After removal of the shoots, roots were delicately
742 placed on the CMC-coated target and a flow of N_2 gas was gently applied for root adhesion to
743 the CMC-coated target. Universal MALDI matrix containing 2,5-dihydroxybenzoic acid (5
744 mg/mL) and α-cyano-4-hydroxycinnamic acid (5 mg/mL) dissolved in 50 % acetonitrile and 0.1

745 % trifluoroacetic acid was sprayed over the whole root-target with a HTX TM-Sprayer (one
746 pass, 0.1 mL/min at 80°C, 10 psi N_2 gas pressure; HTX Technologies LLC, USA). A mixture of
747 peptide calibration standard (Bruker Daltonics) and universal matrix was added on the target
748 edge and let dry for a few minutes for subsequent mass calibration. MALDI-IMS experiments
749 were carried out with an autoflex maX MALDI-TOF/TOF mass spectrometer equipped with the
750 Smartbeam-II laser (Bruker Daltonics, Bremen, Germany) operated by flexControl (version 3.4,
751 Bruker Daltonics). Positive ion mass spectra were acquired in reflectron mode, in *m/z* 160–
752 1500 range with deflection of the ions below *m/z* 160. Laser settings were as follows: 333 Hz
753 repetition rate, 75% intensity, 'medium' laser size corresponding to ~45 µm diameter laser
754 footprint. Mass spectrometer settings were as follows: ion source 1: 19.00 kV; ion source 2:
755 16.65 kV; lens: 8.35 kV; reflector: 21 kV; reflector 2: 9.40 kV; pulsed ion extraction: 150 nsec.
756 The detector was set to 2190 V, and the digitizer was set to 5 GS sec^{-1}. FlexImaging (version
757 3.0) was employed to visualize the spatial distribution of molecules in the sample. Each pixel
758 in the MS image is related to a signal in a single mass spectrum acquired as a sum of 500 laser
759 shots. The IMS experiments of roots were performed at a spatial resolution of 50 µm. The
760 masses of CMC and CMC plus 1/2 MS media only were tested as negative controls.

761

762 **Statistical analysis**

763 The experiments reported here were repeated at least three times with similar results unless
764 otherwise mentioned. Statistical analyses were performed using GraphPad Prism version
765 9.4.1.681 for Windows, GraphPad Software, San Diego, California USA (www.graphpad.com).
766 Unpaired t-test or one-way ANOVA followed by Tukey's honestly significant difference (HSD)
767 post hoc test were used. For pairwise comparisons and repeated experiments, 2-way ANOVA
768 or mixed model ANOVA with random effects for different experiments were applied, followed
769 by Tukey's or Dunnett's multiple comparisons tests. In the case of non-normal count data (e.g.,
770 number of cells), a Poisson mixed model was applied to identify differences between
771 genotypes using R software (R Core Team, https://www.R-project.org). Significant differences
772 for all statistical analyses were considered at *P* values ≤ 0.05 between compared samples.

773 **Funding**

774 The work was supported by the Ministry of Education, Youth and Sports of CR, TowArds Next
775 GENeration Crops (TANGENC) CZ.02.01.01/00/22_008/0004581 and LUAUS24277. The work
776 of E.Z. was supported by the Russian State Budgetary Project (FWNR-2022- 0020). The IJPB
777 benefits from the support of Saclay Plant Sciences-SPS (ANR-17-EUR-0007).

778

779 **Author contributions**

780 J.H. conceived the research and secured funding, A.M., F.P., C.M.P., S.-C. C., L.-M. H., E.Z., and
781 D.A. performed the research, A.M, F.P., S.-C. C., Y.-L. Y., G.M., D.A. and J.H. analyzed and
782 interpreted the data and A.M., D.A. and J.H. wrote the manuscript with the contribution of
783 other co-authors.

784

785 **Acknowledgments**

786 We are grateful to Niko Geldner for providing the CASP1-GFP, ESB1-mCherry, *esb1-1,* and
787 *casp1-1;3-1* lines. We also thank Plant and Imaging (CELLIM) core facilities for helping with the
788 growth of the plant material under controlled conditions and confocal microscopy. This work
789 has benefited from the support of IJPB's Plant Observatory platform P0-Chem.

790

791 **Declaration of interests**

792 The authors declare no competing interests.

References

Achard, P. *et al.* (2008) 'Plant DELLAs Restrain Growth and Promote Survival of Adversity by Reducing the Levels of Reactive Oxygen Species', *Current Biology*, 18(9), pp. 656–660. Available at: https://doi.org/10.1016/j.cub.2008.04.034.

Adlercreutz, H. (2007) 'Lignans and Human Health', *Critical Reviews in Clinical Laboratory Sciences*, 44(5–6), pp. 483–525. Available at: https://doi.org/10.1080/10408360701612942.

Alassimone, J., Naseer, S. and Geldner, N. (2010) 'A developmental framework for endodermal differentiation and polarity', *Proceedings of the National Academy of Sciences of the United States of America*, 107(11), pp. 5214–5219. Available at: https://doi.org/10.1073/pnas.0910772107.

Argyros, R.D. *et al.* (2008) 'Type B response regulators of Arabidopsis play key roles in cytokinin signaling and plant development', *Plant Cell*, 20(8), pp. 2102–2116. Available at: https://doi.org/10.1105/tpc.108.059584.

Arnaud, D. *et al.* (2017) 'Cytokinin-Mediated Regulation of Reactive Oxygen Species Homeostasis Modulates Stomatal Immunity in Arabidopsis', *The Plant Cell*, 29(3), pp. 543–559. Available at: https://doi.org/10.1105/tpc.16.00583.

Arnaud, D., Deeks, M.J. and Smirnoff, N. (2023) 'Organelle-targeted biosensors reveal distinct oxidative events during pattern-triggered immune responses', *Plant Physiology*, 191(4), pp. 2551–2569. Available at: https://doi.org/10.1093/plphys/kiac603.

Balasubramaniam, T. *et al.* (2023) 'Plants' Response Mechanisms to Salinity Stress', *Plants*, 12(12), p. 2253. Available at: https://doi.org/10.3390/plants12122253.

Baxter, I. *et al.* (2009) 'Root suberin forms an extracellular barrier that affects water relations and mineral nutrition in Arabidopsis', *PLoS Genetics*, 5(5). Available at: https://doi.org/10.1371/journal.pgen.1000492.

Bhargava, A. *et al.* (2013) 'Identification of cytokinin-responsive genes using microarray meta-analysis and RNA-seq in Arabidopsis', *Plant Physiology*, 162(1), pp. 272–294. Available at: https://doi.org/10.1104/pp.113.217026.

Bolwell, G.P. *et al.* (2002) 'The apoplastic oxidative burst in response to biotic stress in plants: a three-component system.', *Journal of experimental botany*, 53(372), pp. 1367–76.

Boughton, B.A. *et al.* (2016) 'Mass spectrometry imaging for plant biology: a review', *Phytochemistry Reviews*. Springer Netherlands, pp. 445–488. Available at: https://doi.org/10.1007/s11101-015-9440-2.

Boutet, S. *et al.* (2022) 'Untargeted metabolomic analyses reveal the diversity and plasticity of the specialized metabolome in seeds of different Camelina sativa genotypes', *Plant Journal*, 110(1), pp. 147–165. Available at: https://doi.org/10.1111/tpj.15662.

Castro, B. *et al.* (2021) 'Stress-induced reactive oxygen species compartmentalization, perception and signalling', *Nature Plants*. Nature Research, pp. 403–412. Available at: https://doi.org/10.1038/s41477-021-00887-0.

Chang, L., Ramireddy, E. and Schmülling, T. (2013) 'Lateral root formation and growth of Arabidopsis is redundantly regulated by cytokinin metabolism and signalling genes', *Journal of Experimental Botany*, 64(16), pp. 5021–5032. Available at: https://doi.org/10.1093/jxb/ert291.

Chapman, J.M. *et al.* (2019) 'RBOH-Dependent ROS Synthesis and ROS Scavenging by Plant Specialized Metabolites To Modulate Plant Development and Stress Responses', *Chemical*

Research in Toxicology, 32(3), pp. 370–396. Available at: https://doi.org/10.1021/acs.chemrestox.9b00028.

Clough, S.J. and Bent, A.F. (1998) 'Floral dip: A simplified method for Agrobacterium-mediated transformation of Arabidopsis thaliana', *Plant Journal*, 16(6), pp. 735–743. Available at: https://doi.org/10.1046/j.1365-313X.1998.00343.x.

Cong, F. *et al.* (2013) 'Covalent bond formation between amino acids and lignin: Cross-coupling between proteins and lignin', *Phytochemistry*, 96, pp. 449–456. Available at: https://doi.org/10.1016/j.phytochem.2013.09.012.

Cortleven, A. *et al.* (2019) 'Cytokinin action in response to abiotic and biotic stresses in plants', *Plant Cell and Environment*. Blackwell Publishing Ltd, pp. 998–1018. Available at: https://doi.org/10.1111/pce.13494.

Davin, L.B. *et al.* (1997) 'Stereoselective Bimolecular Phenoxy Radical Coupling by an Auxiliary (Dirigent) Protein Without an Active Center'. Available at: https://www.science.org.

Davin, L.B. and Lewis, N.G. (2003) 'An historical perspective on lignan biosynthesis: Monolignol, allylphenol and hydroxycinnamic acid coupling and downstream metabolism', *Phytochemistry Reviews*, 2(3), pp. 257–288. Available at: https://doi.org/10.1023/B:PHYT.0000046175.83729.b5.

Djoumbou Feunang, Y. *et al.* (2016) 'ClassyFire: automated chemical classification with a comprehensive, computable taxonomy', *Journal of Cheminformatics*, 8(1), pp. 1–20. Available at: https://doi.org/10.1186/s13321-016-0174-y.

Dührkop, K. *et al.* (2021) 'Systematic classification of unknown metabolites using high-resolution fragmentation mass spectra', *Nature Biotechnology*, 39(4), pp. 462–471. Available at: https://doi.org/10.1038/s41587-020-0740-8.

Dunand, C., Crèvecoeur, M. and Penel, C. (2007) 'Distribution of superoxide and hydrogen peroxide in Arabidopsis root and their influence on root development: Possible interaction with peroxidases', *New Phytologist*, 174(2), pp. 332–341. Available at: https://doi.org/10.1111/j.1469-8137.2007.01995.x.

Eklund, P.C. *et al.* (2005) 'Chemical studies on antioxidant mechanisms and free radical scavenging properties of lignans', *Organic & Biomolecular Chemistry*, 3(18), p. 3336. Available at: https://doi.org/10.1039/b506739a.

Eljebbawi, A. *et al.* (2020) 'iScience Highlighting reactive oxygen species as multitaskers in root development'. Available at: https://doi.org/10.1016/j.isci.

Felix, G. *et al.* (1999) 'Plants have a sensitive perception system for the most conserved domain of bacterial flagellin', *Plant Journal*, 18(3), pp. 265–276. Available at: https://doi.org/10.1046/j.1365-313X.1999.00265.x.

Feng, X. *et al.* (2022) 'Secondary metabolite pathway of SDG (secoisolariciresinol) was observed to trigger ROS scavenging system in response to Ca2+ stress in cotton', *Genomics*, 114(4). Available at: https://doi.org/10.1016/j.ygeno.2022.110398.

Fernández-Marcos, M. *et al.* (2017) 'Control of Arabidopsis lateral root primordium boundaries by MYB36', *New Phytologist*, 213(1), pp. 105–112. Available at: https://doi.org/10.1111/nph.14304.

Fujita, S. *et al.* (2020) 'SCHENGEN receptor module drives localized ROS production and lignification in plant roots', *The EMBO Journal*, 39(9). Available at: https://doi.org/10.15252/embj.2019103894.

Gang, D.R. *et al.* (1999) 'Regiochemical control of monolignol radical coupling: a new paradigm for lignin and lignan biosynthesis'. Available at: http://biomednet.com/elecref/1074552100600143.

Gao, Y.-Q. *et al.* (2023) 'A dirigent protein complex directs lignin polymerization and assembly of the root diffusion barrier', *Science*, 382(6669), pp. 464–471. Available at: https://doi.org/10.1126/science.adi5032.

Gasper, R. *et al.* (2016) 'Dirigent Protein Mode of Action Revealed by the Crystal Structure of AtDIR6', *Plant Physiology*, 172(4), pp. 2165–2175. Available at: https://doi.org/10.1104/pp.16.01281.

Halls, S.C. *et al.* (2004) 'Kinetic Study of Coniferyl Alcohol Radical Binding to the (+)-Pinoresinol Forming Dirigent Protein', *Biochemistry*, 43(9), pp. 2587–2595. Available at: https://doi.org/10.1021/bi035959o.

Hellens, R.P. *et al.* (2000) 'pGreen: a versatile and flexible binary Ti vector for Agrobacterium-mediated plant transformation', *Plant Molecular Biology*, 42(6), pp. 819–832. Available at: https://doi.org/10.1023/A:1006496308160.

Higuchi, M. *et al.* (2004) '*In planta* functions of the *Arabidopsis* cytokinin receptor family', *Proceedings of the National Academy of Sciences*, 101(23), pp. 8821–8826. Available at: https://doi.org/10.1073/pnas.0402887101.

Hill, K. *et al.* (2013) 'Functional characterization of type-B response regulators in the Arabidopsis cytokinin respons', *Plant Physiology*, 162(1), pp. 212–224. Available at: https://doi.org/10.1104/pp.112.208736.

Hosmani, P.S. *et al.* (2013) 'Dirigent domain-containing protein is part of the machinery required for formation of the lignin-based Casparian strip in the root', *Proceedings of the National Academy of Sciences*, 110(35), pp. 14498–14503. Available at: https://doi.org/10.1073/pnas.1308412110.

Hossain, M.A. *et al.* (2015) 'Hydrogen peroxide priming modulates abiotic oxidative stress tolerance: insights from ROS detoxification and scavenging', *Frontiers in Plant Science*, 6. Available at: https://doi.org/10.3389/fpls.2015.00420.

Hwang, J.H. *et al.* (2012) '(+)-Medioresinol leads to intracellular ROS accumulation and mitochondria-mediated apoptotic cell death in Candida albicans', *Biochimie*, 94(8), pp. 1784–1793. Available at: https://doi.org/10.1016/j.biochi.2012.04.010.

Dello Ioio, R. *et al.* (2007) 'Cytokinins Determine Arabidopsis Root-Meristem Size by Controlling Cell Differentiation', *Current Biology*, 17(8), pp. 678–682. Available at: https://doi.org/10.1016/j.cub.2007.02.047.

Dello Ioio, R. *et al.* (2008) 'A Genetic Framework for the Control of Cell Division and Differentiation in the Root Meristem', *Science*, 322(5906), pp. 1380–1384. Available at: https://doi.org/10.1126/science.1164147.

Jiang, C. *et al.* (2012) 'ROS-mediated vascular homeostatic control of root-to-shoot soil Na delivery in *Arabidopsis*', *The EMBO Journal*, 31(22), pp. 4359–4370. Available at: https://doi.org/10.1038/emboj.2012.273.

Jiao, Y. *et al.* (2013) 'AtrbohD and AtrbohF positively regulate abscisic acid-inhibited primary root growth by affecting Ca2+ signalling and auxin response of roots in Arabidopsis', *Journal of Experimental Botany*, 64(14), pp. 4183–4192. Available at: https://doi.org/10.1093/jxb/ert228.

Kesawat, M.S. *et al.* (2023) 'Regulation of Reactive Oxygen Species during Salt Stress in Plants and Their Crosstalk with Other Signaling Molecules—Current Perspectives and Future Directions', *Plants*, 12(4), p. 864. Available at: https://doi.org/10.3390/plants12040864.

Khan, A. *et al.* (2018) 'Genome-wide analysis of dirigent gene family in pepper (Capsicum annuum L.) and characterization of CaDIR7 in biotic and abiotic stresses', *Scientific Reports*, 8(1). Available at: https://doi.org/10.1038/s41598-018-23761-0.

Kieber, J.J. and Schaller, G.E. (2018) 'Cytokinin signaling in plant development', *Development*, 145(4). Available at: https://doi.org/10.1242/dev.149344.

Kim, K.W. *et al.* (2012) 'Opposite stereoselectivities of dirigent proteins in Arabidopsis and Schizandra species', *Journal of Biological Chemistry*, 287(41), pp. 33957–33972. Available at: https://doi.org/10.1074/jbc.M112.387423.

Kim, S.G. *et al.* (2010) 'Overexpression of rice isoflavone reductase-like gene (OsIRL) confers tolerance to reactive oxygen species', *Physiologia Plantarum*, 138(1), pp. 1–9. Available at: https://doi.org/10.1111/j.1399-3054.2009.01290.x.

Ko, Y.H. *et al.* (2021) 'Gomisin L1, a Lignan Isolated from Schisandra Berries, Induces Apoptosis by Regulating NADPH Oxidase in Human Ovarian Cancer Cells', *Life*, 11(8), p. 858. Available at: https://doi.org/10.3390/life11080858.

Köllmer, I. *et al.* (2014) 'Overexpression of the cytosolic cytokinin oxidase/dehydrogenase (CKX7) from Arabidopsis causes specific changes in root growth and xylem differentiation', *The Plant Journal*, 78(3), pp. 359–371. Available at: https://doi.org/10.1111/tpj.12477.

Kuderová, A. *et al.* (2008) 'Effects of Conditional IPT-Dependent Cytokinin Overproduction on Root Architecture of Arabidopsis Seedlings', *Plant and Cell Physiology*, 49(4), pp. 570–582. Available at: https://doi.org/10.1093/pcp/pcn029.

Laplaze, L. *et al.* (2008) 'Cytokinins Act Directly on Lateral Root Founder Cells to Inhibit Root Initiation', *The Plant Cell*, 19(12), pp. 3889–3900. Available at: https://doi.org/10.1105/tpc.107.055863.

Lee, B. *et al.* (2012) 'Matairesinol inhibits angiogenesis via suppression of mitochondrial reactive oxygen species', *Biochemical and Biophysical Research Communications*, 421(1), pp. 76–80. Available at: https://doi.org/10.1016/j.bbrc.2012.03.114.

Lee, Y., Rubio, Maria C., *et al.* (2013) 'A mechanism for localized lignin deposition in the endodermis', *Cell*, 153(2), pp. 402–412. Available at: https://doi.org/10.1016/j.cell.2013.02.045.

Lee, Y., Rubio, Maria C., *et al.* (2013) 'A Mechanism for Localized Lignin Deposition in the Endodermis', *Cell*, 153(2), pp. 402–412. Available at: https://doi.org/10.1016/j.cell.2013.02.045.

Li, N. *et al.* (2015) 'AtrbohD and AtrbohF negatively regulate lateral root development by changing the localized accumulation of superoxide in primary roots of Arabidopsis', *Planta*, 241(3), pp. 591–602. Available at: https://doi.org/10.1007/s00425-014-2204-1.

Li, X. *et al.* (2006) 'Cytokinin-Mediated Cell Cycling Arrest of Pericycle Founder Cells in Lateral Root Initiation of Arabidopsis', *Plant and Cell Physiology*, 47(8), pp. 1112–1123. Available at: https://doi.org/10.1093/pcp/pcj082.

Li, X. *et al.* (2022) 'Overexpression of Sugarcane ScDIR Genes Enhances Drought Tolerance in Nicotiana benthamiana', *International Journal of Molecular Sciences*, 23(10). Available at: https://doi.org/10.3390/ijms23105340.

Luo, R. *et al.* (2022) 'The barley DIR gene family: An expanded gene family that is involved in stress responses', *Frontiers in Genetics*, 13. Available at: https://doi.org/10.3389/fgene.2022.1042772.

Ma, L. *et al.* (2012) 'NADPH oxidase AtrbohD and AtrbohF function in ROS-dependent regulation of Na+/K+ homeostasis in Arabidopsis under salt stress', *Journal of Experimental Botany*, 63(1), pp. 305–317. Available at: https://doi.org/10.1093/jxb/err280.

di Mambro, R. *et al.* (2019) 'The Lateral Root Cap Acts as an Auxin Sink that Controls Meristem Size', *Current Biology*, 29(7), pp. 1199-1205.e4. Available at: https://doi.org/10.1016/j.cub.2019.02.022.

Mangano, S. *et al.* (2017) 'Molecular link between auxin and ROS-mediated polar growth', *Proceedings of the National Academy of Sciences of the United States of America*, 114(20), pp. 5289–5294. Available at: https://doi.org/10.1073/pnas.1701536114.

Manzano, C. *et al.* (2014) 'The emerging role of reactive oxygen species signaling during lateral root development', *Plant Physiology*, 165(3), pp. 1105–1119. Available at: https://doi.org/10.1104/pp.114.238873.

Mase, K. and Tsukagoshi, H. (2021) 'Reactive Oxygen Species Link Gene Regulatory Networks During Arabidopsis Root Development', *Frontiers in Plant Science*. Frontiers Media S.A. Available at: https://doi.org/10.3389/fpls.2021.660274.

Mason, M.G. *et al.* (2005) 'Multiple type-B response regulators mediate cytokinin signal transduction in Arabidopsis', *Plant Cell*, 17(11), pp. 3007–3018. Available at: https://doi.org/10.1105/tpc.105.035451.

Masuda, T. *et al.* (2010) 'Antioxidation reaction mechanism studies of phenolic lignans, identification of antioxidation products of secoisolariciresinol from lipid oxidation', *Food Chemistry*, 123(2), pp. 442–450. Available at: https://doi.org/10.1016/j.foodchem.2010.04.065.

Metsalu, T. and Vilo, J. (2015) 'ClustVis: a web tool for visualizing clustering of multivariate data using Principal Component Analysis and heatmap', *Nucleic Acids Research*, 43(W1), pp. W566–W570. Available at: https://doi.org/10.1093/nar/gkv468.

Mhamdi, A. and Van Breusegem, F. (2018) 'Reactive oxygen species in plant development', *Development (Cambridge)*, 145(15). Available at: https://doi.org/10.1242/dev.164376.

Miller, G. *et al.* (2010) 'Reactive oxygen species homeostasis and signalling during drought and salinity stresses', *Plant, Cell and Environment*, 33(4), pp. 453–467. Available at: https://doi.org/10.1111/j.1365-3040.2009.02041.x.

Mittler, R. (2017) 'ROS Are Good', *Trends in Plant Science*. Elsevier Ltd, pp. 11–19. Available at: https://doi.org/10.1016/j.tplants.2016.08.002.

Mittler, R. and Blumwald, E. (2015) 'The Roles of ROS and ABA in Systemic Acquired Acclimation', *The Plant Cell*, 27(1), pp. 64–70. Available at: https://doi.org/10.1105/tpc.114.133090.

Miyawaki, K. *et al.* (2006) 'Roles of Arabidopsis ATPADP isopentenyltransferases and tRNA isopentenyltransferases in cytokinin biosynthesis'. Available at: www.pnas.orgcgidoi10.1073pnas.0603522103.

Moss, G.P. (2000) 'Nomenclature of Lignans and Neolignans (IUPAC Recommendations 2000)', *Pure and Applied Chemistry*, 72(8), pp. 1493–1523. Available at: https://doi.org/10.1351/pac200072081493.

Niculaes, C. *et al.* (2014) 'Phenylcoumaran benzylic ether reductase prevents accumulation of compounds formed under oxidative conditions in poplar xylem', *Plant Cell*, 26(9), pp. 3775–3791. Available at: https://doi.org/10.1105/tpc.114.125260.

Nishimura, C. *et al.* (2004) 'Histidine kinase homologs that act as cytokinin receptors possess overlapping functions in the regulation of shoot and root growth in arabidopsis', *Plant Cell*, 16(6), pp. 1365–1377. Available at: https://doi.org/10.1105/tpc.021477.

Nishiyama, R. *et al.* (2011) 'Analysis of cytokinin mutants and regulation of cytokinin metabolic genes reveals important regulatory roles of cytokinins in drought, salt and abscisic acid

responses, and abscisic acid biosynthesis', *Plant Cell*, 23(6), pp. 2169–2183. Available at: https://doi.org/10.1105/tpc.111.087395.

Nongpiur, R.C. *et al.* (2024) 'OsRR26, a type-B response regulator, modulates salinity tolerance in rice via phytohormone-mediated ROS accumulation in roots and influencing reproductive development', *Planta*, 259(5), p. 96. Available at: https://doi.org/10.1007/s00425-024-04366-6.

Novák, J. *et al.* (2013) 'High cytokinin levels induce a hypersensitive-like response in tobacco', *Annals of Botany*, 112(1), pp. 41–55. Available at: https://doi.org/10.1093/aob/mct092.

Orman-Ligeza, B. *et al.* (2016) 'RBOH-mediated ROS production facilitates lateral root emergence in Arabidopsis', *Development (Cambridge)*, 143(18), pp. 3328–3339. Available at: https://doi.org/10.1242/dev.136465.

Paniagua, C. *et al.* (2017) 'Dirigent proteins in plants: modulating cell wall metabolism during abiotic and biotic stress exposure', *Journal of Experimental Botany*. Oxford University Press, pp. 3287–3301. Available at: https://doi.org/10.1093/jxb/erx141.

Passardi, F. *et al.* (2006) 'Two cell wall associated peroxidases from Arabidopsis influence root elongation', *Planta*, 223(5), pp. 965–974. Available at: https://doi.org/10.1007/s00425-005-0153-4.

Qadir, M. *et al.* (2014) 'Economics of salt-induced land degradation and restoration', *Natural Resources Forum*, 38(4), pp. 282–295. Available at: https://doi.org/10.1111/1477-8947.12054.

Ralph, S. *et al.* (2006) 'Dirigent proteins in conifer defense: Gene discovery, phylogeny, and differential wound- and insect-induced expression of a family of DIR and DIR-like genes in spruce (Picea spp.)', *Plant Molecular Biology*, 60(1), pp. 21–40. Available at: https://doi.org/10.1007/s11103-005-2226-y.

Ralph, S.G., Jancsik, S. and Bohlmann, J. (2007) 'Dirigent proteins in conifer defense II: Extended gene discovery, phylogeny, and constitutive and stress-induced gene expression in spruce (Picea spp.)', *Phytochemistry*, 68(14), pp. 1975–1991. Available at: https://doi.org/10.1016/j.phytochem.2007.04.042.

Ramireddy, E., Chang, L. and Schmülling, T. (2014) 'Cytokinin as a mediator for regulating root system architecture in response to environmental cues', *Plant Signaling & Behavior*, 9(1), p. e27771. Available at: https://doi.org/10.4161/psb.27771.

Rani Debi, B., Taketa, S. and Ichii, M. (2005) 'Cytokinin inhibits lateral root initiation but stimulates lateral root elongation in rice (Oryza sativa)', *Journal of Plant Physiology*, 162(5), pp. 507–515. Available at: https://doi.org/10.1016/j.jplph.2004.08.007.

Reguera, M. *et al.* (2013) 'Stress-induced cytokinin synthesis increases drought tolerance through the coordinated regulation of carbon and nitrogen assimilation in rice', *Plant Physiology*, 163(4), pp. 1609–1622. Available at: https://doi.org/10.1104/pp.113.227702.

Ben Rejeb, K. *et al.* (2015) 'NADPH oxidase-dependent H2O2 production is required for salt-induced antioxidant defense in Arabidopsis thaliana', *Journal of Plant Physiology*, 174, pp. 5–15. Available at: https://doi.org/10.1016/j.jplph.2014.08.022.

Richter, J. *et al.* (2018) 'Multiplex mutagenesis of four clustered CrRLK1L with CRISPR/Cas9 exposes their growth regulatory roles in response to metal ions', *Scientific Reports*, 8(1). Available at: https://doi.org/10.1038/s41598-018-30711-3.

Roppolo, D. *et al.* (2011) 'A novel protein family mediates Casparian strip formation in the endodermis', *Nature*, 473(7347), pp. 381–384. Available at: https://doi.org/10.1038/nature10070.

Routaboul, J.M. *et al.* (2006) 'Flavonoid diversity and biosynthesis in seed of Arabidopsis thaliana', *Planta*, 224(1), pp. 96–107. Available at: https://doi.org/10.1007/s00425-005-0197-5.

de Rybel, B.D. *et al.* (2011) 'A versatile set of ligation-independent cloning vectors for functional studies in plants', *Plant Physiology*, 156(3), pp. 1292–1299. Available at: https://doi.org/10.1104/pp.111.177337.

Sakai, H. *et al.* (2001) 'ARR1, a Transcription Factor for Genes Immediately Responsive to Cytokinins', *Science*, 294(5546), pp. 1519–1521. Available at: https://doi.org/10.1126/science.1065201.

Samalova, M. *et al.* (2023) 'Hormone-regulated expansins: Expression, localization, and cell wall biomechanics in Arabidopsis root growth', *Plant Physiology* [Preprint]. Available at: https://doi.org/10.1093/plphys/kiad228.

dos Santos, C. *et al.* (2022) 'Overexpression of cotton genes GhDIR4 and GhPRXIIB in Arabidopsis thaliana improves plant resistance to root-knot nematode (Meloidogyne incognita) infection', *3 Biotech*, 12(9). Available at: https://doi.org/10.1007/s13205-022-03282-4.

Shimada, T.L., Shimada, T. and Hara-Nishimura, I. (2010) 'A rapid and non-destructive screenable marker, FAST, for identifying transformed seeds of Arabidopsis thaliana: TECHNICAL ADVANCE', *Plant Journal*, 61(3), pp. 519–528. Available at: https://doi.org/10.1111/j.1365-313X.2009.04060.x.

Skalak, J. *et al.* (2021) 'Signal Integration in Plant Abiotic Stress Responses via Multistep Phosphorelay Signaling', *Frontiers in Plant Science*, 12. Available at: https://doi.org/10.3389/fpls.2021.644823.

Smirnoff, N. and Arnaud, D. (2019) 'Hydrogen peroxide metabolism and functions in plants', *New Phytologist*. Blackwell Publishing Ltd, pp. 1197–1214. Available at: https://doi.org/10.1111/nph.15488.

Sparzak-Stefanowska, B. and Krauze-Baranowska, M. (2022) 'Phyllanthus amarus shoot cultures as a source of biologically active lignans: the influence of selected plant growth

regulators', *Scientific Reports*, 12(1). Available at: https://doi.org/10.1038/s41598-022-15309-0.

Street, I.H. *et al.* (2016) 'Cytokinin acts through the auxin influx carrier AUX1 to regulate cell elongation in the root', *Development* [Preprint]. Available at: https://doi.org/10.1242/dev.132035.

Suzuki, N. *et al.* (2011) 'Respiratory burst oxidases: the engines of ROS signaling', *Current Opinion in Plant Biology*, 14(6), pp. 691–699. Available at: https://doi.org/10.1016/j.pbi.2011.07.014.

Suzuki, S. and Umezawa, T. (2007) 'Biosynthesis of lignans and norlignans', *Journal of Wood Science*, pp. 273–284. Available at: https://doi.org/10.1007/s10086-007-0892-x.

Svolacchia, N. and Sabatini, S. (2023) 'Cytokinins', *Current Biology*, 33(1), pp. R10–R13. Available at: https://doi.org/10.1016/j.cub.2022.11.022.

Takeda, S. *et al.* (2008) 'Local Positive Feedback Regulation Determines Cell Shape in Root Hair Cells', *Science*, 319(5867), pp. 1241–1244. Available at: https://doi.org/10.1126/science.1152505.

Taniguchi, M. *et al.* (2007) 'ARR1 directly activates cytokinin response genes that encode proteins with diverse regulatory functions', *Plant and Cell Physiology*, 48(2), pp. 263–277. Available at: https://doi.org/10.1093/pcp/pcl063.

Tsukagoshi, H. (2016) 'Control of root growth and development by reactive oxygen species', *Current Opinion in Plant Biology*, 29, pp. 57–63. Available at: https://doi.org/10.1016/j.pbi.2015.10.012.

Tsukagoshi, H., Busch, W. and Benfey, P.N. (2010) 'Transcriptional regulation of ROS controls transition from proliferation to differentiation in the root', *Cell*, 143(4), pp. 606–616. Available at: https://doi.org/10.1016/j.cell.2010.10.020.

Umezawa, T. (2003) 'Diversity in lignan biosynthesis', *Phytochemistry Reviews*, 2(3), pp. 371–390. Available at: https://doi.org/10.1023/B:PHYT.0000045487.02836.32.

Ursache, R. *et al.* (2018) 'A protocol for combining fluorescent proteins with histological stains for diverse cell wall components', *Plant Journal*, 93(2), pp. 399–412. Available at: https://doi.org/10.1111/tpj.13784.

Wang, P. *et al.* (2024) 'Reactive oxygen species: Multidimensional regulators of plant adaptation to abiotic stress and development', *Journal of Integrative Plant Biology* [Preprint]. Available at: https://doi.org/10.1111/jipb.13601.

Wang, Y. *et al.* (2015) 'Endogenous cytokinin overproduction modulates ROS homeostasis and decreases salt stress resistance in Arabidopsis thaliana', *Frontiers in Plant Science*, 6(NOVEMBER). Available at: https://doi.org/10.3389/fpls.2015.01004.

Xie, M. *et al.* (2018) 'A B-ARR-mediated cytokinin transcriptional network directs hormone cross-regulation and shoot development', *Nature Communications*, 9(1). Available at: https://doi.org/10.1038/s41467-018-03921-6.

Yamauchi, S. *et al.* (2006) 'Radical and Superoxide Scavenging Activities of Matairesinol and Oxidized Matairesinol', *Bioscience, Biotechnology, and Biochemistry*, 70(8), pp. 1934–1940. Available at: https://doi.org/10.1271/bbb.60096.

Yamoune, A. *et al.* (2021) 'Hormonal orchestration of root apical meristem formation and maintenance in Arabidopsis', *Journal of Experimental Botany*. Oxford University Press, pp. 6768–6788. Available at: https://doi.org/10.1093/jxb/erab360.

Yang, W. *et al.* (2021) 'Molecular mechanism of cytokinin-activated cell division in *Arabidopsis*', *Science*, 371(6536), pp. 1350–1355. Available at: https://doi.org/10.1126/science.abe2305.

Yonekura-Sakakibara, K. *et al.* (2021) 'Seed-coat protective neolignans are produced by the dirigent protein AtDP1 and the laccase AtLAC5 in Arabidopsis', *Plant Cell*, 33(1), pp. 129–152. Available at: https://doi.org/10.1093/plcell/koaa014.

Zálešák, F., Bon, D.J.Y.D. and Pospíšil, J. (2019) 'Lignans and Neolignans: Plant secondary metabolites as a reservoir of biologically active substances', *Pharmacological Research*. Academic Press. Available at: https://doi.org/10.1016/j.phrs.2019.104284.

Zhao, C. *et al.* (2020) 'Mechanisms of Plant Responses and Adaptation to Soil Salinity', *Innovation*. Cell Press. Available at: https://doi.org/10.1016/j.xinn.2020.100017.

Zou, Y., Zhang, Y. and Testerink, C. (2022) 'Root dynamic growth strategies in response to salinity', *Plant, Cell & Environment*, 45(3), pp. 695–704. Available at: https://doi.org/10.1111/pce.14205.

Zubo, Y.O. *et al.* (2017) 'Cytokinin induces genome-wide binding of the type-B response regulator ARR10 to regulate growth and development in *Arabidopsis*', *Proceedings of the National Academy of Sciences*, 114(29). Available at: https://doi.org/10.1073/pnas.1620749114.

Figure legends

Figure 1. Cytokinin-inducible *DIR13* is active in all root tissues including lateral root primordia. (A) Representative images of the root differentiation zone from 7-day-old seedlings expressing *pDIR13:NLS-3xGFP* and radial optical cross-sections of the root cells (1–3). The fluorescent signal was detected in all layers of *Arabidopsis* root. **(B)** 9-day-old seedlings show the activity of *DIR13* promoter in lateral root primordia. In (A and B), the plasma membrane signal from PI staining is shown in magenta and GFP is in green. Scale bars represent 50 µm in

(A) and 20 µm in (B). ep, epidermis; en, endodermis; co, cortex; pe, pericycle; LRP, lateral root primordia. **(C)** The promoter of *DIR13* is activated by cytokinin in the root apical meristem (RAM). Representative images of 5-day-old roots expressing *pDIR13:NLS-3xGFP* after 24h of 5 µM BAP and control (0.1% DMSO) treatments. The plasma membrane signal from PI staining is shown in magenta and GFP is in green. Scale bars represent 50 µm. **(D)** Left panel - number of fluorescent nuclei per root at the RAM of 5-day-old seedlings expressing *pDIR13:NLS-3xGFP* after 4h and 24h of 5 µM BAP and control (0.1% DMSO) treatments. Data are presented as the mean +/- SE (n ≥ 10). Asterisks indicate statistically significant differences between BAP and control treatments based on Poisson mixed model analysis and Tukey test (**$P < 0.01$, ***$P < 0.001$). Right panel - the fluorescence intensity of individual nuclei after 4h and 24h of 5 µM BAP and control (0.1% DMSO) treatments was quantified in RAM. Results are the means +/- SE (n ≥ 10). Asterisks indicate statistically significant differences between BAP and control treatments based on two-way ANOVA followed by Tukey's HSD test (**$P < 0.01$, ***$P < 0.001$). **(E)** *DIR13* expression is inducible by cytokinin. *DIR13* expression was analyzed by RT-qPCR in roots of 11-day-old seedlings after 5 µM BAP and control (0.1% DMSO) treatments for 0, 0.5, 1, 3, and 5 hours. **(F)** *DIR13* expression is regulated by type-B ARR transcription factors. The expression level of *DIR13* was examined by RT-qPCR in *arr1,10, arr1,12* and *arr10,12* double mutants after 5 µM BAP and control (0.1% DMSO) treatments for 1h. In (C-D), transcript levels were normalized to the reference *EF-1α* gene, and the relative *DIR13/EF-1α* expression ratio is shown. Data are the means of a representative experiment. Error bars indicate +/- SE (n = 3). Asterisks indicate statistically significant differences between BAP and control treatments (C) or between genotypes (D) based on two-way ANOVA followed by Tukey's HSD test (*$P < 0.05$, **$P < 0.01$, ***$P < 0.001$).

Figure 2. DIR13 localizes in the root endodermis and peripheral cells of lateral root primordia. (A-C) DIR13-mCherry localizes in the endodermal cells of the root differentiation zone. Representative confocal images of roots from 7-day-old seedlings expressing *pDIR13:DIR13-mCherry.* Median section (A), Z-stack overview (B), and radial optical cross-section (C) of the root. **(D, E)** Cytokinin treatment enhances DIR13-mCherry expression in roots. Representative Z-stack confocal images of 7-day-old seedlings after 24h of 5 µM BAP and control (0.1% DMSO) treatments. BAP shifts DIR13 localization closer to the root apical

meristem, indicated by arrowheads. **(F-I)** DIR13-mCherry protein is detected in the peripheral cells of lateral root (LR) primordia (F) and emerged lateral root (G-I). Representative confocal images of different stages of LR development in 9-day-old seedlings. In (A-I), cleared roots were stained with Calcofluor White, the cell wall is shown in blue and mCherry is in red. Scale bars represent 50 µm in (A–C) and (F–I), and 100 µm in (D, E). en, endodermis; LRP, lateral root primordia; ELR, emerged lateral root.

Figure 3. DIR13 promotes lateral root growth. (A) The phenotype of 11-day-old Col-0 WT, *DIR13* overexpressing lines (*35S:DIR13* #6 and #8) and **(B)** *dir13-4* knock-out mutant seedlings growing under normal conditions. Scale bars represent 1 cm. **(C, D, F**, and **G**) Average number of emerged lateral roots (C and F) and LR density expressed as the number of lateral roots per mm of primary root length (D and G) in 11-day-old Col-0 WT, *35S:DIR13* #6 and #8 (C and D) and *dir13-4* mutant (F and G) seedlings. In (B, C, F, and G), data show the median and upper and lower quartiles of a representative experiment (n ≥ 30). Asterisks indicate statistically significant differences between genotypes at $*P < 0.05$, $**P < 0.01$ and $***P < 0.001$ based on Poisson mixed model analysis (C and F), one-way ANOVA followed by Tukey's HSD test (D), and unpaired t-test (G). (**E** and **H**) Total lateral root length per seedling (in cm) in 11-day-old Col-0 WT, *DIR13* overexpressing (E) and *dir13-4* mutant (H) seedlings. In (E and H), data are the means of a representative experiment. Error bars indicate +/- SE (n ≥ 30). Asterisks indicate statistically significant differences between genotypes at $*P < 0.05$, $**P < 0.01$ and $***P < 0.001$ based on one-way ANOVA followed by Tukey's HSD test (D) and unpaired t-test (H).

Figure 4. *DIR13* improves plant tolerance to salt stress. (A, B) Seed germination rates of Col-0 WT, *35S:DIR13* #6 and #8 overexpressing lines (A) and *dir13-4* mutant (B) under salt stress treatment. The germination rate was recorded for 7 days after stratification in the presence of 150 mM NaCl (for 0, 50 and 100 mM NaCl treatments see Suppl. Fig. 6). Data are the averages of three individual experiments. Error bars indicate +/- SE, (n ≥ 100). Asterisks indicate statistically significant differences between Col-0 WT and *DIR13* OE in (A) and between Col-0 WT and *dir13-4* in (B) based on repeated measures two-way ANOVA followed by Dunnett's HSD test ($*P < 0.05$, $**P < 0.01$). **(C-F)** DIR13 promotes lateral root growth in the

presence of salt. The average number of emerged lateral roots (C, E) and total lateral root length in cm per seedling (D, F) were measured 9 days after the transfer of Col-0 WT, *35S:DIR13* #6, #8 (C-D) and *dir13-4* (E-F) seedlings to 150 mM NaCl. Data show the means of a representative experiment +/- SE (n ≥ 38). Asterisks indicate statistically significant differences between genotypes at *$P < 0.05$, **$P < 0.01$ and ***$P < 0.001$ based on Poisson mixed model analysis (C and E), and two-way ANOVA followed by Tukey's HSD test (D and F). Numbers in rectangles show the relative difference compared to Col-0 in percentage. **(G, H)** Phenotypes of 8-week-old Col-0 WT and *35S:DIR13* #8 plants growing in short-day conditions after 4 weeks of progressive salt stress by application of increasing NaCl concentrations (100, 150, 200, and 300 mM) each week. Scale bar represents 1 cm. **(I)** Quantification of Photosystem II maximum quantum yield efficiency (*Fv*/*Fm*) of Col-0 WT and *35S:DIR13* #8 plants after 23 days of progressive salt stress. Data are the averages of a representative experiment. Error bars indicate +/- SE, (n ≥ 7). Asterisks indicate statistically significant differences between Col-0 WT and *35S:DIR13* #8 based on two-way ANOVA followed by Tukey's HSD test (*$P < 0.05$).

Figure 5. Salt stress-induced ROS accumulation in root cells is promoted by *DIR13*. (A) Representative confocal images and **(B)** quantification of ROS production measured with the fluorescent dye H_2DCFDA in the root differentiation zone of 7-day-old Col-0 WT, *35S:DIR13* #8 and *dir13-4* seedlings pretreated for 2 hours with 5 µM BAP or 0.1% DMSO as control and exposed to 150 mM NaCl or control solution (0 mM NaCl) for 30 min. In (A), H_2DCFDA fluorescence is shown in green and scale bars represent 20 µm. In (B), data show the median and upper and lower quartiles of three independent experiments (n ≥ 20). Different letters indicate statistically significant differences at $P < 0.05$ between genotypes and treatments based on repeated measures two-way ANOVA followed by Tukey's HSD test.

Figure 6. DIR13 mediates (neo)lignan formation in planta. (A) Principal Component Analysis (PCA) of HPLC-MS/MS data in ElectroSpray Ionization in positive (ESI+) mode from root biological replicates of 10-day-old Col-0 WT and *35S:DIR13* #8 (left panel) and Col-0 WT and *dir13-4* (right panel). PCA demonstrates the difference genotypes in the accumulation of significantly different abundant compounds. **(B)** *DIR13* overexpression leads to the

accumulation of putative lignans and neolignans in roots. Selected differentially abundant compounds annotated as putative (neo)-lignans were extracted from Col-0 WT, *35S:DIR13* #8 and *dir13-4* roots and detected by HPLC-MS/MS in ESI+ mode. Data are shown as relative to Col-0 WT and are the means +/- SE (n ≥ 5). Asterisks indicate statistically significant differences between Col-0 WT and *35S:DIR13* #8, and Col-0 WT and *dir13-4* based on two-way ANOVA followed by Tukey's HSD test. (*$P < 0.05$, **$P < 0.01$, ***$P < 0.001$). **(C)** Spatial distribution of putative lignans in the roots of *DIR13* overexpressing and *dir13-4* mutant lines. Imaging Mass Spectrometry (IMS) of roots from 10-day-old Col-0 WT, *35S:DIR13* #8 overexpressing and *dir13-4* mutant lines. Signals at *m/z* 355.1 (3) (14), *m/z* 343.1 (4) (13), *m/z* 480.2 (5) correspond to putative matairesinol (5), and metabolites annotated as lignans (3), (4), (13) and (14). The spatial resolution is 50 µm. MS signal intensity is indicated by color bars and the scale bar represents 5 mm. The experiment was repeated at least twice with similar results.

Figure 7. Proposed mechanism of DIR13 action in the abiotic stress response. In a response to different developmental and/or environmental signals, *DIR13* is activated, at least partially via the cytokinin-regulated multistep phosphorelay (MSP) signaling. (A)biotic stresses may activate the MSP either via controlling the abundance of endogenous cytokinins and/or by affecting some of the numerous stress-related MSP inputs e.g. ABA signaling (Skalak et al., 2021) affecting directly the type-B response regulators. DIR13-mediated (neo)lignans accumulation upregulates NOX/PER-mediated ROS production. ROS act as effector molecules modulating the stress adaptive response by inducing systemic acquired acclimation and root architecture. The ROS production induced by abiotic stress seems to be sensitized by cytokinins via unknown mechanism.

Figures

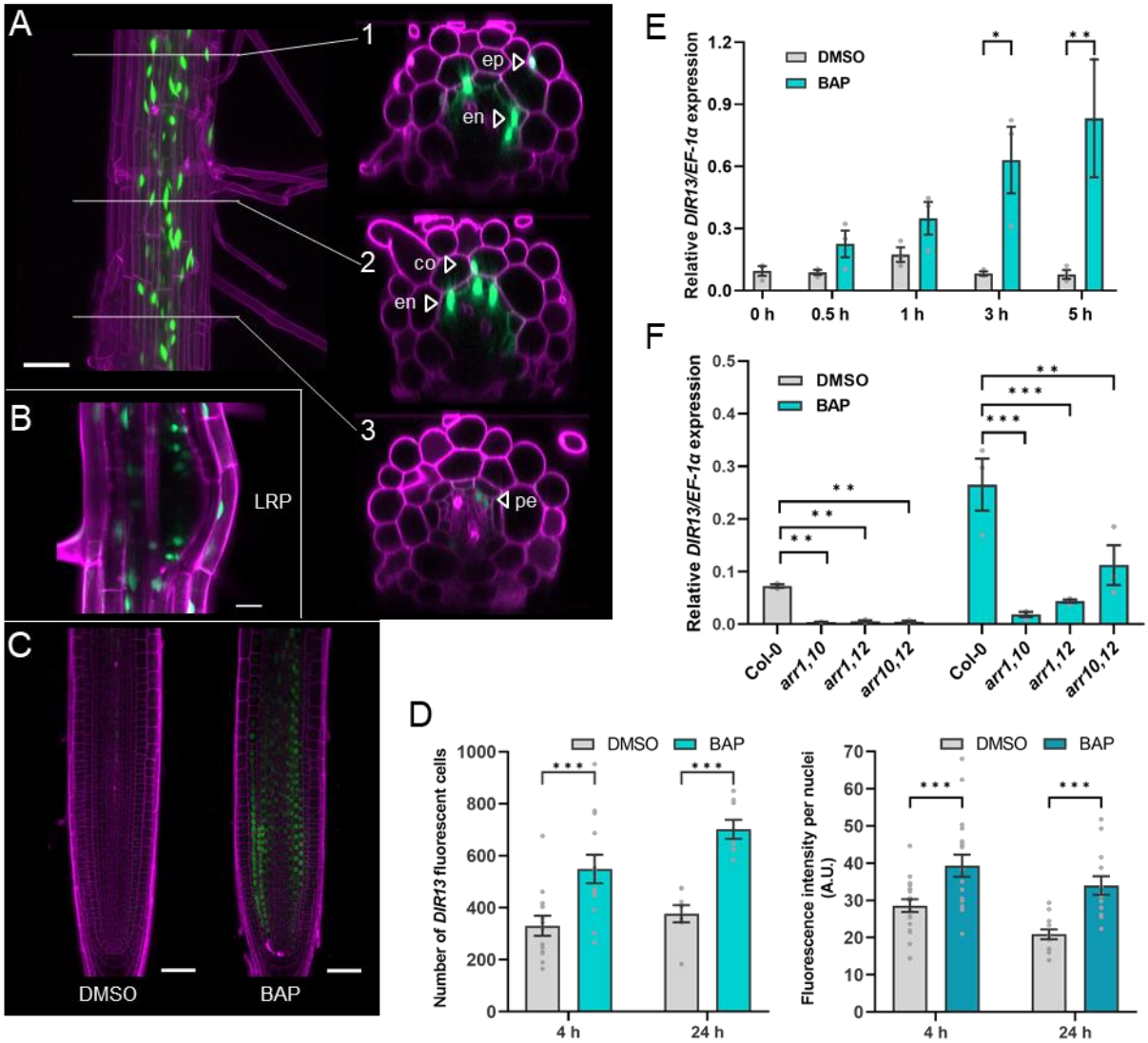

Figure 1. Cytokinin-inducible *DIR13* is active in all root tissues including lateral root primordia. (A) Representative images of the root differentiation zone from 7-day-old seedlings expressing *pDIR13:NLS-3xGFP* and radial optical cross-sections of the root cells (1–3). The fluorescent signal was detected in all layers of *Arabidopsis* root. **(B)** 9-day-old seedlings show the activity of *DIR13* promoter in lateral root primordia. In (A and B), the plasma membrane signal from PI staining is shown in magenta and GFP is in green. Scale bars represent 50 µm in (A) and 20 µm in (B). ep, epidermis; en, endodermis; co, cortex; pe, pericycle; LRP, lateral root primordia. **(C)** The promoter of *DIR13* is activated by cytokinin in the root apical meristem (RAM). Representative images of 5-day-old roots expressing *pDIR13:NLS-3xGFP* after 24h of 5 µM BAP and control (0.1% DMSO) treatments. The plasma membrane signal from PI staining

is shown in magenta and GFP is in green. Scale bars represent 50 µm. **(D)** Left panel - number of fluorescent nuclei per root at the RAM of 5-day-old seedlings expressing *pDIR13:NLS-3xGFP* after 4h and 24h of 5 µM BAP and control (0.1% DMSO) treatments. Data are presented as the mean +/- SE (n ≥ 10). Asterisks indicate statistically significant differences between BAP and control treatments based on Poisson mixed model analysis and Tukey test (**$P < 0.01$, ***$P < 0.001$). Right panel - the fluorescence intensity of individual nuclei after 4h and 24h of 5 µM BAP and control (0.1% DMSO) treatments was quantified in RAM. Results are the means +/- SE (n ≥ 10). Asterisks indicate statistically significant differences between BAP and control treatments based on two-way ANOVA followed by Tukey's HSD test (**$P < 0.01$, ***$P < 0.001$). **(E)** *DIR13* expression is inducible by cytokinin. *DIR13* expression was analyzed by RT-qPCR in roots of 11-day-old seedlings after 5 µM BAP and control (0.1% DMSO) treatments for 0, 0.5, 1, 3, and 5 hours. **(F)** *DIR13* expression is regulated by type-B ARR transcription factors. The expression level of *DIR13* was examined by RT-qPCR in *arr1,10, arr1,12* and *arr10,12* double mutants after 5 µM BAP and control (0.1% DMSO) treatments for 1h. In (C-D), transcript levels were normalized to the reference *EF-1α* gene, and the relative *DIR13/EF-1α* expression ratio is shown. Data are the means of a representative experiment. Error bars indicate +/- SE (n = 3). Asterisks indicate statistically significant differences between BAP and control treatments (C) or between genotypes (D) based on two-way ANOVA followed by Tukey's HSD test (*$P < 0.05$, **$P < 0.01$, ***$P < 0.001$).

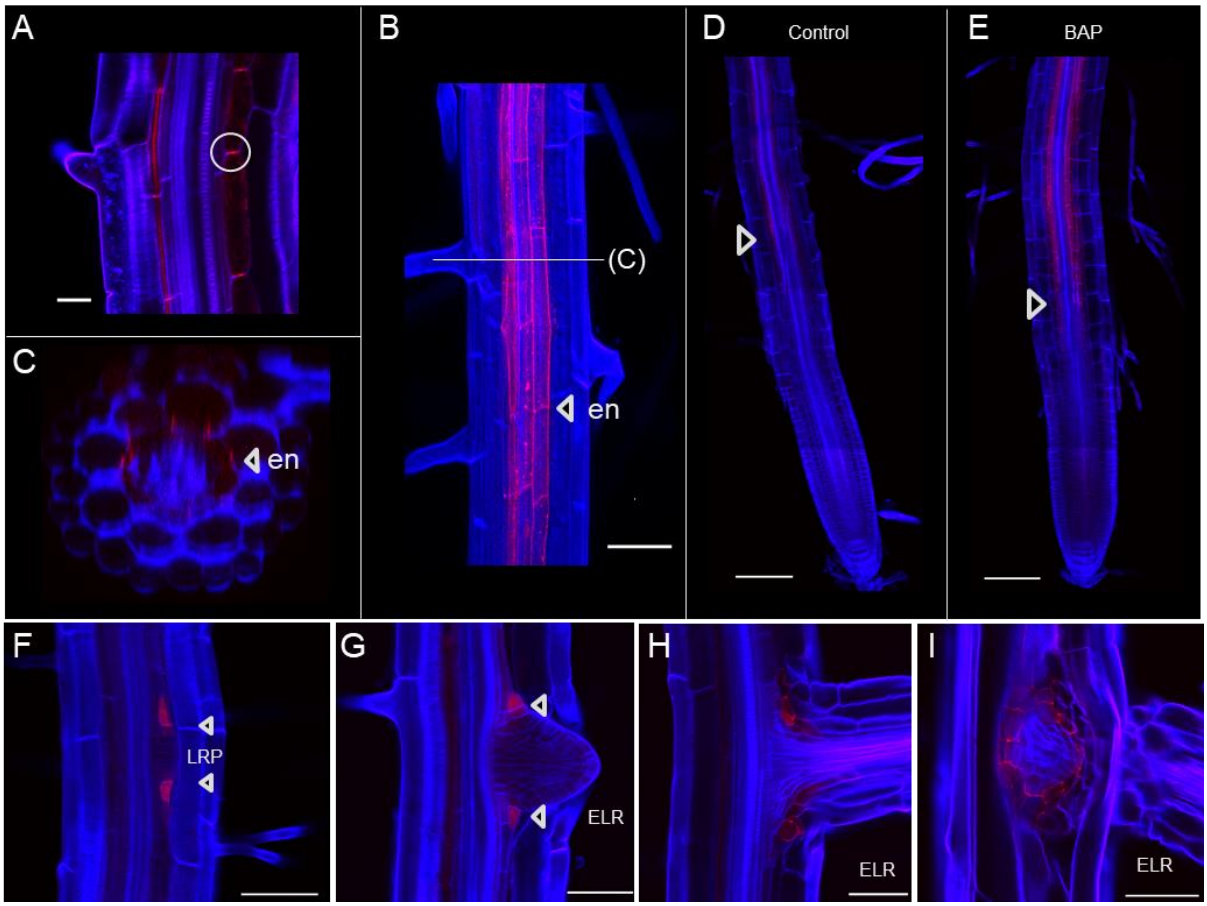

Figure 2. DIR13 localizes in the root endodermis and peripheral cells of lateral root primordia. (A-C) DIR13-mCherry localizes in the endodermal cells of the root differentiation zone. Representative confocal images of roots from 7-day-old seedlings expressing *pDIR13:DIR13-mCherry.* Median section (A), Z-stack overview (B), and radial optical cross-section (C) of the root. **(D, E)** Cytokinin treatment enhances DIR13-mCherry expression in roots. Representative Z-stack confocal images of 7-day-old seedlings after 24h of 5 µM BAP and control (0.1% DMSO) treatments. BAP shifts DIR13 localization closer to the root apical meristem, indicated by arrowheads. **(F-I)** DIR13-mCherry protein is detected in the peripheral cells of lateral root (LR) primordia (F) and emerged lateral root (G-I). Representative confocal images of different stages of LR development in 9-day-old seedlings. In (A-I), cleared roots were stained with Calcofluor White, the cell wall is shown in blue and mCherry is in red. Scale bars represent 50 µm in (A–C) and (F–I), and 100 µm in (D, E). en, endodermis; LRP, lateral root primordia; ELR, emerged lateral root.

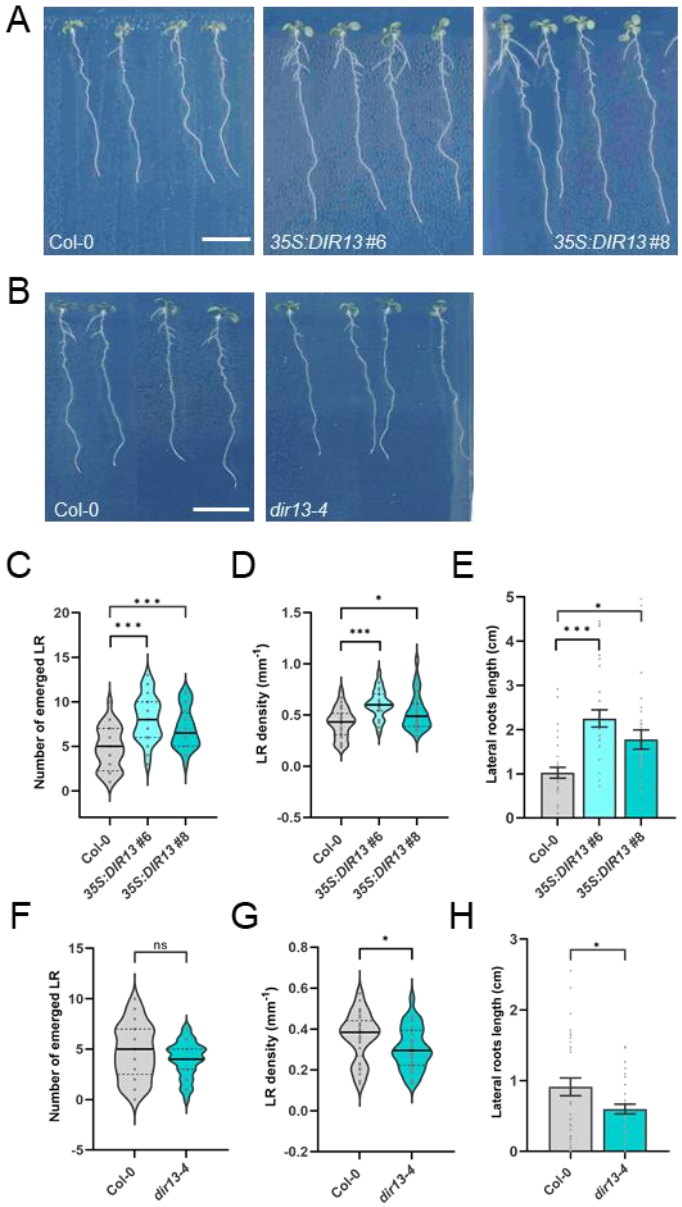

Figure 3. DIR13 promotes lateral root growth. (A) The phenotype of 11-day-old Col-0 WT, *DIR13* overexpressing lines (*35S:DIR13* #6 and #8) and **(B)** *dir13-4* knock-out mutant seedlings growing under normal conditions. Scale bars represent 1 cm. **(C, D, F**, and **G**) Average number of emerged lateral roots (C and F) and LR density expressed as the number of lateral roots per mm of primary root length (D and G) in 11-day-old Col-0 WT, *35S:DIR13* #6 and #8 (C and D) and *dir13-4* mutant (F and G) seedlings. In (B, C, F, and G), data show the median and upper and lower quartiles of a representative experiment (n ≥ 30). Asterisks indicate statistically significant differences between genotypes at **P* < 0.05, ***P* < 0.01 and ****P* < 0.001 based on Poisson mixed model analysis (C and F), one-way ANOVA followed by Tukey's HSD test (D), and unpaired t-test (G). (**E** and **H**) Total lateral root length per seedling (in cm) in 11-day-old

Col-0 WT, *DIR13* overexpressing (E) and *dir13-4* mutant (H) seedlings. In (E and H), data are the means of a representative experiment. Error bars indicate +/- SE (n ≥ 30). Asterisks indicate statistically significant differences between genotypes at $*P < 0.05$, $**P < 0.01$ and $***P < 0.001$ based on one-way ANOVA followed by Tukey's HSD test (D) and unpaired t-test (H).

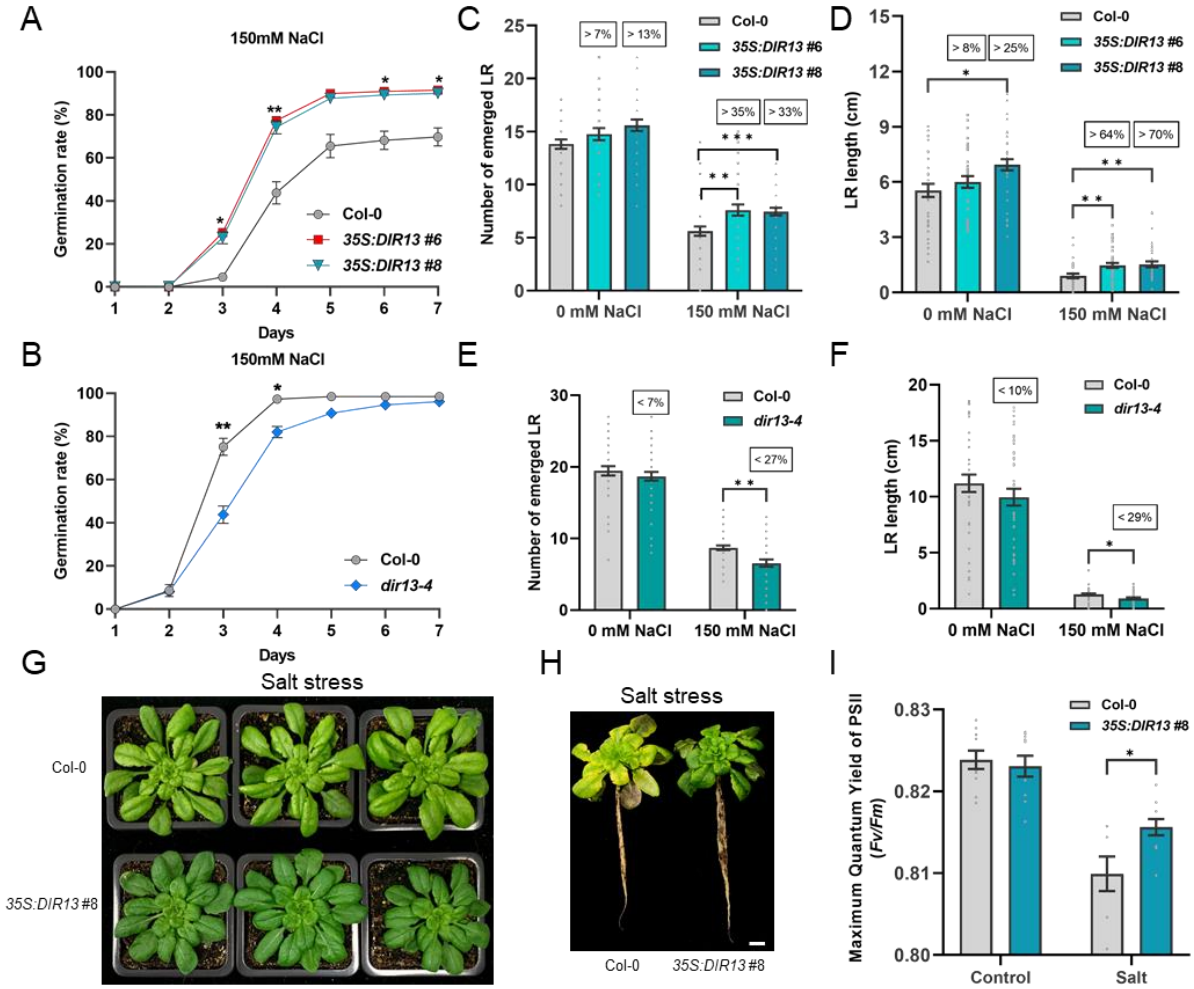

Figure 4. *DIR13* improves plant tolerance to salt stress. (A, B) Seed germination rates of Col-0 WT, *35S:DIR13* #6 and #8 overexpressing lines (A) and *dir13-4* mutant (B) under salt stress treatment. The germination rate was recorded for 7 days after stratification in the presence of 150 mM NaCl (for 0, 50 and 100 mM NaCl treatments see Suppl. Fig. 6). Data are the averages of three individual experiments. Error bars indicate +/- SE, (n ≥ 100). Asterisks indicate statistically significant differences between Col-0 WT and *DIR13* OE in (A) and between Col-0 WT and *dir13-4* in (B) based on repeated measures two-way ANOVA followed by Dunnett's HSD test (**P* < 0.05, ***P* < 0.01). **(C-F)** DIR13 promotes lateral root growth in the presence of salt. The average number of emerged lateral roots (C, E) and total lateral root length in cm per seedling (D, F) were measured 9 days after the transfer of Col-0 WT, *35S:DIR13* #6, #8 (C-D) and *dir13-4* (E-F) seedlings to 150 mM NaCl. Data show the means of a representative experiment +/- SE (n ≥ 38). Asterisks indicate statistically significant differences between genotypes at **P* < 0.05, ***P* < 0.01 and ****P* < 0.001 based on Poisson mixed model

analysis (C and E), and two-way ANOVA followed by Tukey's HSD test (D and F). Numbers in rectangles show the relative difference compared to Col-0 in percentage. **(G, H)** Phenotypes of 8-week-old Col-0 WT and *35S:DIR13* #8 plants growing in short-day conditions after 4 weeks of progressive salt stress by application of increasing NaCl concentrations (100, 150, 200, and 300 mM) each week. Scale bar represents 1 cm. **(I)** Quantification of Photosystem II maximum quantum yield efficiency (*Fv*/*Fm*) of Col-0 WT and *35S:DIR13* #8 plants after 23 days of progressive salt stress. Data are the averages of a representative experiment. Error bars indicate +/- SE, ($n \geq 7$). Asterisks indicate statistically significant differences between Col-0 WT and *35S:DIR13* #8 based on two-way ANOVA followed by Tukey's HSD test (*$P < 0.05$).

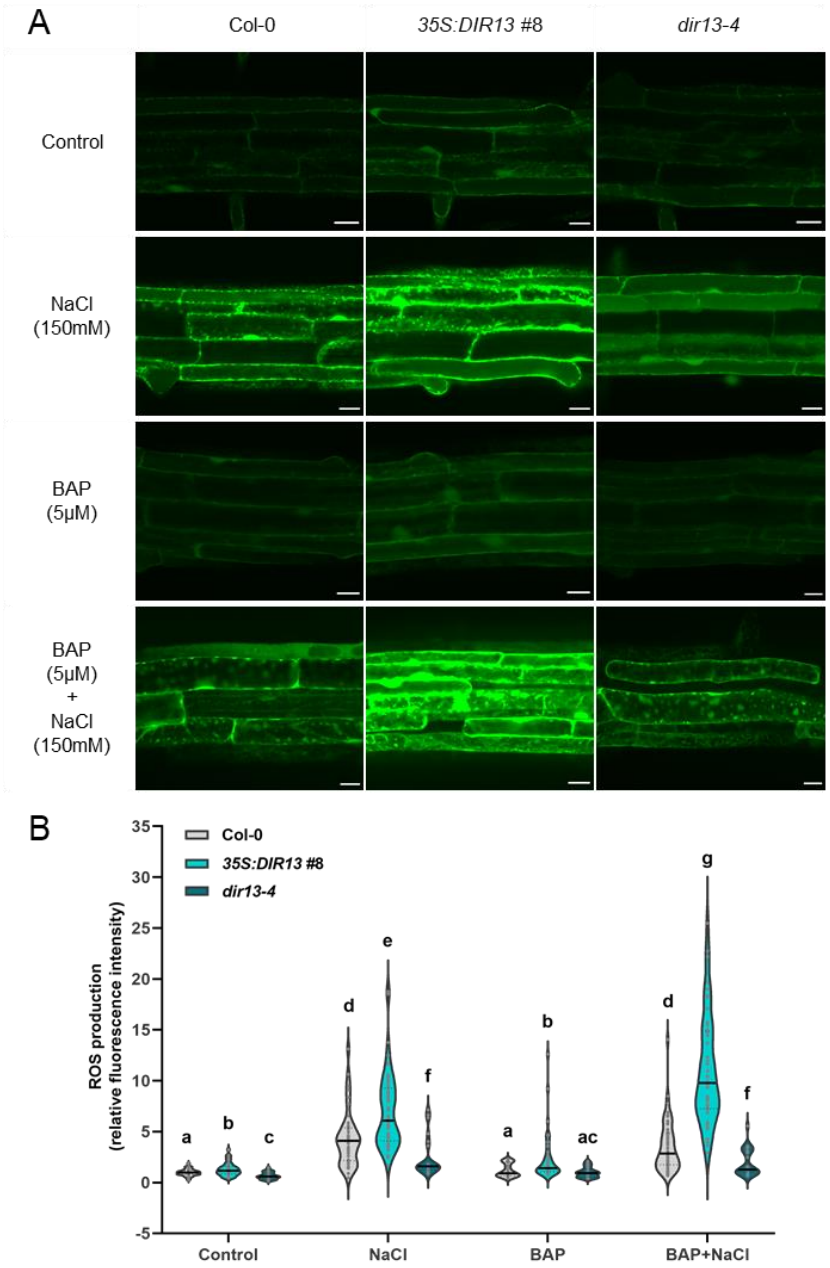

Figure 5. Salt stress-induced ROS accumulation in root cells is promoted by *DIR13*. (A) Representative confocal images and **(B)** quantification of ROS production measured with the fluorescent dye H_2DCFDA in the root differentiation zone of 7-day-old Col-0 WT, *35S:DIR13* #8 and *dir13-4* seedlings pretreated for 2 hours with 5 µM BAP or 0.1% DMSO as control and exposed to 150 mM NaCl or control solution (0 mM NaCl) for 30 min. In (A), H_2DCFDA fluorescence is shown in green and scale bars represent 20 µm. In (B), data show the median and upper and lower quartiles of three independent experiments (n ≥ 20). Different letters indicate statistically significant differences at $P < 0.05$ between genotypes and treatments based on repeated measures two-way ANOVA followed by Tukey's HSD test.

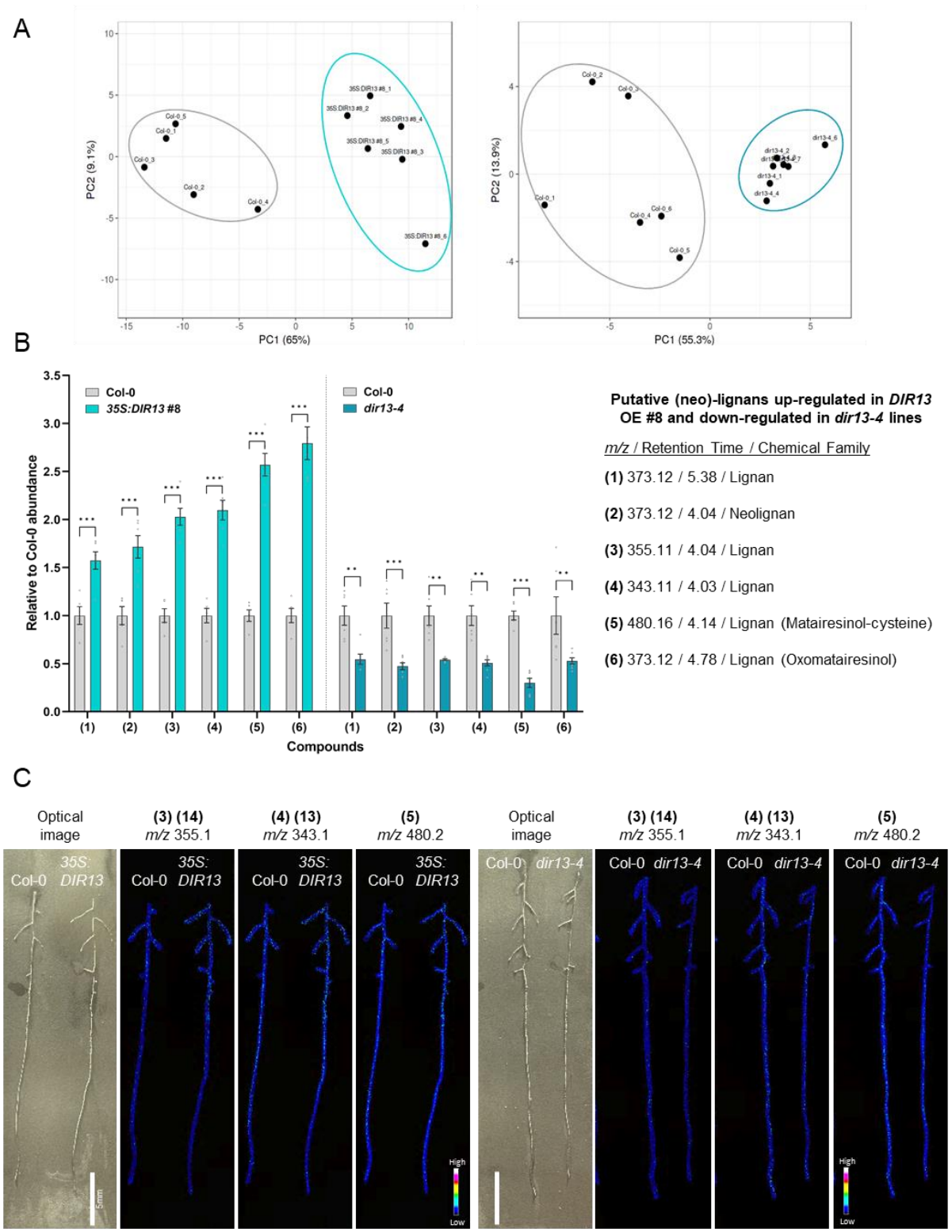

Figure 6. DIR13 mediates (neo)lignan formation in planta. (A) Principal Component Analysis (PCA) of HPLC-MS/MS data in ElectroSpray Ionization in positive (ESI+) mode from root biological replicates of 10-day-old Col-0 WT and *35S:DIR13* #8 (left panel) and Col-0 WT and *dir13-4* (right panel). PCA demonstrates the difference genotypes in the accumulation of significantly different abundant compounds. **(B)** *DIR13* overexpression leads to the

accumulation of putative lignans and neolignans in roots. Selected differentially abundant compounds annotated as putative (neo)-lignans were extracted from Col-0 WT, *35S:DIR13* #8 and *dir13-4* roots and detected by HPLC-MS/MS in ESI+ mode. Data are shown as relative to Col-0 WT and are the means +/- SE (n ≥ 5). Asterisks indicate statistically significant differences between Col-0 WT and *35S:DIR13* #8, and Col-0 WT and *dir13-4* based on two-way ANOVA followed by Tukey's HSD test. (*$P < 0.05$, **$P < 0.01$, ***$P < 0.001$). **(C)** Spatial distribution of putative lignans in the roots of *DIR13* overexpressing and *dir13-4* mutant lines. Imaging Mass Spectrometry (IMS) of roots from 10-day-old Col-0 WT, *35S:DIR13* #8 overexpressing and *dir13-4* mutant lines. Signals at *m/z* 355.1 (3) (14), *m/z* 343.1 (4) (13), *m/z* 480.2 (5) correspond to putative matairesinol (5), and metabolites annotated as lignans (3), (4), (13) and (14). The spatial resolution is 50 µm. MS signal intensity is indicated by color bars and the scale bar represents 5 mm. The experiment was repeated at least twice with similar results.

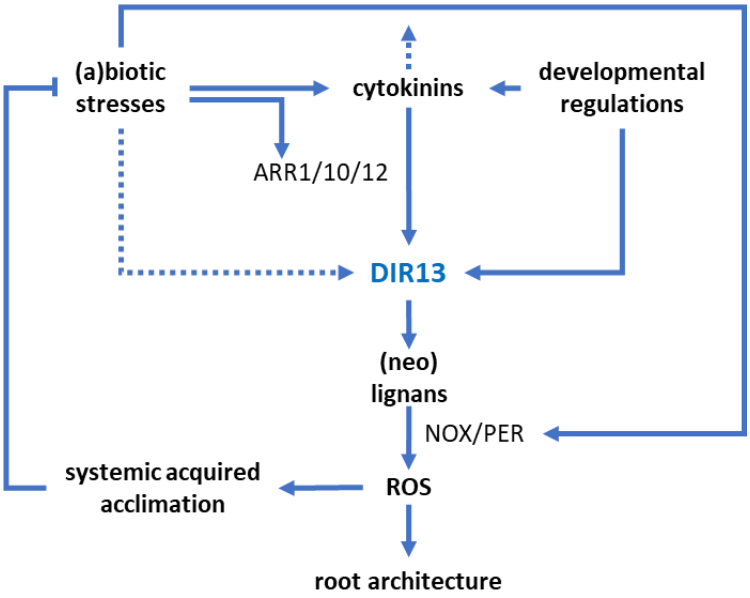

Figure 7. Proposed mechanism of DIR13 action in the abiotic stress response. In a response to different developmental and/or environmental signals, *DIR13* is activated, at least partially via the cytokinin-regulated multistep phosphorelay (MSP) signaling. (A)biotic stresses may activate the MSP either via controlling the abundance of endogenous cytokinins and/or by affecting some of the numerous stress-related MSP inputs e.g. ABA signaling (Skalak et al., 2021) affecting directly the type-B response regulators. DIR13-mediated (neo)lignans accumulation upregulates NOX/PER-mediated ROS production. ROS act as effector molecules modulating the stress adaptive response by inducing systemic acquired acclimation and root architecture. The ROS production induced by abiotic stress seems to be sensitized by cytokinins via unknown mechanism.

Supplemental Information

Supplemental Figures

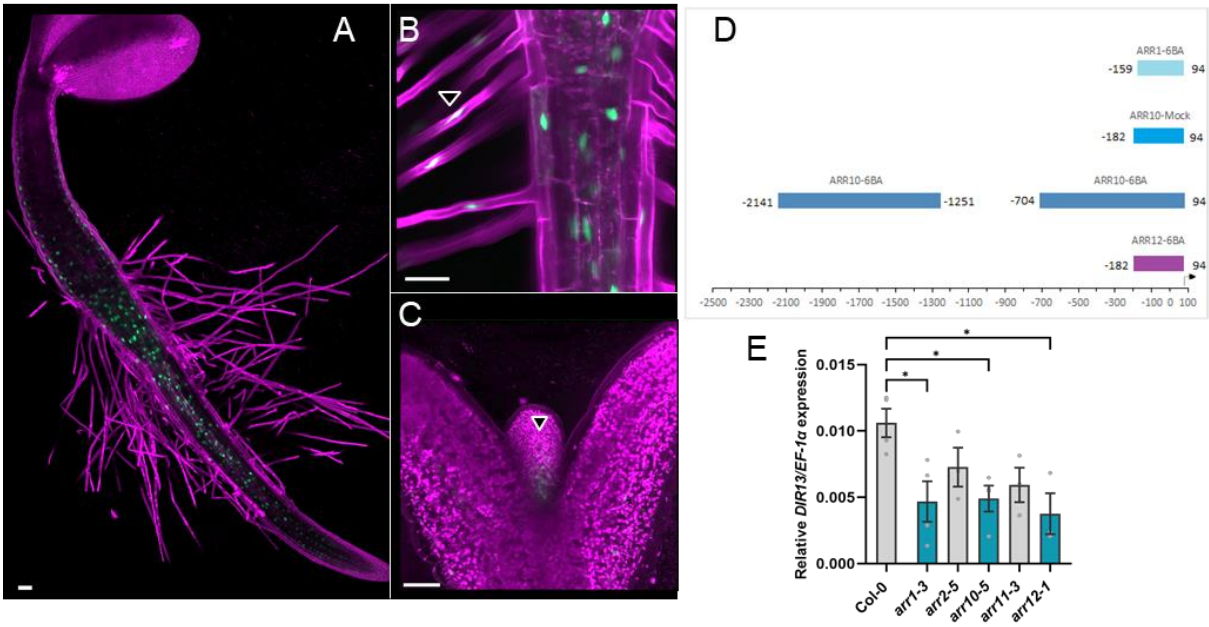

Supplemental Figure 1. *DIR13* promoter is active in all root tissues at early developmental stage and is the target of type-B ARR1, ARR10 and ARR12 transcription factors. (A - C) Activity of *DIR13* promoter in 3-day-old seedling expressing *pDIR13:NLS-3xGFP*. The fluorescent signal was detected mostly in the root (A), also in root hairs (B) and in the shoot apical meristem (C) as indicated by arrowheads. The plasma membrane signal from PI staining is shown in magenta and GFP is in green. Scale bars represent 50 µm. **(D)** *DIR13* promoter analysis identifies ChIP-Seq-derived binding events (from Xie et al., 2018) for type-B ARR transcription factors (TFs) involved in cytokinin signaling pathway, in particular ARR1, ARR10 and ARR12. The coordinates represent positions relative to the transcription start site (value = 0) whereas translation start site is indicated by an arrow. **(E)** *DIR13* expression is regulated by type-B ARR1, ARR10 and ARR12 TFs. The expression level of *DIR13* was examined by RT-qPCR in *arr1-3, arr2-5, arr10-5, arr11-3* and *arr12-1* single mutants. Transcript levels were normalized to the reference *EF-1α* gene and the relative *DIR13/EF-1α* expression ratio is shown. Data are the means of a representative experiment. Error bars indicate +/- SE (n = 4). Asterisks indicate statistically significant differences at $P < 0.05$ between Col-0 WT and mutant genotypes based on one-way ANOVA followed by Dunnett's HSD test.

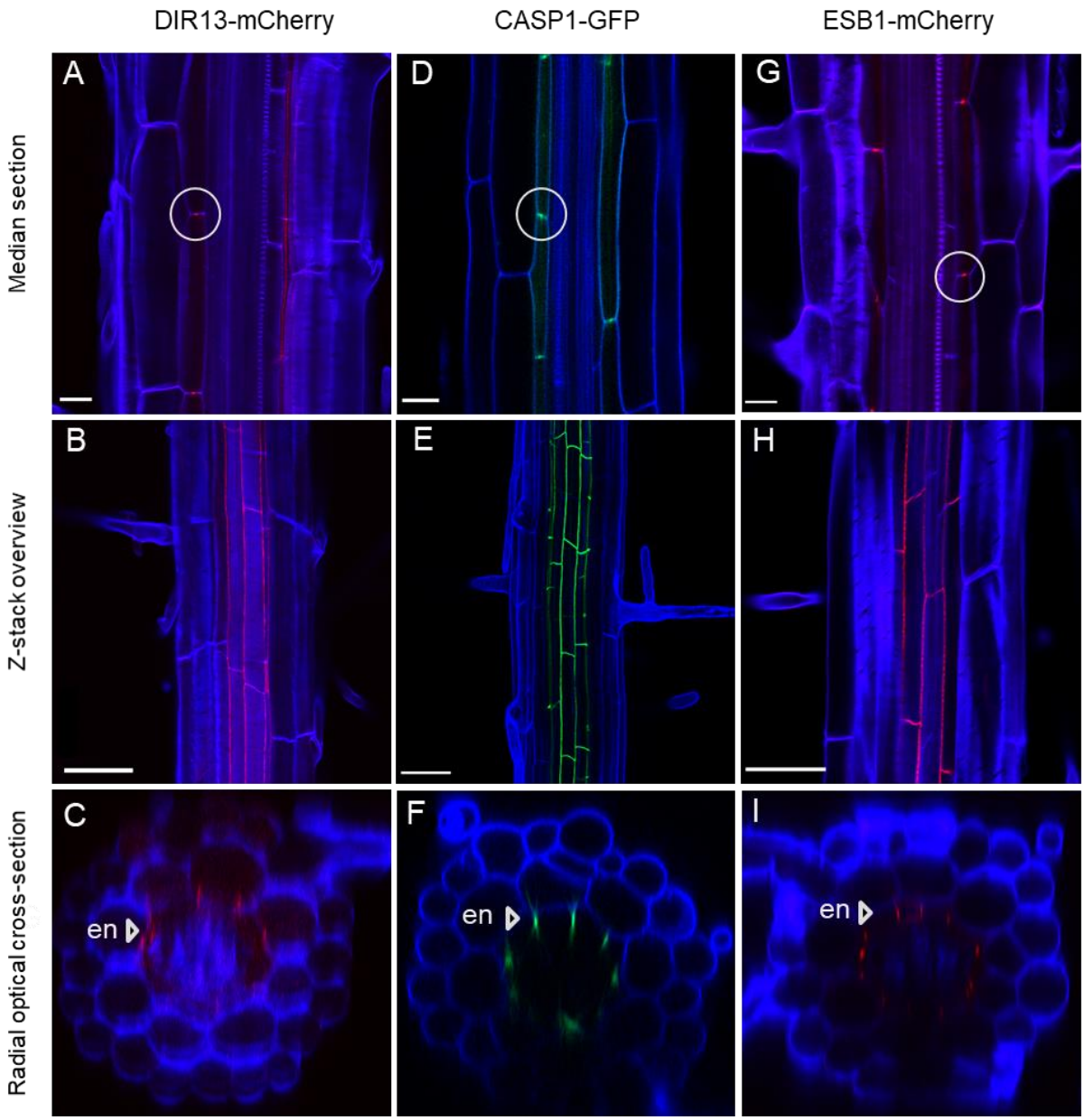

Supplemental Figure 2. Comparison of the localization patterns of DIR13-mCherry, CASP1-GFP and ESB1-mCherry. Representative images of root differentiation zone from 7-day-old seedlings expressing *DIR13-mCherry* **(A – C),** *CASP1-GFP* **(D – F)** and *ESB1-mCherry* **(G – I)** under their native promoters. The tested reporters show similar pattern of protein localization in median sections as indicated by white circles (A, D, G), in Z-stack overview (B, E, H) and in radial optical cross-sections as indicated by arrowheads (C, F, I) respectively. Cleared roots were stained with Calcofluor White, the cell wall is shown in blue, GFP is in green, and mCherry is in red. Scale bars represent 50 µm. en, endodermis.

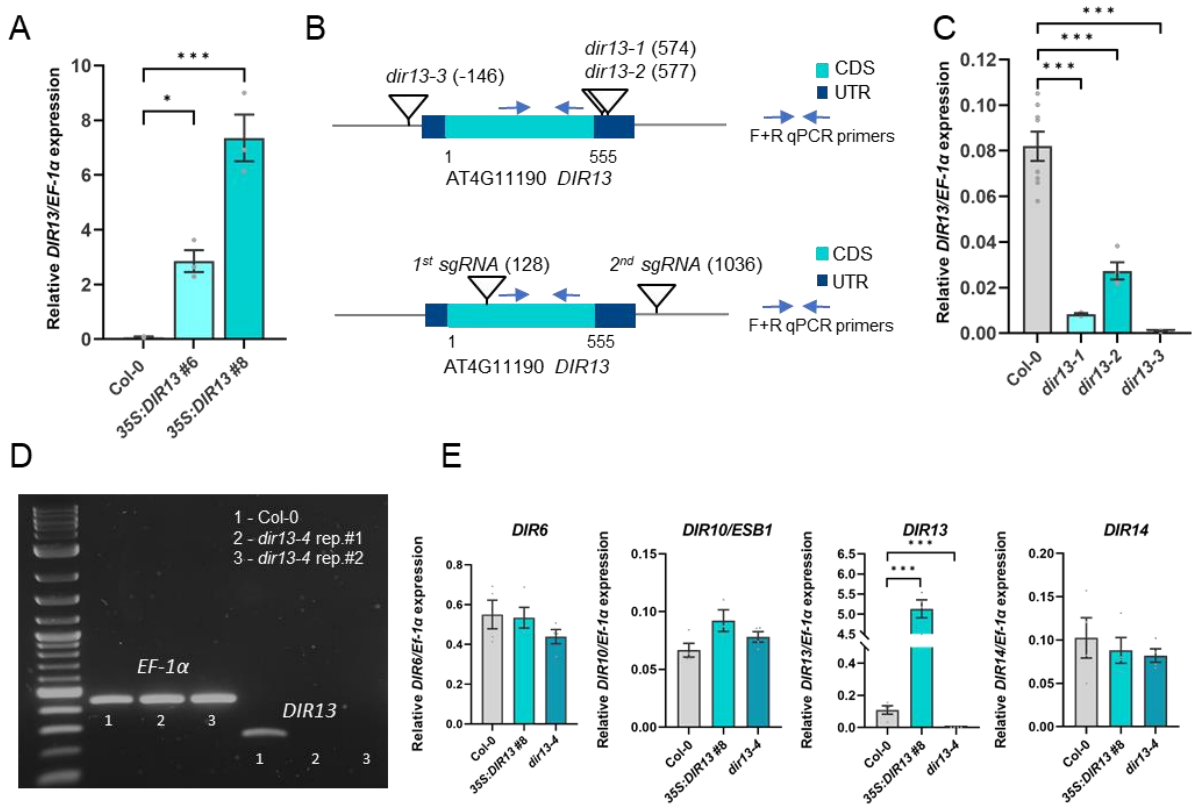

Supplemental Figure 3. Characterization of *DIR13* overexpressing and mutant lines. (A) *DIR13* expression level in *DIR13* overexpressing lines. *DIR13* expression was analyzed by RT-qPCR in the roots of 11-day-old *35S:DIR13* #6 and #8 seedlings. **(B)** Schemes representing the structure of *DIR13* gene, the position of T-DNA insertions in *dir13-1*, *dir13-2* and *dir13-3* mutants (top panel), and sgRNAs used for CRISPR-Cas9 (low panel). Coding sequence (CDS) and untranslated regions (UTR) are depicted in cyan and dark blue respectively. Blue arrows indicate the positions of the primers used for RT-qPCR and semi-quantitative RT-PCR amplification of *DIR13*. **(C)** *DIR13* expression was detected by RT-qPCR in the roots of 11-day-old *dir13-1*, *dir13-2* and *dir13-3* T-DNA insertion mutants. **(D)** Semi-quantitative RT-PCR gel electrophoresis shows the absence of *DIR13* transcripts in *dir13-4* mutant line. *EF-1α* was used as a control. **(E)** The expression levels of *DIR13* closest homologs are not affected by *DIR13* overexpression or *dir13-4* knock-out mutation. Expression levels of *DIR6, DIR10 (ESB1), DIR13 and DIR14* were verified by RT-qPCR in the roots of 11-day-old Col-0 WT, *35S:DIR13* #8 and *dir13-4* seedlings. In (A, C and E), transcript levels were normalized to the reference *EF-1α* gene and the relative *DIR* target gene to *EF-1α* expression ratios are shown. Data are the means of a representative experiment. Error bars indicate +/- SE (n ≥ 3). Asterisks indicate statistically significant

differences between genotypes based on one-way ANOVA followed by Tukey's HSD test (*$P < 0.05$, ***$P < 0.001$).

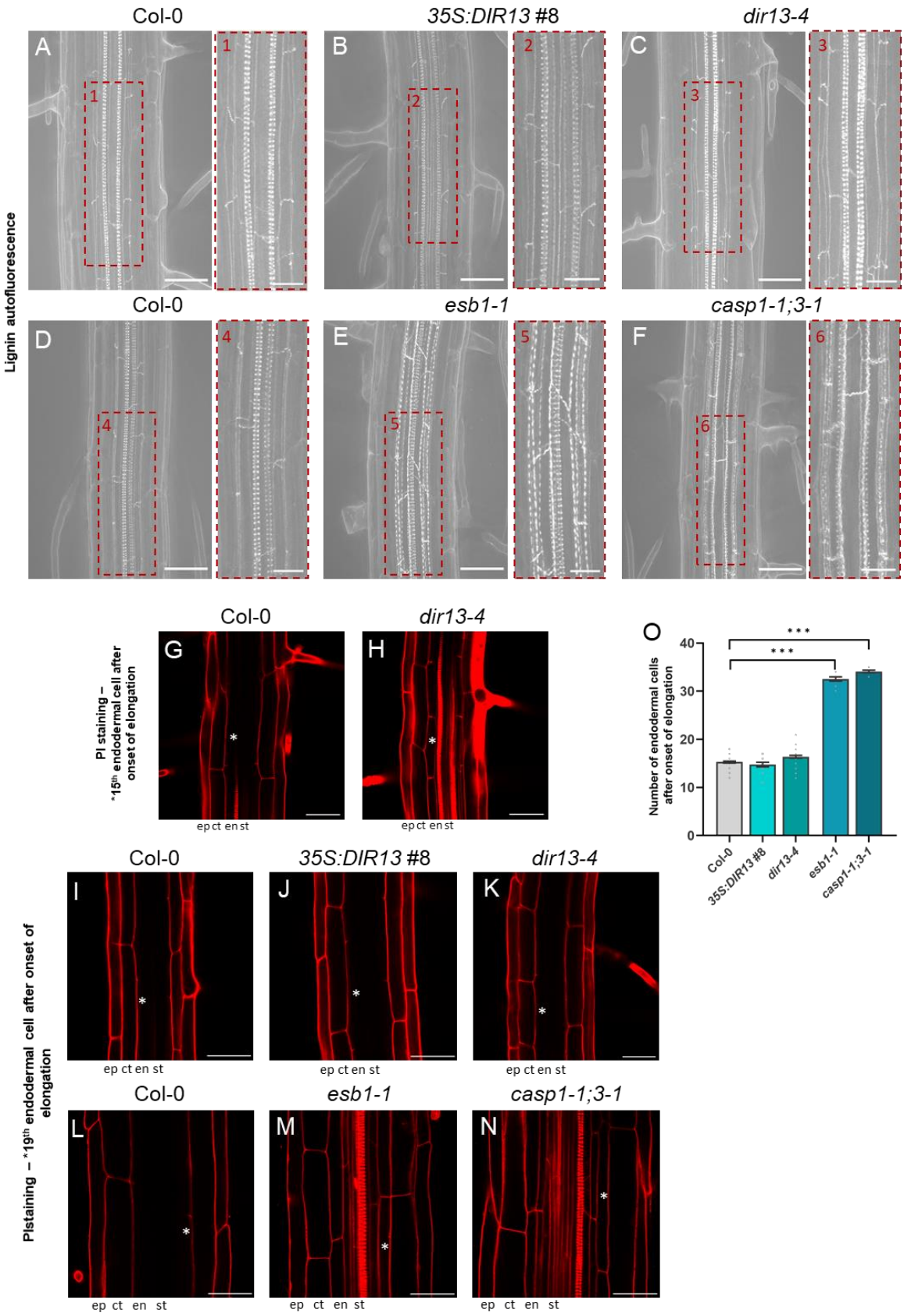

Supplemental Figure 4. DIR13 is not required for normal morphology and function of Casparian strip. (A – F) Visualization of lignin autofluorescence after clearing roots of 7-day-

old Col-0 WT (A, D), *35S:DIR13* #8 (B), *dir13-4* (C), *esb1-1* (E), and c*asp1-1;3-1* (F), and their close-up images (1 - 6) shown respectively in red dashed rectangles. **(G – N)** Propidium iodide (PI) penetration into the stele in 5-day-old Col-0 WT (G, I, L), *dir13-4* (H, K), *35S:DIR13* #8 (J), *esb1-1* (M) and c*asp1-1;3-1* (N). Asterisks mark the 15th (G, H) and 19th (I - N) endodermal cell after onset of elongation. The onset of elongation (e.g., fully expanded cell) is defined as the zone where the length of an endodermal cell was observed to be more than twice its width. Scale bars represent 50 µm in (A - O) and 20 µm in (1 - 6). ep, epidermis; ct, cortex; en, endodermis; st, stele. **(O)** Quantification of PI penetration in Col-0 WT, *35S:DIR13* #8, *dir13-4*, *esb1-1*, and *casp1-1;3-1* roots. The number of endodermal cells showing PI staining into the stele were counted from the first fully expanded endodermal cell. Data are the means of a representative experiment. Error bars indicate +/- SE, ($n \geq 10$). Asterisks indicate statistically significant differences between Col-0 WT and mutant lines based on Poisson mixed model analysis and Tukey test (**$P < 0.01$, ***$P < 0.001$).

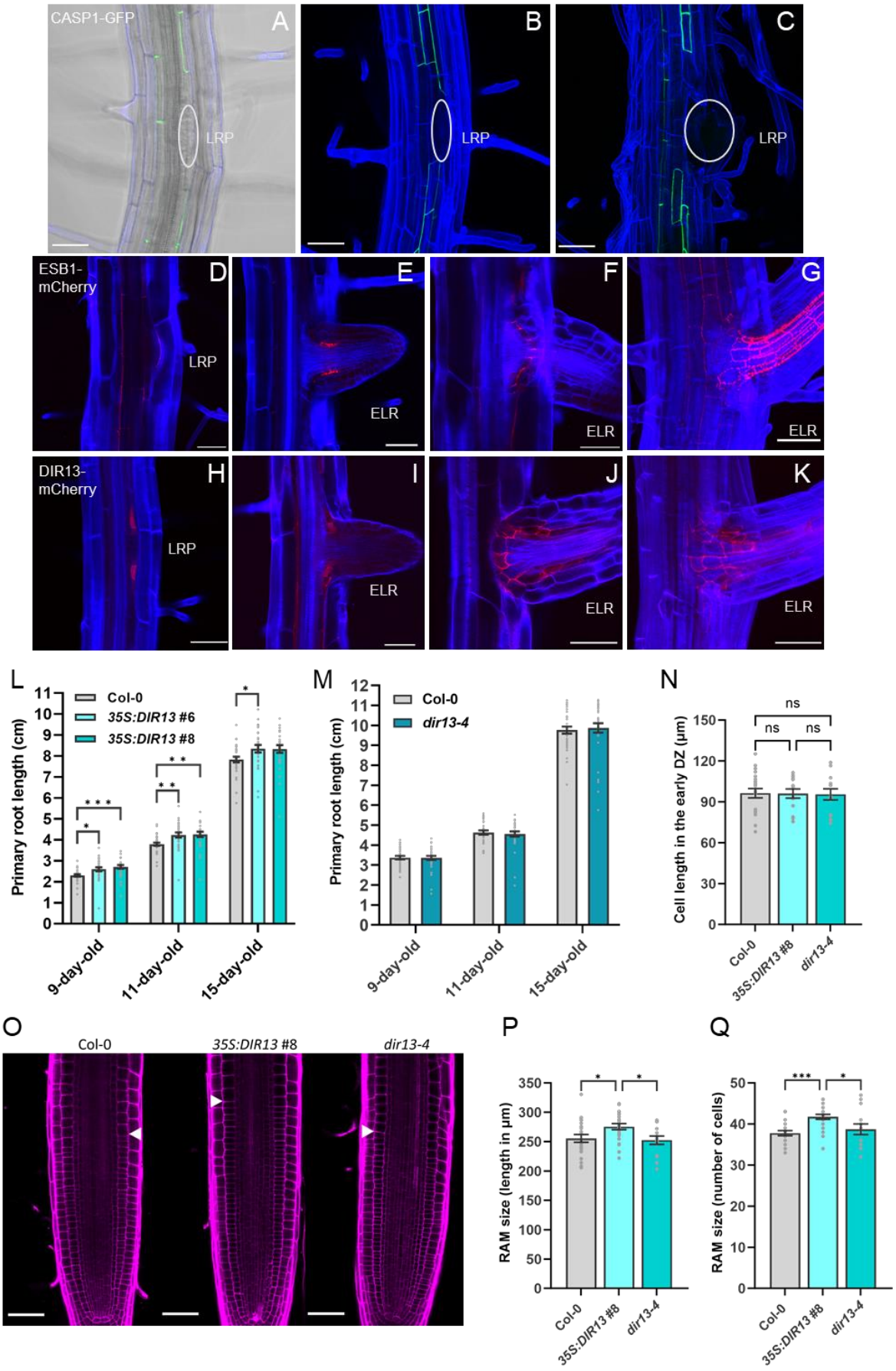
CASP1-GFP
A
B
C
LRP
ESB1-mCherry
D
E
F
G
ELR
DIR13-mCherry
H
I
J
K
L
Col-0
35S:DIR13 #6
35S:DIR13 #8
Primary root length (cm)
9-day-old
11-day-old
15-day-old
M
dir13-4
N
Cell length in the early DZ (µm)
ns
O
P
Q
RAM size (length in µm)
RAM size (number of cells)

Supplemental Figure 5. DIR13, CASP1 and ESB1 show distinct localization patterns during lateral root formation. (A – C) CASP1-GFP signal is not detected in lateral root primordia (LRP) as indicated by white ovals. Representative images of 9-day-old seedlings where (A) is confocal image merged with transmission image and (B, C) are Z-stack overviews. **(D – G)** ESB1-mCherry localizes in both LRP and emerged lateral root (ELR). Representative images of Z-stack overviews of 9-day-old seedlings expressing *pESB1:ESB1-mCherry* in the developing lateral root area of LRP (D) and ELR (E – G). **(H – K)** DIR13-mCherry localization partially resembles ESB1-mCherry expression pattern but is more localized to the LR peripheral basal cells throughout LR development. Representative images of Z-stack overviews of 9-day-old seedlings expressing *pDIR13:DIR13-mCherry* in the developing lateral root area of LRP (H) and ELR (I – K). Cleared roots were stained with Calcofluor White, the cell wall is shown in blue, GFP is in green and mCherry is in red. Scale bars represent 50 µm. **(L – M)** Comparison of the primary root length (in cm) in Col-0 WT, *35S:DIR13* #6 and #8 (F) and *dir13-4* mutant (G) seedlings grown vertically for 9, 11 and 15 days. Data are the means of a representative experiment. Error bars indicate +/- SE (n ≥ 30). Asterisks indicate statistically significant differences between genotypes based on two-way ANOVA followed by Dunnett's HSD test (**P* < 0.05, ***P* < 0.01, ****P* < 0.001). **(N)** Cell length measured in the early differentiation zone (DZ) of Col-0 WT, *35S:DIR13* #8 and *dir13-4* mutant. Data are presented as the mean +/-SE (n≥14). No statistically significant difference was found between tested genotypes based on one-way followed by Tukey's HSD test. **(O)** Representative images of 7-day-old roots of Col-0 WT, *35S:DIR13* #8 and *dir13-4* mutant. The plasma membrane signal from PI staining is shown in magenta. The end of the measured RAM size indicated by white arrowheads. Scale bars represent 50 µm. **(P, Q)** RAM size measured as total length from QC until the distal end of TZ (in µm) (P) and as number of cortex cells in the same area (Q). Asterisks indicate statistically significant differences between tested genotypes based on one-way ANOVA (P) or Poisson mixed model analysis (Q) followed by Tukey's HSD test (**P* < 0.05, ****P* < 0.001).

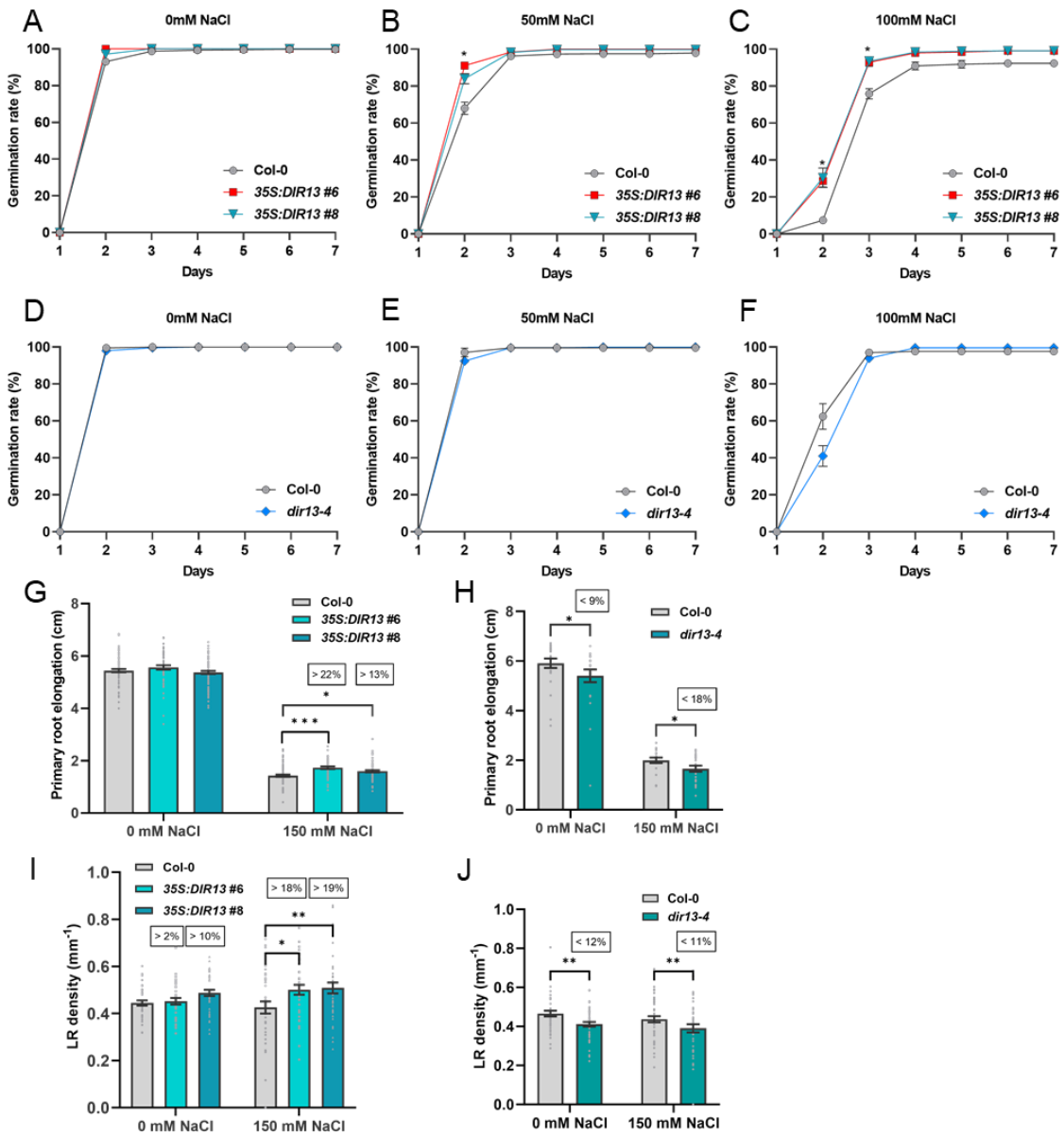

Supplemental Figure 6. DIR13 improves tolerance to salt stress. (A - F) Seed germination rates of *35S:DIR13* #6 and #8 overexpressing lines (A - C) and *dir13-4* mutant (D - F) under salt stress treatment. The germination rate was recorded for 7 days after stratification in the presence of 0, 50 and 100 mM NaCl. Data are the averages of three independent experiments. Error bars indicate +/- SE (n ≥ 100). Asterisks indicate statistically significant differences at $P < 0.05$ between Col-0 WT and *DIR13* OE in (A - C) based on repeated measures two-way ANOVA followed by Dunnett's HSD test. **(G - H)** DIR13 attenuates salt stress-mediated inhibition of primary root growth. 5-day-old Col-0 WT, *35S:DIR13* #6 and #8 lines (G) and *dir13-4* mutant (H) seedlings grown on MS/2 media were transferred to MS/2 media supplemented with 0 mM (control) or 150 mM NaCl. Primary root elongation (in cm) was measured 7 days after

transfer. Data are the averages of three independent experiments. Error bars indicate +/- SE (n ≥ 60). Asterisks indicate statistically significant differences between genotypes based on two-way ANOVA followed by Tukey's HSD test (*P < 0.05, ***P < 0.001). Numbers in rectangles show the relative difference compared to Col-0 WT in percentage. **(I - J)** DIR13 promotes lateral root growth even in the presence of salt. LR density (lateral root number per mm of primary root length) was measured 9 days after the transfer of Col-0 WT, *35S:DIR13* #6 and #8 (I) and *dir13-4* (J) seedlings to 150 mM NaCl. Data show the means of a representative experiment +/- SE (n ≥ 20). Asterisks indicate statistically significant differences between genotypes based on two-way ANOVA followed by Tukey's HSD test (**P < 0.01, ***P < 0.001). Numbers in rectangles show the relative difference compared to Col-0 in percentage.

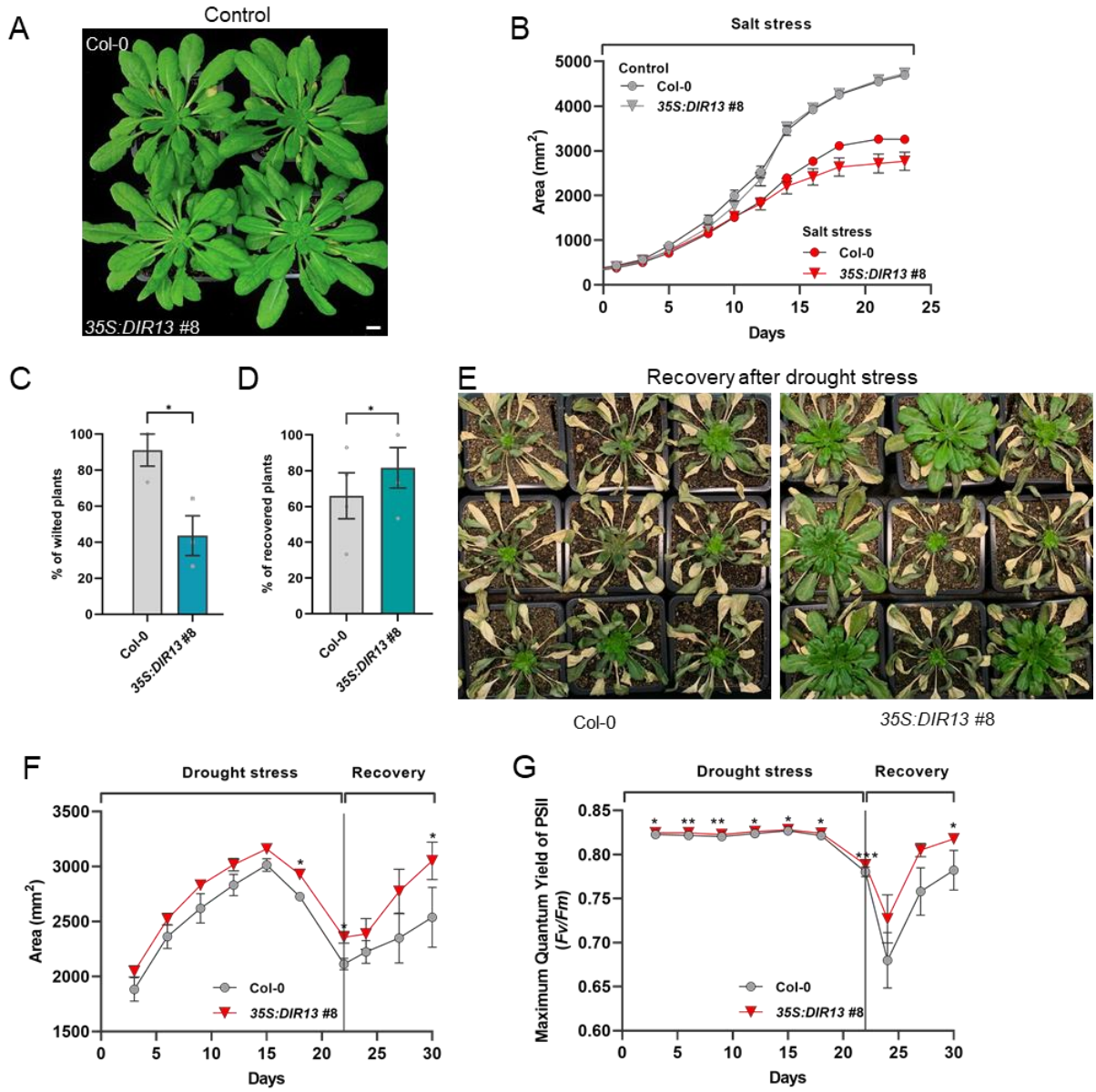

Supplemental Figure 7. Tolerance to drought stress of *DIR13* overexpressing plants is higher than Col-0 WT. **(A)** Phenotypes of 8-week-old Col-0 WT and *35S:DIR13* #8 plants growing under normal short-day conditions. Scale bar represents 1 cm. **(B)** Area (in mm^2) of the plant rosette (A; Fig. 4 G) was recorded in Col-0 WT and *35S:DIR13* #8 plants during the control and salt stress conditions. Data are the means of a representative experiment. Error bars indicate +/- SE (n ≥ 7). No statistically significant differences between Col-0 WT and *35S:DIR13* #8 in control or salt stress conditions was found based on mixed model analysis followed by Tukey's HSD test. **(C, D)** *DIR13* overexpression promotes plant tolerance to drought stress. Percentage of wilted Col-0 WT and *35S:DIR13* #8 plants (B) was calculated 3 weeks after water withholding and percentage of recovered plants (C) was calculated 5 days after rewatering. The data are

means of three independent experiments. Error bars indicate +/- SE (n = 45). Asterisks indicate statistically significant differences at $P < 0.05$ between Col-0 WT and *35S:DIR13* #8 based on repeated measures one-way ANOVA followed by Tukey's HSD test. **(E)** Representative images of the recovery phenotype after 5 days of rewatering drought stressed Col-0 WT and *35S:DIR13* #8 plants. **(F, G)** Area (in mm^2) of the plant rosette (E) and Photosystem II maximum quantum yield (*Fv*/*Fm*) efficiency (F) were recorded in Col-0 WT and *35S:DIR13* #8 plants during the drought stress and recovery phases. Data are the means of a representative experiment. Error bars indicate +/- SE (n = 13). Asterisks indicate statistically significant differences between Col-0 WT and *35S:DIR13* #8 based on mixed model analysis followed by Tukey's HSD test (*$P < 0.05$, **$P < 0.01$).

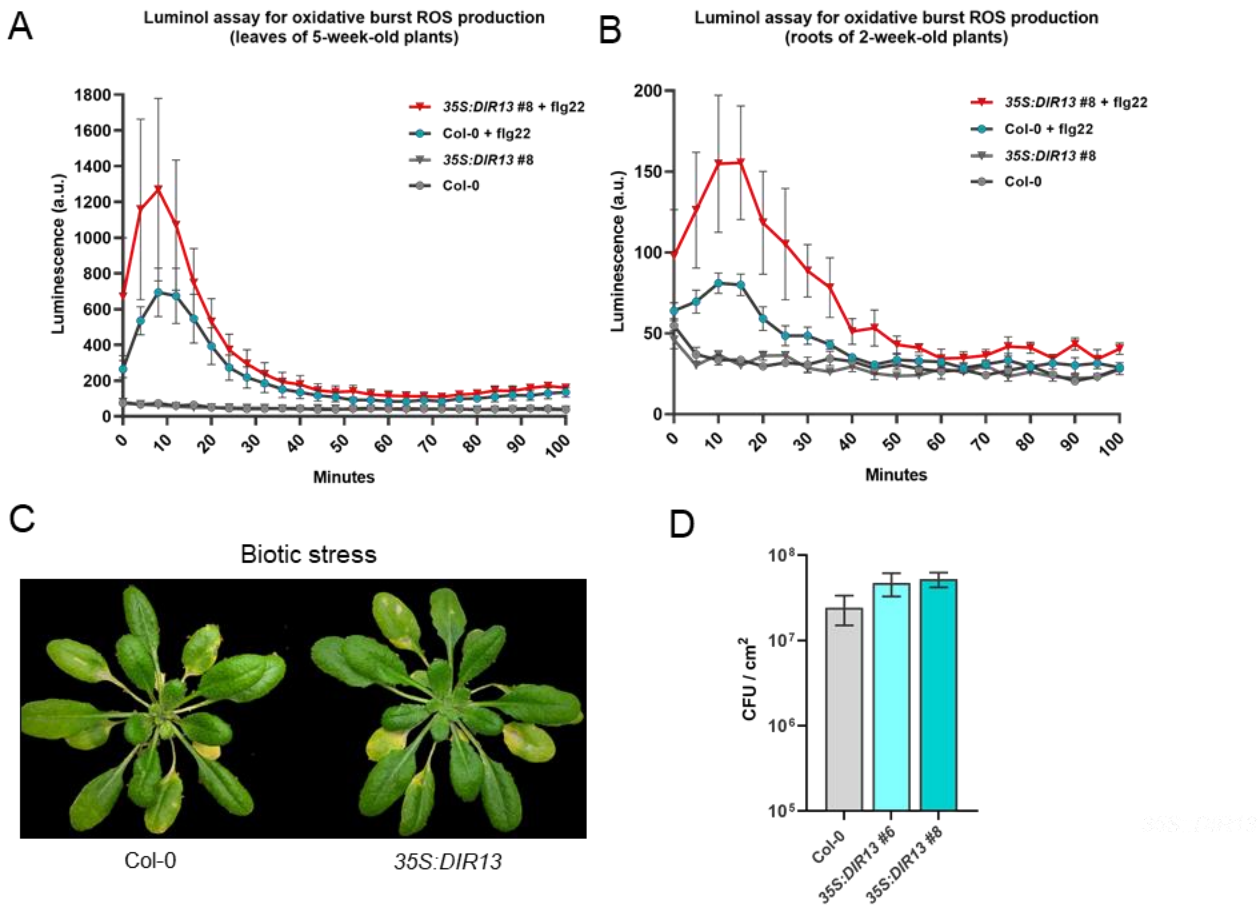

Supplemental Figure 8. Biotic stress responses in Col-0 WT and *35S:DIR13* #8 plants. (A, B) *35S:DIR13* #8 plants show enhanced ROS production triggered by flg22. Oxidative burst induced by 1 µM flg22 was measured by luminol assays in 5-week-old leaves (A) and 2-week-old roots (B) of Col-0 WT and *35S:DIR13* #8 plants. Data show the means of a representative experiment. Error bars indicate +/- SE (n = 6). Statistically significant difference at $P < 0.05$ between Col-0 WT and *35S:DIR13* #8 was not found based on repeated measures mixed model analysis followed by Tukey's HSD test. **(C)** Disease symptoms in 5-week-old Col-0 WT and *35S:DIR13* #8 plants 5 days after spray-inoculation with *Pseudomonas syringae* pv. tomato (*Pst*) DC3000 at 10^8 cfu/mL. **(D)** Quantification of *Pst* DC3000 bacterial growth (colony forming units – CFU per cm^2 of leaf area) in Col-0 WT and *35S:DIR13* #6, #8 leaves 3 days after spraying with 10^8 cfu/mL *Pst* DC3000. Results are the means of two independent experiments. Error bars indicate +/- SE (n = 16). No significant difference at $P < 0.05$ between Col-0 WT and *35S:DIR13* #6, #8 was found based on repeated measures one-way ANOVA followed by Tukey's HSD test.

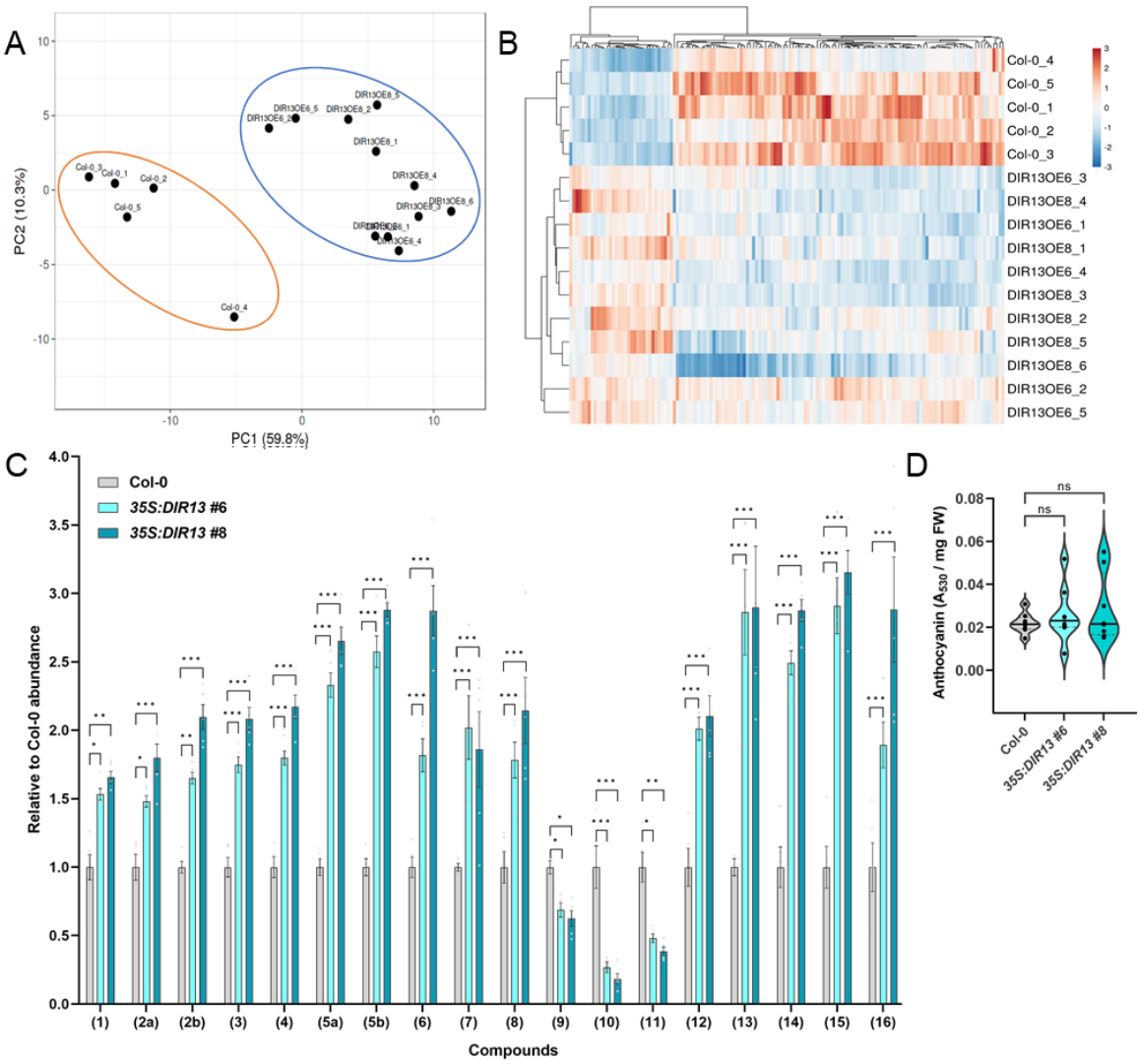

Putative compounds differently accumulated in *DIR13* OE #6 and #8 compared to Col-0 WT

m/z / Retention Time / Chemical Family

(1) 373.12 / 5.38 / Lignan

(2a) 373.12 / 4.04 / Dibenzylbutyrolactone lignans

(2b) 373.12 / 4.27 / Dibenzylbutyrolactone lignans, might be an isomer of **(2a)**

(3) 355.11 / 4.04 / Lignan

(4) 343.11 / 4.03 / Lignan

(5a) 480.16 / 4.14 / Lignan (Matairesinol-cysteine)

(5b) 359.15 / 4.14 / in source fragment of (5a) by loss of cysteine (Matairesinol)

(6) 373.12 / 4.65 / Lignan

(7) 335.25 / 22.4 / Lipids, fatty acids

(8) 570.21 / 4.24 / 2-arylbenzofuran flavonoids

(9) 595.16 / 3.98 / Kaempferol-hexoside-rhamnoside (flavonols)

(10) 373.14 / 3.52 / Syringin (Phenolic glycosides)

(11) 540.24 / 4.70 / Lariciresinol 4-O-glucoside (Lignan glycosides)

(12) 512.16 / 5.36 / Lignan

(13) 343.12 / 4.84 / Lignan

(14) 355.12 / 4.30 / Lignan

(15) 583.17 / 4.50 / Neolignan

(16) 556.24 / 3.91 / Neolignan

Supplemental Figure 9. Untargeted metabolomic analyses reveal changes in the accumulation of putative lignans and neolignans in *DIR13* overexpressing lines. (A) Principal

Component Analysis (PCA) of HPLC-MS/MS data in ElectroSpray Ionization in positive (ESI+) mode from root biological replicates of 10-day-old Col-0 WT, *35S:DIR13* #6 and #8. PCA demonstrates the difference between Col-0 WT and *DIR13* OE lines in the accumulation of significantly different abundant compounds. **(B)** Clustering of compounds detected by HPLC-MS/MS (ESI+ mode) which are significantly different abundant between Col-0 WT and *DIR13* OE roots. Columns were centered, unit variance scaling was applied to columns. Both rows and columns were clustered using correlation distance and average linkage. **(C)** *DIR13* overexpression leads to the accumulation of putative lignans and neolignans in roots. Selected differentially abundant compounds annotated mostly as putative (neo)-lignans were extracted from Col-0 WT, *35S:DIR13* #6, #8 roots and detected by HPLC-MS/MS in ESI+ mode. Data are shown as relative to Col-0 WT and are the means +/- SE ($n \geq 5$). Asterisks indicate statistically significant differences between Col-0 WT and *35S:DIR13* #6, #8 based on two-way ANOVA followed by Dunnett's HSD test. (*$P < 0.05$, **$P < 0.01$, ***$P < 0.001$). **(D)** Quantification of anthocyanins Abs_{530}/mg of fresh weight (FW) in the shoots of 11-day-old Col-0 WT and *35S:DIR13* #6 and #8 seedlings. No significant difference at $P < 0.05$ between Col-0 WT and *35S:DIR13* #6, #8 was found based on one-way ANOVA followed by Tukey's HSD test.

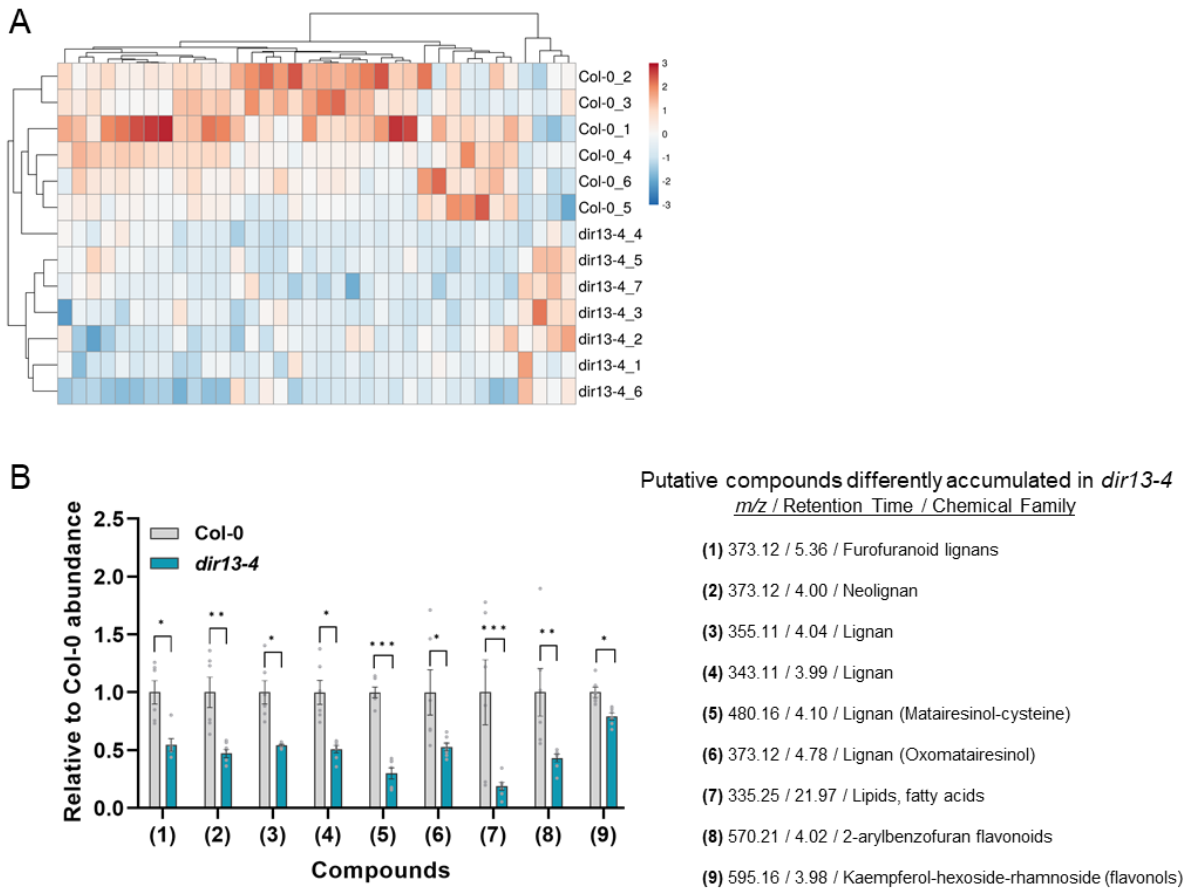

Supplemental Figure 10. Untargeted metabolomic analyses reveal changes in the accumulation of putative lignans and neolignans in *dir13-4* mutant line in ESI+ mode. (A) Clustering of compounds detected by HPLC-MS/MS which are significantly different presented in Col-0 WT and *dir13-4* plants. Columns are centered, unit variance scaling is applied to columns. Both rows and columns are clustered using correlation distance and average linkage. **(B)** Differential accumulation of phenolic compounds in *dir13-4* mutant. Selected differentially abundant compounds annotated mostly as putative (neo)-lignans were extracted from Col-0 WT, *dir13-4* roots and detected by HPLC-MS/MS in ESI+ mode. Data are shown as relative to Col-0 WT and are the means +/- SE (n = 6). Asterisks indicate statistically significant differences between Col-0 WT and *dir13-4* based on two-way ANOVA followed by Tukey's HSD test. (**P* < 0.05, ***P* < 0.01, ****P* < 0.001).

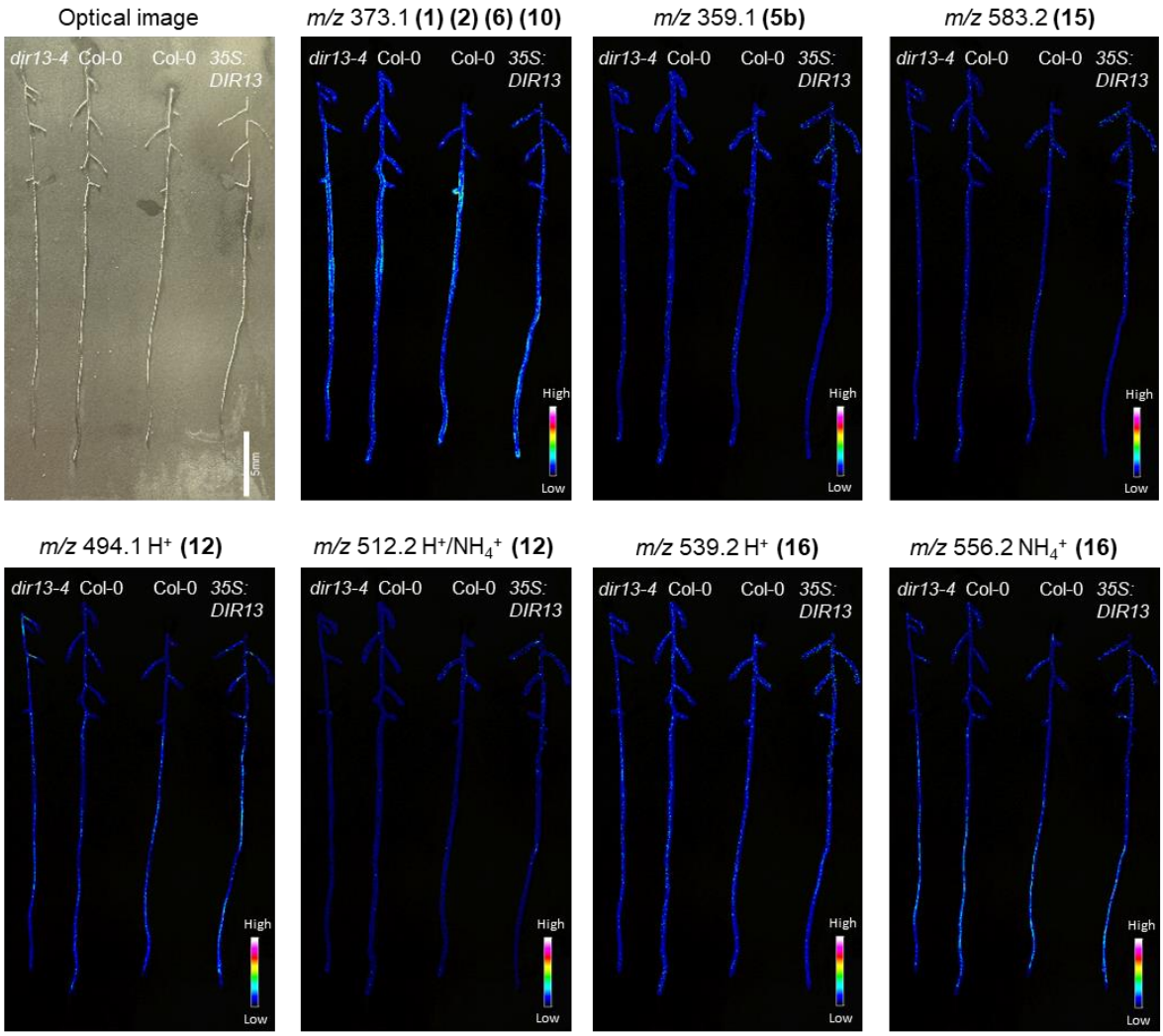

Supplemental Figure 11. Spatial distribution of putative lignans in the roots of *dir13-4* mutant and *DIR13* overexpressing lines. Imaging Mass Spectrometry (IMS) of roots from 10-day-old Col-0 WT, *dir13-4* mutant and *35S:DIR13* #8 overexpressing lines. Signals at *m/z* 373.1 (1) (2) (6) (10), *m/z* 359.1 (5b), 583.2 (15), 494.1 H^+ (12), 512.2 H^+/NH_4^+ (12), 539.2 H^+ (16) and 556.2 NH_4^+ (16) correspond to putative matairesinol (5b), oxomatairesinol (6), syringin (10) and metabolites annotated as lignans (1), (12) or neolignans (2), (15) and (16). For metabolites (12) and (16) the *m/z* signals from two possible ionizations by H^+ or NH_4^+ are shown. The spatial resolution is 50 µm. MS signal intensity is indicated by color bars and the scale bar represents 5 mm. The experiment was repeated at least twice with similar results.

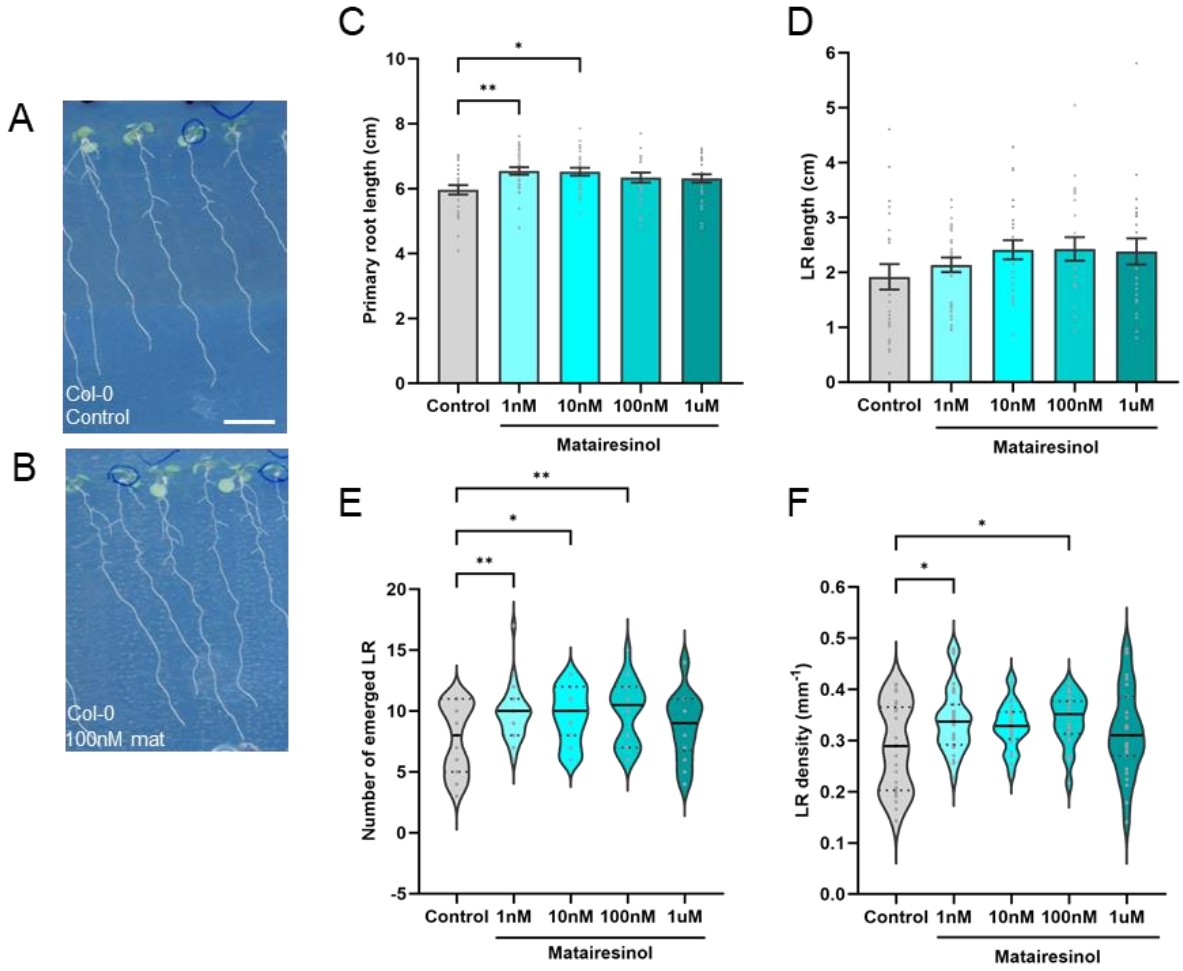

Supplemental Figure 12. Matairesinol promotes lateral root growth. (A - B) Phenotype of 11-day-old Col-0 WT seedlings growing in normal conditions (A) or on plates supplemented with 100nM matairesinol (B). Scale bars represent 1 cm. **(C - D)** Comparison of the primary root length (in cm) (C) and total lateral root length per seedling (in cm) (D) in 11-day-old Col-0 WT seedlings. Data are the means of a representative experiment. Error bars indicate +/- SE (n ≥ 22). Asterisks indicate statistically significant differences between genotypes at $^{**}P < 0.01$ based on one-way ANOVA followed by Dunnett's HSD test. **(E - F)** Average number of emerged lateral roots (E) and LR density expressed as the number of lateral roots per cm of primary root length (F) in 11-day-old Col-0 WT seedlings. Data show the median and upper and lower quartiles of a representative experiment (n ≥ 22). Asterisks indicate statistically significant differences between genotypes at $^{*}P < 0.05$ based on Poisson mixed model analysis (E), one-way ANOVA followed by Dunnett's HSD test (F).

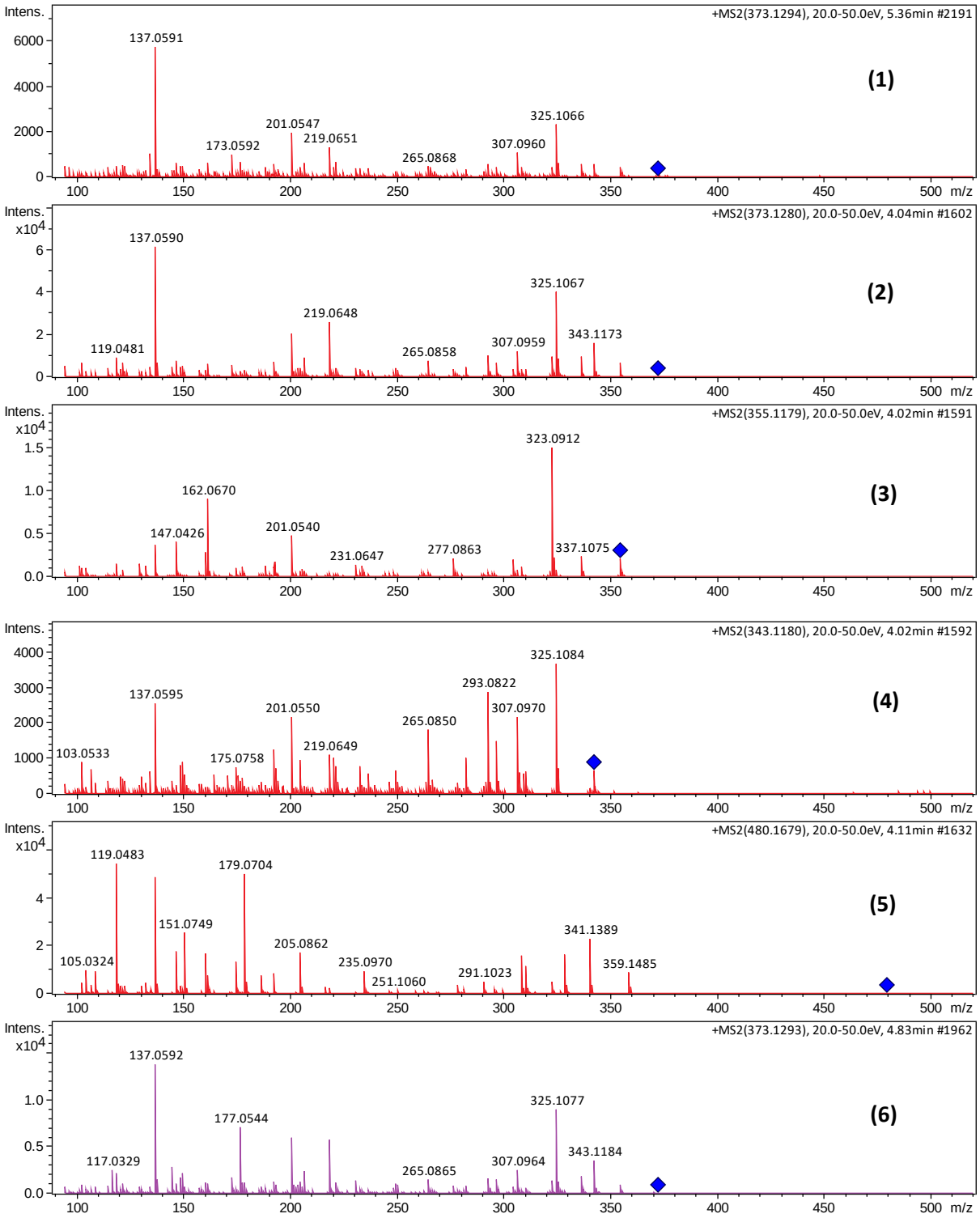

Supplemental Figure 13. **ESI+ MS/MS spectra of accumulated putative lignans and neolignans in roots overexpressing *DIR13***. For the compounds numbering see Figure 6B, HPLC-MS/MS analyses were performed using *35S:DIR13* #8.

Supplemental Materials and Methods

Lignin autofluorescence

Lignin autofluorescence experiment was performed as described by (Hosmani et al., 2013). 5- to 6-day-old seedlings were transferred to a Petri dish containing 0.24 M HCl and 20 % methanol and incubated for 15 minutes at 57 °C. The solution was replaced with 7 % NaOH and 60 % ethanol and incubated for 15 minutes at room temperature. After these clearing steps, roots were rehydrated at room temperature by sequential replacement of the solution using 40 % ethanol for 5 minutes, 20 % ethanol for 5 minutes, 10 % ethanol for 5 minutes, 5 % ethanol for 15 minutes, and finally 25 % glycerol was added. For mounting root on glass slides, 50 % glycerol was used. Autofluorescence of the Casparian strip was observed on cleared roots (Malamy & Benfey, 1997) by using a Zeiss LSM880 confocal microscope with excitation at 488 nm and with band path filter of 500–600 nm.

PI staining and quantification

For assay of the apoplastic barrier, PI staining was done as described previously (Alassimone et al., 2010). Briefly, 5- to 6-day-old Col-0 WT, *35S:DIR13, dir13-4, esb1-1, and casp1-1;3-1* seedlings were incubated in the dark for 10 min in a fresh solution of 15 µM (10 µg/mL) PI and rinsed twice in water. For quantification, the “onset of elongation” was defined as the point where an endodermal cell in a median optical section was more than twice its width and the number of cells were counted until PI could not penetrate into the stele.

ClearSee-adapted cell wall staining

ClearSee-adapted cell wall staining was performed as described before by (Ursache et al., 2018). Briefly, 5- to 6-day -old seedlings were fixed in 3 ml 1 × PBS containing 4 % paraformaldehyde for 1 hour at room temperature in 6- well plates and washed twice with 3 ml 1 × PBS. Following fixation, the seedlings were cleared in 3 ml ClearSee solution under gentle shaking. After overnight clearing, the solution was exchanged to new ClearSee solution containing 0.1% Calcofluor White for cell wall staining. The dye solution was removed after 1 hour of staining and rinsed once with fresh ClearSee solution. The samples were washed in

new ClearSee solution for 30 minutes with gentle shaking and washed again in another fresh ClearSee solution for at least 1 hour before observation.

Drought stress tolerance tests

For the drought tolerance test, different genotypes randomly mixed and initially grown on soil under normal watering conditions for 4 weeks were subjected to a 21-day dehydration period by withholding water, during which observations were made. The percentage of wilted plants was counted when wild-type plants exhibited wilting on young/meristematic leaves. Subsequently, watering was resumed, and the percentage of recovered plants was calculated 5 days after rewatering and counted as plants with newly green meristematic leaves. Control plants grown in parallel under well-watered conditions were used as a control. During the drought experiment, the morphologic and fluorescent parameters were monitored using the automatic phenotyping platform (PlantScreen^{TM} SC Root System, PSI). Particularly, measurements of "Area (mm^2)" and "Maximum quantum yield of PSII (*Fv/Fm*)" representing the maximal photochemical efficiency were taken every 3 days for each plant.

Luminol assay

Apoplastic oxidative burst evaluation ROS released by leaf and root tissue was assayed as described by (Arnaud et al., 2023). 6 mm leaf discs of 4.5-week-old Arabidopsis plants were cut in 4 equal pieces or 2-week-old roots were collected from 16 seedlings for each genotype and transferred into the wells of 96-well plate containing distilled water. The plates were incubated for 3 hours at room temperature for recovery after wounding. Then water was exchanged with a solution containing 20 µM luminol (Sigma) and 10 µg/mL horseradish peroxidase (Sigma). After adding water as a control solution or 1 µM flg22, the luminescence was measured immediately using a PROMEGA microplate reader (BMG Labtech) with a reading time of 2 sec.

Bacterial infection assay

Bacterial infection assay was performed as previously described by (Arnaud et al., 2017). Bacterial strain *Pseudomonas syringae* pv. tomato DC3000 (Pst DC3000) was cultivated overnight at 28°C in King's B medium supplemented with rifampicin (100 µg/ml) and kanamycin (50 µg/ml) antibiotics. Bacteria were collected by centrifugation at 3000 *g* for 5 min at room temperature and washed twice in 10 mM $MgCl_2$. Plants were surface inoculated by spraying with a bacterial solution of $1x10^8$ colony-forming units (cfu)/mL in 10 mM MgCl2 containing 0.02 % Silwet L-77, and plants were covered to maintain high humidity until disease symptoms developed. After 3 days, bacterial growth in the apoplast of three leaves per plant and four plants per genotype was determined as previously described (Katagiri et al., 2002).

Supplemental References

Alassimone, J., Naseer, S., & Geldner, N. (2010). A developmental framework for endodermal differentiation and polarity. *Proceedings of the National Academy of Sciences of the United States of America*, *107*(11), 5214–5219. https://doi.org/10.1073/pnas.0910772107

Arnaud, D., Deeks, M. J., & Smirnoff, N. (2023). Organelle-targeted biosensors reveal distinct oxidative events during pattern-triggered immune responses. *Plant Physiology*, *191*(4), 2551–2569. https://doi.org/10.1093/plphys/kiac603

Arnaud, D., Lee, S., Takebayashi, Y., Choi, D., Choi, J., Sakakibara, H., & Hwang, I. (2017). Cytokinin-Mediated Regulation of Reactive Oxygen Species Homeostasis Modulates Stomatal Immunity in Arabidopsis. *The Plant Cell*, *29*(3), 543–559. https://doi.org/10.1105/tpc.16.00583

Hosmani, P. S., Kamiya, T., Danku, J., Naseer, S., Geldner, N., Guerinot, M. Lou, & Salt, D. E. (2013). Dirigent domain-containing protein is part of the machinery required for formation of the lignin-based Casparian strip in the root. *Proceedings of the National Academy of Sciences*, *110*(35), 14498–14503. https://doi.org/10.1073/pnas.1308412110

Katagiri, F., Thilmony, R., & He, S. Y. (2002). The Arabidopsis Thaliana-Pseudomonas Syringae Interaction. *The Arabidopsis Book*, *1*, e0039. https://doi.org/10.1199/tab.0039

Malamy, J. E., & Benfey, P. N. (1997). Organization and cell differentiation in lateral roots of Arabidopsis thaliana. *Development*, *124*(1), 33–44. https://doi.org/10.1242/dev.124.1.33

Ursache, R., Andersen, T. G., Marhavý, P., & Geldner, N. (2018). A protocol for combining fluorescent proteins with histological stains for diverse cell wall components. *Plant Journal*, *93*(2), 399–412. https://doi.org/10.1111/tpj.13784